

1 Newly identified climatically and environmentally significant high- 2 latitude dust sources

3 Outi Meinander¹, Pavla Dagsson-Waldhauserová^{2,3}, Pavel Amosov⁴, Elena Aseyeva⁵, Cliff Atkins⁶,
4 Alexander Baklanov⁷, Clarissa Baldo⁸, Sarah Barr⁹, Barbara Barzycka¹⁰, Liane G. Benning^{11,23}, Bojan
5 Cvetkovic¹², Polina Enchilik⁵, Denis Frolov⁵, Santiago Gassó¹³, Konrad Kandler¹⁴, Nikolay Kasimov⁵,
6 Jan Kavan¹⁵, James King¹⁶, Tatyana Koroleva⁵, Viktoria Krupskaya^{5,6}, Markku Kulmala¹⁸, Monika
7 Kusiak¹⁹, Hanna K Lappalainen¹⁸, Michał Laska¹¹, Jerome Lasne²⁰, Marek Lewandowski¹⁹, Bartłomiej
8 Luks¹⁹, James B McQuaid¹⁰, Beatrice Moroni²¹, Benjamin J Murray¹⁰, Ottmar Möhler²², Adam Nawrot¹⁹,
9 Slobodan Nickovic¹³, Norman T. O'Neill²³, Goran Pejanovic¹³, Olga B. Popovicheva⁵, Keyvan
10 Ranjbar^{23,a}, Manolis N. Romanias²⁰, Olga Samonova⁵, Alberto Sanchez-Marroquin¹⁰, Kerstin
11 Schepanski²⁴, Ivan Semenov⁵, Anna Sharapova¹¹, Elena Shevnina¹, Zongbo Shi⁹, Mikhail Sofiev¹,
12 Frédéric Thevenet²⁰, Throstur Thorsteinsson²⁵, Mikhail A. Timofeev⁵, Nsikanabasi Silas Umo²², Andreas
13 Uppstu¹, Darya Urupina²⁰, György Varga²⁶, Tomasz Werner¹⁹, Olafur Arnalds², and Ana Vukovic
14 Vimic²⁷

15

16 ¹Finnish Meteorological Institute, Helsinki, 00101, Finland

17 ²Agricultural University of Iceland, Reykjavik, 112, Iceland

18 ³Czech University of Life Sciences Prague, Prague, 16521, Czech Republic

19 ⁴INEP Kola Science Center RAS, Apatity, Russia

20 ⁵Lomonosov Moscow State University, Moscow, 119991, Russia

21 ⁶Institute of Geology of Ore Deposits, Petrography, Moscow, 119017, Russia

22 ⁷Te Herenga Waka—Victoria University of Wellington, Wellington, 6012, New Zealand

23 ⁸World Meteorological Organization, WMO, Geneva, 1211, Switzerland

24 ⁹University of Birmingham, Birmingham, B15 2TT, United Kingdom

25 ¹⁰University of Leeds, Leeds, LS2 9JT, United Kingdom

26 ¹¹University of Silesia in Katowice, Sosnowiec, 41-200, Poland

27 ¹²German Research Centre for Geosciences, Helmholtz Centre Potsdam, 14473, Germany

28 ¹³Republic Hydrometeorological Service of Serbia, 11030, Belgrade, Serbia

29 ¹⁴University of Maryland, College Park MD, 20742, United States of America

30 ¹⁵Technical University of Darmstadt, Darmstadt, 64287, Germany

31 ¹⁶Masaryk University, Brno, 61137, Czech Republic

32 ¹⁷University of Montreal, Montreal, H3T 1J4, Canada

33 ¹⁸Institute for Atmospheric and Earth System Research, University of Helsinki, Helsinki, 00101, Finland

34 ¹⁹Institute of Geophysics, Polish Academy of Sciences, Warsaw, 01-452, Poland

35 ²⁰IMT Lille Douai, SAGE, Université de Lille, 59000 Lille, France

36 ²¹University of Perugia, Perugia, 06123, Italy

37 ²²Institute of Meteorology and Climate Research, Karlsruhe Institute of Technology, Karlsruhe, 76227, Germany.

38 ²³Université de Sherbrooke, Sherbrooke, J1K, Canada

39 ²⁴Free University of Berlin, Berlin, 12165, Germany

40 ²⁵University of Iceland, Reykjavik, 102, Iceland

41 ²⁶Research Centre for Astronomy and Earth Sciences, Budapest, 1112, Hungary

42 ²⁷University of Belgrade, Faculty of Agriculture, Belgrade, 11080, Serbia

43 ^anow at: Flight Research Laboratory, National Research Council Canada, Ottawa, ON, Canada

44

45

46 *Correspondence to:* Outi Meinander (outi.meinander@fmi.fi)

47 **Abstract.** Dust particles from high latitudes have a potentially large local, regional, and global significance to climate and the
48 environment as short-lived climate forcers, air pollutants, and nutrient sources. Identifying the locations of local dust sources
49 and their emission, transport, and deposition processes is important for understanding the multiple impacts of High Latitude
50 Dust (HLD, $\geq 50^\circ\text{N}$ and $\geq 40^\circ\text{S}$) on the Earth's systems. Here, we identify, describe, and quantify the Source Intensity (SI)
51 values, which show the potential of soil surfaces for dust emission scaled to values 0 to 1 concerning globally best productive
52 sources, using the Global Sand and Dust Storms Source Base Map (G-SDS-SBM). This includes sixty-four HLD sources in
53 our collection for the Northern (Alaska, Canada, Denmark, Greenland, Iceland, Svalbard, Sweden, and Russia) and Southern
54 (Antarctica and Patagonia) high latitudes. Activity from most of these HLD dust sources shows seasonal character. It is
55 estimated that high-latitude land areas with higher ($\text{SI} \geq 0.5$), very high ($\text{SI} \geq 0.7$), and the highest potential ($\text{SI} \geq 0.9$) for dust
56 emission cover $>1\,670\,000\text{ km}^2$, $>560\,000\text{ km}^2$, and $>240\,000\text{ km}^2$, respectively. In the Arctic HLD region ($\geq 60^\circ\text{N}$), land area
57 with $\text{SI} \geq 0.5$ is 5.5% ($1\,035\,059\text{ km}^2$), area with $\text{SI} \geq 0.7$ is 2.3% ($440\,804\text{ km}^2$), and with $\text{SI} \geq 0.9$ is 1.1% ($208\,701\text{ km}^2$).
58 Minimum SI values in the north HLD region are about three orders of magnitude smaller, indicating that the dust sources of
59 this region greatly depend on weather conditions. Our spatial dust source distribution analysis modeling results showed
60 evidence supporting a northern High Latitude Dust (HLD) belt, defined as the area north of 50°N , with a 'transitional HLD-
61 source area' extending at latitudes $50\text{--}58^\circ\text{N}$ in Eurasia and $50\text{--}55^\circ\text{N}$ in Canada, and a 'cold HLD-source area' including areas
62 north of 60°N in Eurasia and north of 58°N in Canada, with currently 'no dust source' area between the HLD and LLD dust
63 belt, except for British Columbia. Using the global atmospheric transport model SILAM, we estimated that 1.0% of the global
64 dust emission originated from the high-latitude regions. About 57% of the dust deposition in snow- and ice-covered Arctic
65 regions was from HLD sources. In the south HLD region, soil surface conditions are favorable for dust emission during the
66 whole year. Climate change can decrease snow cover duration, retrieval of glaciers, and increase drought, heatwave intensity,
67 and frequency, leading to the increasing frequency of topsoil conditions favorable for dust emission, which increases the
68 probability of dust storms. Our study provides a step forward to improve the representation of HLD in models and to monitor,
69 quantify, and assess the environmental and climate significance of HLD going forward.

70 **1 Introduction**

71 Mineral dust is an essential and relevant climate and environmental variable with multiple socioeconomic effects on, e.g.,
72 weather and air quality, marine life, climate, and health (Creamean et al., 2013; Terradellas et al., 2015; Shepherd et al., 2016;
73 Querol et al., 2019; Nemuc et al., 2020). Mineral dust is transported from local sources of high-latitude dust (HLD, $\geq 50^\circ\text{N}$ and

74 $\geq 40^{\circ}\text{S}$), low-latitude dust (LLD, mostly $0\text{-}35^{\circ}\text{N}$), and the so-called ‘global dust belt’ (GDB, Prospero et al., 2002), defined to
75 extend into the Northern Hemisphere from the west coast of North Africa, over the Middle East (West Asia), Central and East
76 Asia, and south-west North America (Ginoux et al., 2012), with only minor sources in Southern Hemisphere (Prospero et al.,
77 2002; Ginoux et al., 2012; Bullard et al., 2016; Terradellas et al., 2017). Dust is often associated with hot, subtropical deserts,
78 but the importance of dust sources in the cold, high latitudes has recently increased (Arnalds et al., 2016; Bullard et al., 2016;
79 Groot Zwaafting et al., 2016, 2017; Kavan et al., 2018, 2020a,b; Boy et al., 2019; Gassó and Torres, 2019; IPCC, 2019; Tobo
80 et al., 2019; Bachelder et al., 2020; Cosentino et al., 2020; Ranjbar et al., 2021; Sanchez-Marroquin et al., 2020). Dust produced
81 in high latitudes and cold climates (Iceland, Greenland, Svalbard, Alaska, Canada, Antarctica, New Zealand, and Patagonia)
82 can have regional and global significance (Bullard et al., 2016). Local HLD dust emissions are increasingly being recognized
83 as driving the local climate, biological productivity, and air quality (Groot Zwaafting et al., 2016, 2017; Moroni et al., 2018;
84 Crocchianti et al., 2021; Varga et al., 2021). HLD can induce significant direct (blocking sunlight) and indirect (clouds and
85 cryosphere) radiative forcing (Kylling et al., 2018) on solar radiation fluxes and snow optical characteristics, strongly
86 impacting Arctic amplification, including glacier melt (Boy et al., 2019).

87

88 HLD aerosols consist of a variety of different dust particle types with various particle sizes and shapes distributions, as well
89 as physical, chemical, and optical properties that differ from the crustal dust of the Sahara or American deserts (Shepherd et
90 al., 2016; Arnalds et al., 2016; Bachelder et al., 2020; Baldo et al., 2020; Crucius, 2021). Therefore, impacts on climate,
91 environment, and human health can differ from those of LLD. For example, Icelandic dust is of volcanic desert origin, often
92 dark, and has higher proportions of heavy metals than crustal dust (Arnalds et al., 2016). The IPCC special report (IPCC, 2019)
93 recognizes dark dust aerosols as a short-lived climate forcer (SLCF) and light-absorbing aerosols connected to cryospheric
94 changes. Light-absorbing HLD particles can induce direct effects on solar radiation fluxes as SLCF and snow optical
95 characteristics impacting cryosphere melt via radiative feedback (Peltoniemi et al. 2015; Boy et al., 2019; Dagsson-
96 Waldhauserová and Meinander, 2019, 2020; IPCC, 2019; Kylling et al., 2018). HLD significantly affects the formation and
97 properties of clouds (Abbatt et al., 2019; Sanchez-Marroquin et al., 2020; Murray et al., 2021).

98

99 Dust is connected to climate change: Historical dust (paleo dust) is not only a contributor to climate change but a record of
100 previous dust and climate conditions (Lamy et al., 2014; Lewandowski et al., 2020). Dust can significantly contribute to air
101 pollution mortalities (Terradellas et al., 2015; Nemuc et al., 2020). Deposition at high latitudes can provide nutrients to the
102 marine system; mineral and organic matter on glaciers, including natural and anthropogenic dust, can form cryoconite granules.
103 Cryoconite, dust, and ice algae can reduce surface albedo and accelerate the melting of glaciers (Lutz et al., 2016; McCutcheon
104 et al., 2021). Monitoring dust in remote, high-latitude areas has crucial value for climate change assessment and understanding
105 the impacts of global warming on natural systems and socioeconomic sectors. Bullard et al. (2016) summarized natural HLD
106 sources as covering over $500\,000\text{ km}^2$ and producing particulate matter of ca. 100 Mt dust per year.

107

108 Dust emissions respond to changes in wind speed, soil moisture, and other parameters affected by climate change; changes in
109 land cover and surface properties by human activities can affect dust emissions (Kylling et al., 2018). The fundamental
110 processes controlling aeolian dust emissions in high latitudes are essentially the same as in temperate regions. However, there
111 are other processes specific to or enhanced in cold regions. Low temperatures, humidity, strong winds, permafrost, and niveo-
112 aeolian processes, which can affect the efficiency of dust emission and distribution of sediments, were listed in Bullard et al.
113 (2016).

114

115 The modeling of emissions, transport, and deposition complemented with available observations, can provide essential
116 information related to dust's impact on the climate and environment in the high latitudes (IPCC, 2019). The locations and
117 characteristics of local dust sources are two of the major observations documented for inputting information into numerical
118 models to predict or simulate the HLD process from its emission to downwind deposition. In some cases, model results can
119 indicate possible but not yet identified dust sources in the HL regions. A general lack of observational and long-range transport
120 modeling studies results in poor HLD monitoring and predicting. Models have predictive capacity and, without the
121 observations, can constitute a source of information and indicate where more direct observations are needed. The first long-
122 range transport modeling studies show that main transport pathways from HLD sources clearly affect the High Arctic (>80°N)
123 and European mainland (Baddock et al., 2017; Beckett et al., 2017; Đorđević et al., 2019; Groot Zwaaving et al., 2016, 2017;
124 Moroni et al., 2018). The World Meteorological Organization Sand and Dust Storm Warning Advisory and Assessment System
125 (WMO SDS-WAS) monitors and predicts dust storms from the world's major deserts (<https://www.wmo.int/sdswas>), where
126 HLD sources have recently been included in the SDS-WAS dust forecasts. Europe's largest desert is at a high latitude in
127 Iceland (Arnalds et al., 2016), with dust transport observed over the North Atlantic to European countries (Ovadnevaite et al.,
128 2009; Prospero et al., 2012; Beckett et al., 2017; Đorđević et al., 2019).

129

130 HLD is a short-lived climate forcer, air pollutant, and nutrient source, showing the need to identify the geographical extent
131 and dust activity of the HLD sources (Dagsson-Waldhauserová et al., 2014, 2015; Terradellas et al., 2015; Arnalds et al., 2014,
132 2016; USGCRP, 2018; IPCC, 2019). Bullard et al. (2016) designed the first HLD map based on visibility and dust observations,
133 combined with field and satellite observations of high-latitude dust storms, resulting in 129 locations described in 39 papers.
134 Here, we compile and describe sixty-four HLD sources in the northern and southern high latitudes. Since dust particles emitted
135 from high latitudes can have a large local, regional, and global significance to climate and the environment, identifying where
136 local dust sources are is important. Climate change and land-use change can further increase the number of dust sources and
137 their emissions when, for example, snow, ice, or glaciers melt, exposing new open soil areas and generating more glacial dust
138 particles. This work's main aim is to:

- 139 (i) identify new and previously unpublished HLD sources using direct observations and measurements, satellite
140 data, literature sources (including media and social media), and include HLD sources identified in recent

- 141 literature from 2017–2021, which have not been part of previously published collections of HLD sources, as
142 well as update some of the previously documented sources
- 143 (ii) estimate the high-latitude land area with potential dust activity and calculate the source intensity (SI) for the
144 identified sources
 - 145 (iii) provide model results on HLD emission, long-range transport and deposition at various scales of time and
146 space
 - 147 (iv) specify key climatic and environmental impacts of HLD and related research questions, which could improve
148 our understanding of HLD sources.
- 149

150 We focus on high latitudes with natural dust sources and include some anthropogenic dust sources, such as road dust, when
151 unpaved roads serve as a significant dust source. Direct emissions of volcanic eruptions and road dust formed via abrasion and
152 wear of pavement or traction control materials are excluded. Identifying new dust sources is the first step to understanding the
153 atmospheric dust life-cycle representation for the HLD life cycle (dust emission, transport, and deposition). After that, impacts
154 and feedback mechanisms, including HLD-atmosphere direct and indirect interactions and HLD-ocean interactions (Boy et
155 al., 2019), can be identified and quantified as physical, chemical, and optical properties of dust from these source areas. Their
156 properties during emission, transport, and deposition are needed to be characterized to allow a holistic understanding.

157 **2 Materials and methods**

158 **2.1 Identification and characteristics of dust sources**

159 Three topical workshops in Russia, Finland, and Iceland (Meinander et al., 2019a,b) on HLD were organized in 2019 to
160 identify, describe, and assess new high-latitude dust sources at $\geq 50^\circ\text{N}$ and $\geq 40^\circ\text{S}$ (including the Arctic as a subregion at \geq
161 60°N). The HLD source map and observations on dust properties provided here are based on:

- 162 (i) field and satellite observations not described in published academic papers
- 163 (ii) newly identified HLD source locations reported in academic literature but not included in previous collections
- 164 (iii) updated observations on previously documented sources.

165 Each location was assessed to classify each source: Category 1 refers to an active dust source with high ecological significance,
166 category 2 to a semi-active source with moderate ecological significance, and category 3 to new sources with unknown activity
167 and importance. Moreover, SI values for each HLD location in the Northern and Southern (Antarctica and Patagonia) high
168 latitudes were quantified, and the potential land surface area for dust emissions in the north, Arctic, and south HLD regions
169 was calculated (Section 2.2).

170 **2.2 High-latitude dust sources from UNCCD G-SDS-SBM**

171 The Global Sand and Dust Storms Source Base Map (G-SDS-SBM), developed by the United Nations Convention to Combat
172 Desertification (UNCCD) in collaboration with the United Nations Environment Programme (UNEP) and World
173 Meteorological Organization (<https://maps.unccd.int/sds/>; Vukovic, 2019, 2021) represents gridded values of SDS source
174 intensity (SI, values 0 to 1) on a resolution of 30 arcsec. The Source Base Map was developed by including the information on
175 soil texture, bare land fraction, and NASA satellite Moderate-resolution Imaging Spectroradiometer Enhanced Vegetation
176 Index, MODIS EVI, as well as the data on land cover, topsoil moisture, and temperature. Values of SI represent topsoil’s
177 potential to emit soil particles under windy conditions, assigning the highest values of source intensity to the most productive
178 surfaces. SI values are derived under the assumption they are exposed to the same velocity of surface wind. Input data, which
179 change depending on the weather (and possibly human activities) for bare land fraction, moisture, and temperature data, are
180 defined for four months (January, April, July, October—each month representing one season) by using extreme values. This
181 was observed from 2014 to 2018, providing favorable conditions for surfaces to act as sources. Thus, sources that may appear
182 during heatwaves and drier conditions (or drought), when the surface in high latitudes is unfrozen, snow-free, and more
183 susceptible to wind erosion, are included in this map. Such weather extremes under climate change are becoming more frequent
184 and are projected to increase (IPCC, 2013), justifying the source mapping approach using the information on extreme topsoil
185 conditions. Using the maps produced for the four seasons, maximum and minimum values are determined for each grid point
186 to explore the potential of high-latitude land surfaces to act as dust sources, their seasonality, and to compare values of source
187 intensity with marked locations of HLD sources.

188 **2.3 Methods used to identify and study the dust sources**

189 Various methods identified the HLD sources (Table 1), including direct observations and measurements; satellite data;
190 emission, long-range transport and deposition modeling; media, social media, and literature sources (e.g., web pages,
191 conference abstracts). More details and literature references can be found in each source section. Dust emission, long-range
192 transport, and deposition modeling calculations were made to study if the HLD sources have local, regional, or global
193 significance. Two well-established dust atmospheric models—SILAM and DREAM—were used to simulate the atmospheric
194 dust process over high latitudes. Both models have been thoroughly evaluated for other deserts where the accuracy of their
195 results has been verified.

196

197 **Table 1. Methods used to identify and study the dust sources**

Method	Sources
--------	---------

Direct observation: photographs and visual observations	Marambio, Antarctic Peninsula, Schirmacher Oasis, East Antarctica McMurdo Sound/Ross Sea
Satellite images: Meteosat-11 images	Denmark, Sweden, Iceland
Instrumentation: SEM	Svalbard
Instrumentation: LOAC	James Ross Island
Instrumentation: SL-501 surface and snow albedo	Marambio, Antarctic Peninsula
Instrumentation: Magnetic susceptibility upon heating, magnetic hysteresis parameters	Svalbard
Instrumentation: ICP-MS, AES-ICP, XRD, XRF	Russia (sources no. 2–5 of Fig.1)
Instrumentation: high performed liquid chromatography, potentiometry	Russia (sources no. 7–8 of Fig.1)
Passive deposition samplers	James Ross Island
Snow samples	Svalbard (Hornsund, Pyramiden), Antarctica
Social media: Twitter account (@SanGasso) and hashtag (#highlatitudedust)	South America (Patagonia), Alaska, Greenland, Iceland
Literature sources	Denmark, Sweden
SILAM model	Arctic
DREAM model	Arctic, Antarctic

198

199

200

201

202

203

204

205

206

207

Estimates of the emission and deposition of global and Arctic dust were computed separately to assess Arctic dust's global impact using the SILAM model (Sofiev et al., 2015)—a global to meso-scale atmospheric dispersion and chemistry model—applied for air quality and atmospheric composition modelling. The dust emission estimate is driven by the European Centre for Medium Range Weather Forecast ECMWF IFS meteorological model at a resolution of 0.1 x 0.1 degrees. The computations were performed using ECMWF ERA5 meteorological reanalysis data for 2017 at a resolution of 0.5 x 0.5 degrees. The dust emission model was validated against AERONET (AERosol RObotic NETwork, www.aeronet.com) aerosol optical density (AOD) data and provided unbiased results for the main dust emission areas. For Arctic areas, where dust is not contributing to the AOD as much, the simulated AOD from all aerosols is unbiased concerning the measurements. While the simulation's

208 relatively coarse resolution cannot capture the smaller point-like dust sources, it is still expected to give a good approximation
209 of the overall patterns and magnitudes of dust emission and deposition. The SILAM results are presented in sections 3.3 (Fig.
210 4) and 3.4 (Fig. 12 and Fig. 15).

211
212 DREAM is a fully dynamic numerical prediction model for atmospheric dust dispersion originating from soil. The dust
213 component of this system (Pejanovic et al., 2011; Nickovic et al., 2016) is online and driven by the atmospheric model NMME
214 (Janjic et al., 2001). Dust concentration in the model is described with eight particle bins, with radii ranging from 0.18 to 9
215 μm . DREAM-ICELAND is the model version to predict dust transport emitted from Iceland's largest European dust sources
216 (Cvetkovic et al., 2021, submitted). The size distribution of particles in the model is specified according to in situ measurements
217 in the Icelandic hot spots. The model horizontal resolution of ~ 3.5 km is sufficiently fine to resolve the Icelandic dust sources'
218 rather heterogeneous and small-scale character. As the first operational numerical HLD model in the international community,
219 DREAM-ICELAND is used daily, having predicted Icelandic dust since April 2018. DREAM results are included in sections
220 3.4 (Fig. 8 and 11) and 3.6 (Fig. 16), and as a supplementary animation.

221

222 **2.4 Literature survey on climatic and environmental impacts**

223

224 Climatic and environmental impacts of HLD were investigated with the help of literature surveys. Each impact section presents
225 an independent literature survey with its own co-author list, as indicated in the author contribution section. Thus, the following
226 sections were created: impacts of HLD on clouds and climate feedback, atmospheric chemistry, marine environment,
227 cryosphere, and cryosphere-atmosphere feedback.

228

229 **3 Results and discussion**

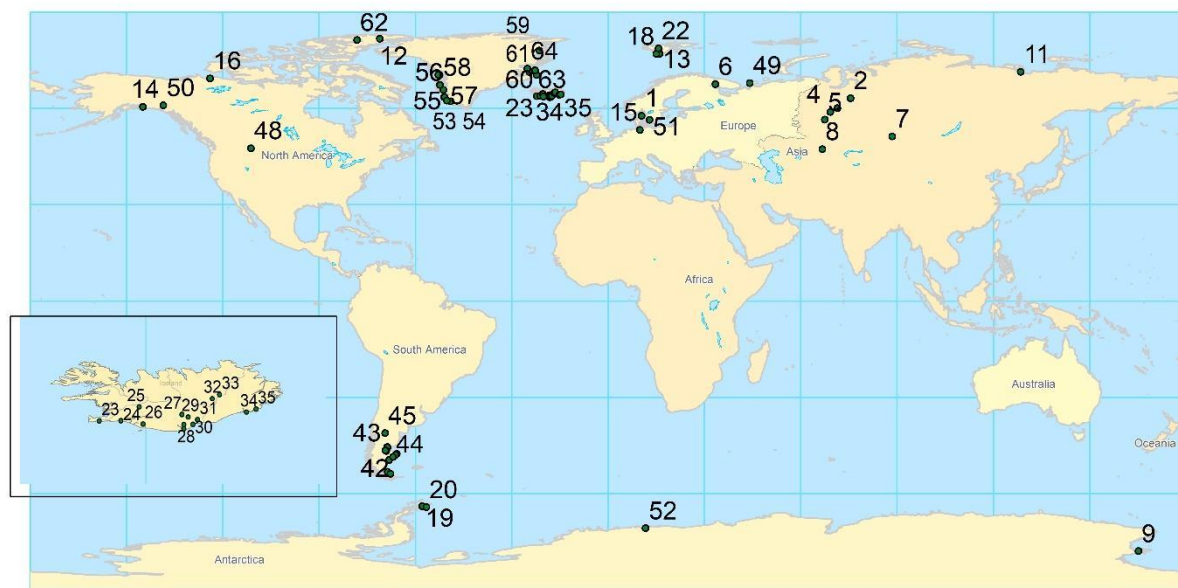
230

231 **3.1 Locations of the HLD sources**

232

233 Sixty-four HLD sources at northern and southern high latitudes (Fig. 1) were identified. In the north HLD region are 49
234 locations in Alaska, Canada, Denmark, Greenland, Iceland, Svalbard, Sweden, and Russia, of 35 are in the Arctic HLD
235 subregion. In the south HLD region, 15 sources were identified in Antarctica and Patagonia, South America. The sources
236 included the Arctic and Antarctic, boreal, remote, rural, mountain, marine and coastal, river sediments, mining, unpaved roads,
237 soils (Podzols, Retisols, Gleysols, Phaeozems, and Stagnosols; USS Working Group WRB, 2015), and glacial dust. The
238 observational periods for these locations varied from days or weeks to multiple years and included data from ground-based
239 measurements, remote sensing data, and modeling results. Results on the calculated source intensity and areas of high-latitude
240 surface land with higher ($SI \geq 0.5$), very high ($SI \geq 0.7$), and the highest potential ($SI \geq 0.9$) for dust emission are shown in Section
241 3.2. Observations and characteristics of the identified dust sources in our collection (Fig. 1) are presented in Section 3.4 and

242 the Supplement Tables S1-S7 (including the contemporary classification for each source into categories 1–3, based on the
243 currently available observations, in S1; satellite observations on new HLD sources in Iceland in S2; observations on new HLD
244 sources in Greenland and Canada in S3; SI values for each source in S4 and S5, including latitude and longitude; and results
245 from Russian HLD sources in S6-S7).



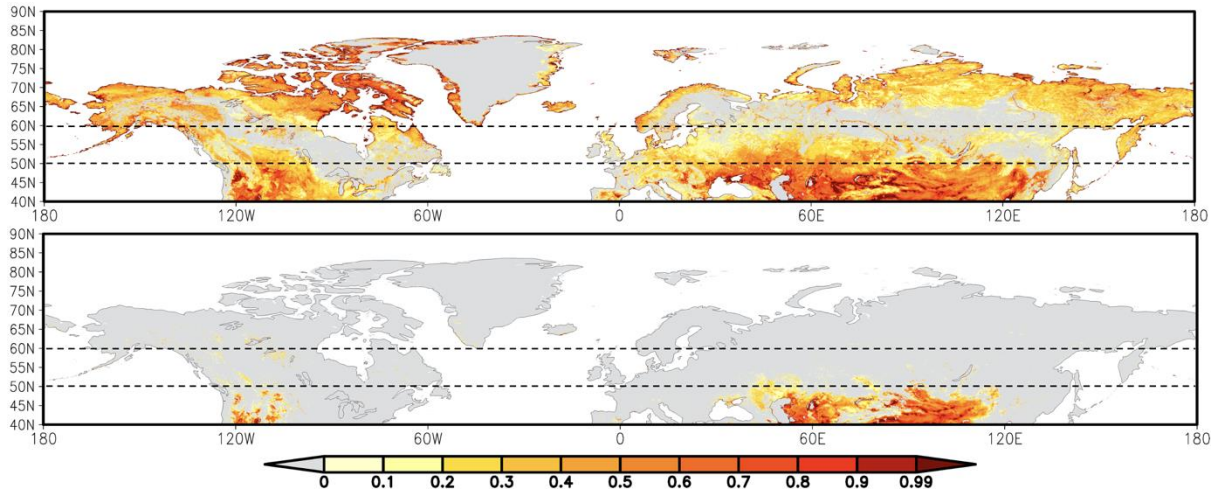
246
247 **Figure 1. Map of the locations of the northern (north of 50°N) and southern (south of 40°S) high-latitude dust (HLD) sources**
248 **identified and included in this study. The numbers are the identified 64 dust sources, as shown in Figure 1.**
249

250 **3.2 Source intensity from UNCCD G-SDS-SBM**

251 Figure 2 presents the G-SDS-SBM source intensity values (maximum and minimum) for the north HLD region. The north
252 HLD region also includes the area north of latitude 50°N and the Arctic region (as a subregion of the HLD region) north of
253 60°N. HLD dust sources show extreme seasonal characteristics, with some exceptions. The sources appear and disappear (or
254 change SI values) seasonally or appear (or increase source intensity values) only during favorable extreme weather conditions.

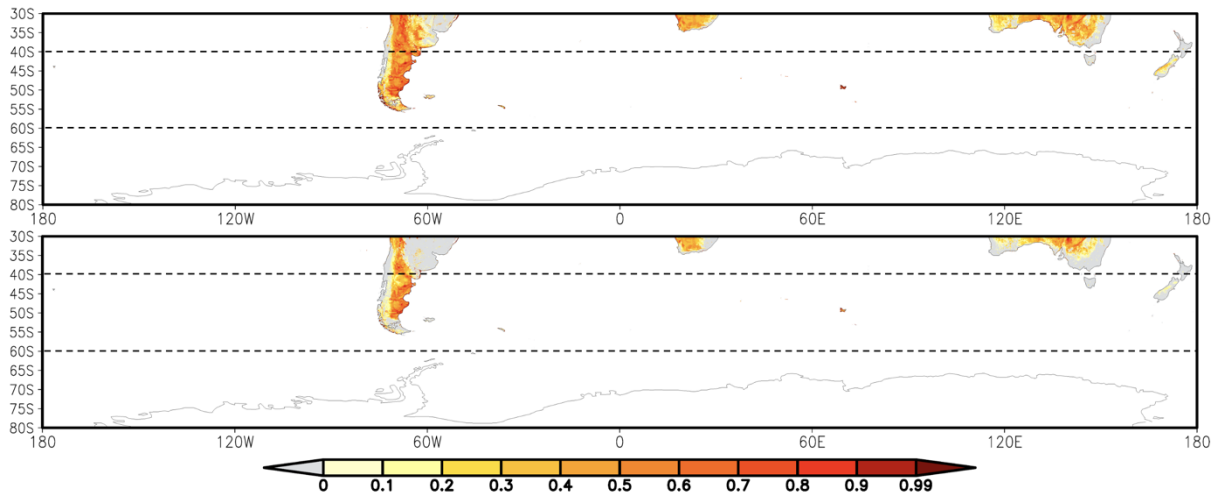
255 Figure 3 shows G-SDS-SBM source intensity values for the south HLD region (south of 40°S) without values for Antarctica
256 since G-SDS-SBM does not include areas south of 60°S. Supplementary Tables S4 and S5 give the values of SI for specific
257 locations marked in Figure 1. Further analysis consists of assessing the areal coverage of sources, with different thresholds for
258 SI values in absolute values (km²) and the percentage they occupy concerning the total land surface area in the defined HLD
259 regions.

260



261
262
263
264
265
266
267
268

Figure 2. UNCCD Global Sand and Dust Storms Source Base Map (G-SDS-SBM) for annual maximum (upper panel) and minimum (lower panel) source intensity for the north HLD region and Arctic sub-region (north of 50°N and 60°N, respectively, marked with dashed lines).



269
270

271 **Figure 3. UNCCD Global Sand and Dust Storms Source Base Map (G-SDS-SBM) for annual maximum (upper panel) and**
 272 **minimum (lower panel) source intensity for the south HLD region (south of 40°S) without Antarctica (south of 60°S), marked with**
 273 **dashed lines.**
 274
 275

276 The total surface area of dust sources with a higher potential for dust emission ($SI \geq 0.5$) over the north HLD region (north of
 277 50°N) is 3.9% of the total land surface (1 364 799 km²). The area with a very high potential for dust emission ($SI \geq 0.7$) is 1.5%
 278 (509 965 km²). The area with the highest dust emission potential ($SI \geq 0.9$) is 0.7% of the total land area (233 336 km²) (Table
 279 2). In the Arctic region (north of 60°N)—the subregion of the north HLD area—dust sources with a higher potential for dust
 280 emission ($SI \geq 0.5$) are 5.5% of the total land surface (1 035 059 km²). The area with a very high potential for dust emission
 281 ($SI \geq 0.7$) is 2.3% (440 804 km²). The area with the highest dust emission potential ($SI \geq 0.9$) is 1.1% (208 701 km²). The surface
 282 of dust-productive areas with minimum seasonal SI values in the north HLD region is about three orders of magnitude smaller
 283 than the maximum, meaning the north HLD dust sources highly depend on weather conditions. Maximum surfaces contain
 284 dust-productive regions that are defined under the most favorable weather conditions for soil exposure to wind erosion
 285 (including extreme weather). All sources defined here are not necessarily active every year nor in the same period, meaning
 286 these surfaces can seasonally or occasionally (under severe weather) appear as dust sources.

287
 288 For the south HLD region (40°S–60°S, area without Antarctica), the land surface is only 2% of the total surface area (Table
 289 3). The surface area of dust sources with $SI \geq 0.5$ is 22.6% of the total land surface (309 520 km²). The area with $SI \geq 0.7$ is 4.5%
 290 (61 527 km²). The area with the highest dust emission potential ($SI \geq 0.9$) is 0.6% (8 630 km²). The surface areas for minimum
 291 SI values above these thresholds are two to three times smaller than the surfaces for maximum SI values compared to the
 292 difference in the north HLD region. This means that soil surface conditions in the south HLD region are favorable for dust
 293 emission over the whole year. Especially in locations of HLD markers, SI maximum and minimum values do not change over
 294 most locations or decrease by 0.1 or 0.2, except for one location (no. 38), which has SI values changing from 0.9 to 0 at the
 295 location of an HLD marker.

296
 297
 298 **Table 2. Relevant surfaces for the north HLD and Arctic regions: surface of total area of the region, surface of land area within**
 299 **the region (in km² and % of total surface), total surface (in km² and % of land surface) of areas with SI values above thresholds**
 300 **(0.5 for surfaces with at least “higher” dust emission potential, 0.7 for surfaces with at least “high” dust emission potential, and 0.9**
 301 **for surfaces with “highest” dust emission potential) in maximum (max) and minimum (min) seasonal values; values are derived**
 302 **from UNCCD G-SDS-SBM.**
 303

NORTH HLD REGION (NORTH OF 50°N)		
total area (km²)	land area (km²)	land area (%)
64392015	34695710	54
	max	min

	surface area (km ²)	surface area (%)	surface area (km ²)	surface area (%)
SI ≥ 0.5	1364799	3.9	1916	0.006
SI ≥ 0.6	803372	2.3	1053	0.003
SI ≥ 0.7	509965	1.5	718	0.002
SI ≥ 0.8	342913	1.0	562	0.002
SI ≥ 0.9	233336	0.7	451	0.001

ARCTIC REGION (NORTH OF 60°N)

	total area (km ²)	land area (km ²)	land area (%)	
	36876709	18853826	51	
	max		min	
	surface area (km ²)	surface area (%)	surface area (km ²)	surface area (%)
SI ≥ 0.5	1035059	5.5	515	0.003
SI ≥ 0.6	665082	3.5	350	0.002
SI ≥ 0.7	440804	2.3	297	0.002
SI ≥ 0.8	303521	1.6	264	0.001
SI ≥ 0.9	208701	1.1	217	0.001

304
305
306
307
308
309
310
311
312
313

Table 3. Relevant surfaces for the south HLD region: surface of total area of the region, surface of land area within the region (in km² and % of total surface), total surface (in km² and % of land surface) of areas with SI values above thresholds (0.5 for surfaces with at least “higher” dust emission potential, 0.7 for surfaces with at least “high” dust emission potential, and 0.9 for surfaces with “highest” dust emission potential) in maximum (max) and minimum (min) seasonal values; values are derived from UNCCD G-SDS-SBM.

SOUTH HLD REGION (SOUTH OF 40°S)

	total area (km ²)	land area (km ²)	land area (%)	
	61435208	1367987	2	
	max		min	
	surface area (km ²)	surface area (%)	surface area (km ²)	surface area (%)
SI ≥ 0.5	309520	22.6	186266	13.616
SI ≥ 0.6	151480	11.1	81522	5.959
SI ≥ 0.7	61527	4.5	29256	2.139
SI ≥ 0.8	25416	1.9	10842	0.793
SI ≥ 0.9	8630	0.6	2747	0.201

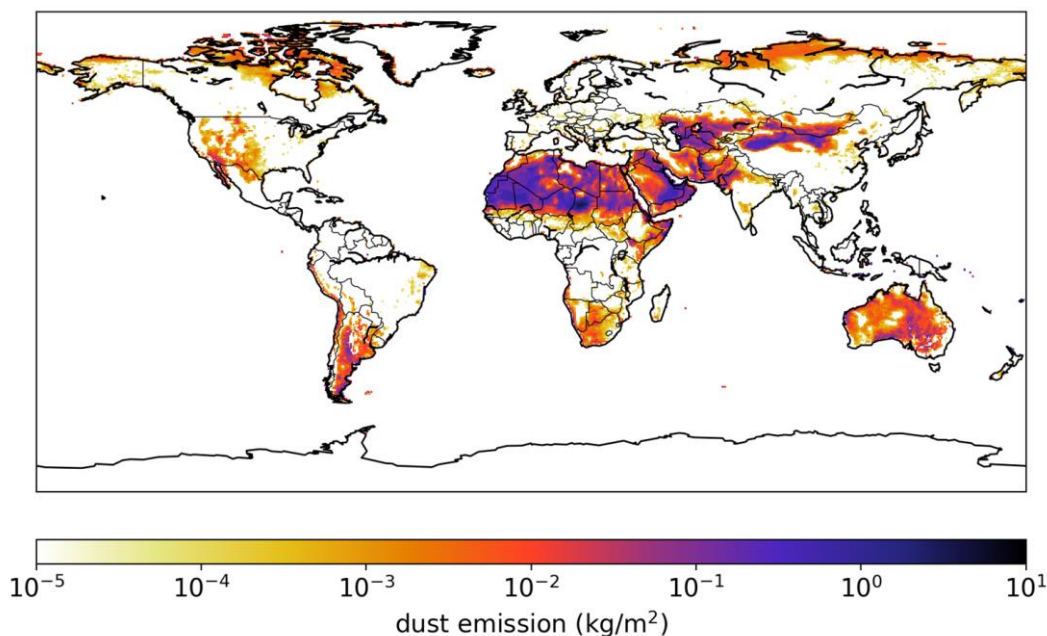
314

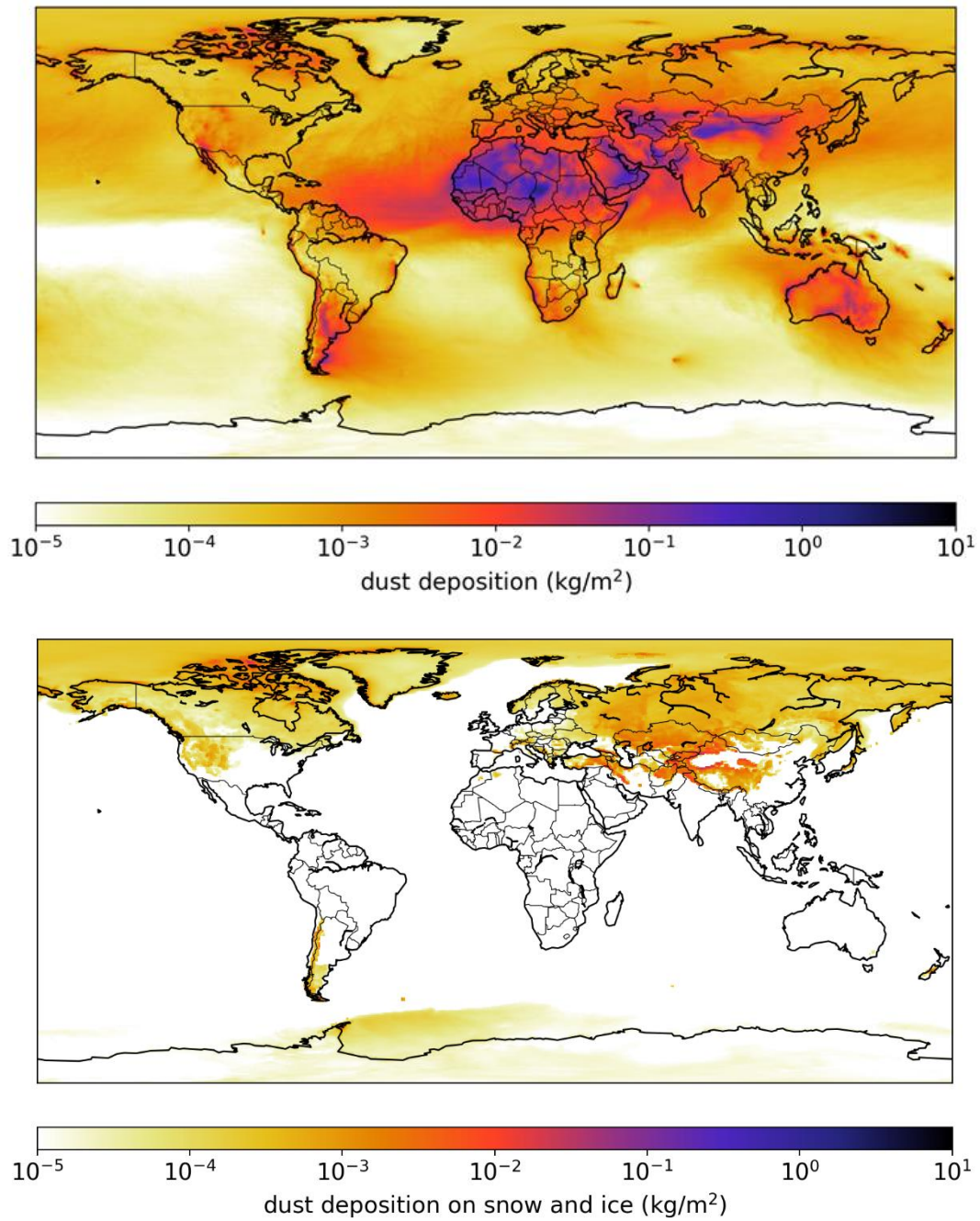
315

316 3.3 Emission and deposition of global and Arctic dust

317 The SILAM model estimated the total emission of annual dust and its deposition (data for 2017) onto snow-covered land,
318 frozen sea, and total sea surfaces (frozen and non-frozen) (Fig. 4). The computations were also performed for Arctic dust and
319 total global dust, with results for overall dust (diameter less than $30\ \mu\text{m}$) and fine dust (diameter less than $2.5\ \mu\text{m}$) separately
320 (Fig. 15 of Section 3.5). Based on the model, the total emission of Arctic dust equals approximately 1.0% of the globe's total
321 dust emission. The deposition of Arctic dust onto snow- and ice-covered surfaces equals about 19% of the total dust deposition
322 onto these areas and around 57% of the deposition onto the areas explicitly located in the Arctic region. For fine dust, the
323 corresponding figures are 7% and 22%. Compared to the deposition of black carbon (anthropogenic sources and wildfires
324 combined; Fig. 15 of Section 3.5) onto snow and ice, the deposition of fine Arctic dust is about 70% higher globally and around
325 580% higher in the Arctic regions. While these figures provide a general quantification of the deposited amounts, detailed
326 calculations of the thermal and optical properties of dust and black carbon deposited on snow would be required to compare
327 the deposited substances' net impacts on the climate.

328





329

330 **Figure 4. SILAM emission and deposition modeling results of dust emission (above), dust deposition (middle) and dust deposition**
331 **on snow and ice (below), in [kg/m²].**

332

333 **3.4 The identified dust sources**

334 Observations of the identified sixty-four dust sources in our collection (Fig. 1) are presented and discussed in alphabetical
335 order as follows: 1. Alaska (sources no. 14 and 50 in Fig. 1); 2. Antarctica (no. 9, 19, 20, 52); 3. Canada (no. 2, 16, 48, 62); 4.
336 Denmark and Sweden (no. 1, 15, 51); 5. Greenland (no. 53–61, 64); 6. Iceland (no. 23–45); 7. Russia (no. 2–11); 8. South
337 America and Patagonia (no. 17, 21, 46, 47, 49, 52, 63); and 9. Svalbard (no. 13, 18, 22). Dust events originating simultaneously
338 from Greenland, Iceland, and northern America are demonstrated in the Supplementary animation. The numbers are the
339 identified 64 dust sources shown in Figure 1. Additional information, including latitude, longitude, and SI values, can be found
340 in Supplement (Tables S1-S4).

341 **3.4.1 Alaska, Copper River Valley, USA**

342 Alaskan dust sources were identified over a century ago (Tarr and Martin, 1913). However, limited satellite detection due to
343 abundant cloud cover and isolated location resulted in sparse information on this region (Crusius et al., 2011). The main
344 identified sources are piedmont glaciers (Malaspina, Bering), resuspension of ash from past eruptions (Hadley et al., 2004),
345 and major rivers carrying glacial sediment (Copper, Yukon, Tanana, and Alsek) (Gassó, 2020a,b; 2021a,b). Resuspension of
346 glacial dust transported by these rivers can be abundant, often triggering air quality alerts by the Alaska Department of
347 Environment (USGCRP, 2018). The largest and most active of such dust sources is the Copper River (Fig. 5), estimated to
348 transport 69 million tons of suspended sediment annually (Brabets, 1997). Transported sediment is deposited on the Copper
349 River Delta, an alluvial floodplain covering an area of 2800 km². When conditions allow, sediment is resuspended, resulting
350 in dust plumes that can extend hundreds of kilometers over the Gulf of Alaska. Dust events, often lasting several days or weeks
351 (Schroth et al., 2017), are most common in late summer and autumn when the river discharge and snow cover are at their
352 minimum and high wind speeds are commonplace (Crusius, 2021). However, these occurrences have been observed year-
353 round (Gassó, 2021a; January 2021). Dust reaches the open waters beyond the continental shelf and the influence of coastal
354 sediments (Crusius et al., 2017). Thus, it has been proposed that dust from coastal sources such as the Copper River Delta can
355 be an important source of bioavailable iron in the Gulf of Alaska (Crusius et al., 2011; Crusius, 2021; Schroth et al., 2017).
356 Further work is also needed to investigate the relative importance of dust emissions from Alaska and East Asia (Bishop et al.,
357 2002) in other areas. Also, dust from this region may initiate ice production in supercooled clouds, which is crucial for climate
358 feedback (Murray et al., 2021). Regarding the magnitude and seasonal variability of emissions of sources in southern Alaska,
359 a few dedicated studies have focused on dust from the Copper River Delta (Crusius, et al., 2017; Schroth et al., 2017; Crusius,
360 2021). However, to our knowledge, no dust activity and source characterization has been carried out along the coast of the
361 Gulf of Alaska. Moreover, resuspended road dust is a major air quality issue throughout Alaska.

362

363

364



365

366

367 **Figure 5. Satellite image (left) of the Copper River region and photo (right) taken at the Copper River Delta on the same day (14th**
368 **October 2019). The common occurrence of clouds prevents directly viewing the dust in suspension, illustrating the difficulty of**
369 **observing dust activity from space. (Satellite image from NASA Worldview; photo by Sarah Barr).**

370

371 **3.4.2 Antarctica**

372 **3.4.2.1 James Ross Island, Ulu Peninsula**

373 The northern part of James Ross Island—Ulu Peninsula—represents one of Antarctica’s largest ice-free areas (312 km²). Its
374 bare surface, consisting mainly of weathered sedimentary rocks, is an active HLD source (Kavan et al., 2018). Suspended
375 sediments originate from outside the local fluvial systems based on the elemental ratios of Sr/Ca and Rb/Sr (Kavan et al.,
376 2017). The wind speed threshold of 10 ms⁻¹ is needed for activating local dust sources, with most of the particles captured (by
377 mass) in size bins between 2.5–10 μm. Mean (median) mass concentrations of the PM₁₀ were 6.4 ± 1.4 (3.9 ± 1) μg m⁻³, while
378 the PM_{2.5} was 3.1 ± 1 (2.3 ± 0.9) μg m⁻³ for the whole measurement period from January to March 2018. Mean PM₁₀ values
379 are comparable to background stations in Northern Europe. The highest daily aerosol concentration was 57 μg m⁻³ for PM₁₀,
380 with hourly PM₁₀ with > 100 μg m⁻³. Higher aerosol concentration occurs in late austral summer when the soil water content
381 in the upper soil layer is significantly lower than in early summer. Long-range transport of dust originating in Patagonia was
382 observed during aerosol measurements (Kavan et al., 2018). A higher proportion of long-range transported dust was found in
383 snow pits on higher elevated glaciers compared to a higher proportion of locally transported dust in lower elevated glaciers
384 (Kavan et al., 2020b). Kňážková et al. (2020) identified a redistribution of mineral material within the HLD source area in
385 Abernethy Flats, impacting the local microtopography.

386 **3.4.2.2 Marambio, Antarctic Peninsula**

387 The Marambio Base (64°14'S, 56°37'W, 198 m a.s.l.) on Marambio Island, Graham Land, Antarctic Peninsula, is a member
388 of the Global Atmosphere Watch (GAW) programme of the WMO, with personnel available year-round. This region has ice-
389 free areas and cold desert soils (Cryosols) that can be seasonally susceptible to wind erosion and weathering. The removal of
390 fine materials occurs mainly by wind action. The Finnish-Argentinian co-operative research in Marambio includes
391 measurements of ozone, solar irradiance, aerosols, and ultraviolet (UV) albedo (Aun et al., 2020). The UV Biometer Model
392 501 from Solar Light Co. (SL501) UV albedo data of 2013–2017 in Marambio were used to analyze the effects of local HLD
393 on measured snow UV albedo and solar UV irradiance and differences in simulated UV irradiances (Meinander et al., 2018;
394 data not presented here). For validating the UV albedo data, surface photos were taken regularly. The surface photos and UV
395 albedo measurements show that local dust can be detected on the snow and ice. Also, the optical dome of the SL-501 sensor
396 was found to be sandblasted by the windblown dust when returning to Finland for maintenance. These findings suggest that in
397 Marambio, local dust can decrease surface snow/ice albedo, possibly enhance the cryosphere melt, and contribute to warming
398 in the Antarctic Peninsula due to the ice-albedo feedback mechanism.

399 **3.4.2.3 McMurdo Sound, Antarctica**

400 The McMurdo Sound area of the Ross Sea region is widely recognized as the dustiest place in Antarctica, where locally sourced
401 aeolian accumulation is up to two to three orders of magnitude above global background and dust fallout rates for the continent
402 (Chewings et al., 2014; Winton et al., 2014). The area includes the McMurdo Dry Valleys (MDV), the largest ice-free area (4
403 800 km²) in Antarctica. The MDV has high but extremely variable fluxes of locally derived aeolian sand (e.g., Speirs et al.,
404 2008; Lancaster et al., 2010; Gillies et al., 2013; Diaz et al., 2020) and common aeolian landforms. Such has led to the
405 assumption that the MDV is a significant regional dust source (e.g., Bullard, 2016). Some modeling studies suggest the MDV
406 could supply large volumes of dust to a wide area of the Southern Ocean (e.g., Bhattachan et al., 2015). However, field-based
407 observations show that very little sediment is transported out of the MDV (Ayling and McGowan, 2006; Atkins and Dunbar,
408 2009; Chewings et al., 2014; Murray et al., 2013) because the valleys have already been extensively winnowed into a well-
409 developed deflation surface and large coastal piedmont glaciers form a topographic barrier, preventing aeolian sediment from
410 escaping. The dominant source of aeolian sediment in the McMurdo Sound area is the debris-covered surface of the McMurdo
411 Ice Shelf (1500 km²), with minor contributions from local ice-free headlands. This ice shelf is unusual because it has high
412 surface ablation and a continuously replenishing supply of fine-grained sediment advected from the seafloor. The sediment is
413 blown off the ice shelf by frequent intense southerly wind events, forming a visible sediment plume onto coastal sea ice. Within
414 a few km of the ice shelf, accumulation rates on sea ice are up to 55g m⁻²yr⁻¹, reducing rapidly downwind to an average of
415 1.14 g m⁻² yr⁻¹, equating to 0.6 kt yr⁻¹ of aeolian sediment entering McMurdo Sound annually (Atkins and Dunbar, 2009;
416 Chewings et al., 2014). Some sediment is transported at least 120 km from the source and could travel much farther,
417 contributing iron-rich dust to the Ross Sea (Winton et al., 2014). Coastal areas and lowland parts of the MDV are on the

418 threshold of climatically driven change with observed increases in ablation and seasonal meltwater flow incising into
419 permafrost (Fountain et al., 2014), suggesting the dust potential of McMurdo Sound and MDV could rapidly change. The
420 McMurdo Dry Valleys (4800 km²) is estimated to best fit Category 3 (source with unknown activity, Table S1). The McMurdo
421 Ice Shelf ‘debris bands’ are estimated to best fit Category 2 (moderately active source).

422 **3.4.2.4 Schirmacher Oasis, East Antarctica**

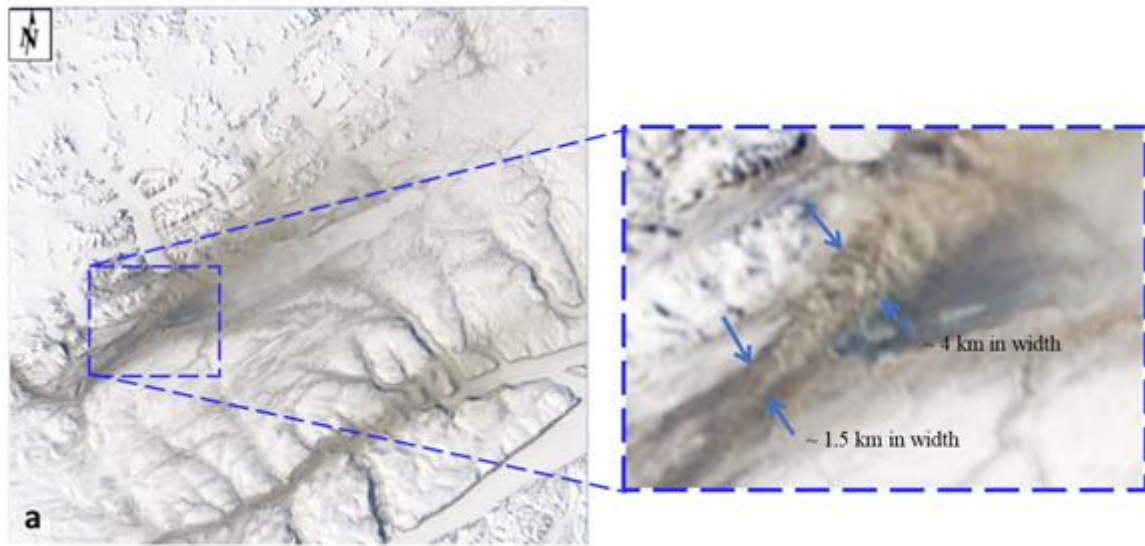
423 The Schirmacher Oasis (70° 45′ 30″ S, 11° 38′ 40″ E) is approximately 80 km from the coast of Lazarev Sea, Queen Maud
424 Land, East Antarctica. The oasis is an ice-free area of over 35 km² with typically hilly relief. The oasis and surrounding
425 area have been explored since the early 1960s. However, no systematic studies of dust on local ice and snow have been done.
426 Most of this region’s dust is assumed to be formed with the soils blown in the air because of strong winds. Human activity
427 produces some of the dust in this region: The oasis shelters four bases, which use diesel oil and petrol to supply heat and
428 transport operations. Two airports are nearby, which operate during the summer—lasting from late November to late February.
429 In December 2019, we collected the snow samples on eleven sites near the local ice roads, bases, and airports. These data will
430 contribute to our future study.

431 **3.4.3 Canada**

432 **3.4.3.1 Lake Hazen, Ellesmere Island**

433 Evidence of dust activity in Canada has been reported, e.g., in the prairie, crater lake, and river valley environments (e.g.,
434 Wheaton et al., 1990; Neuman, 1990; Wheaton, 1992; Hugenholz and Wolfe, 2010; Fox et al., 2012). Satellite observations
435 of high-latitude dust events over water are relatively common (see, for example, Bullard et al., 2016). Whether directly
436 concerning explicit plume remote sensing or indirectly regarding plume deposition, the detection of such events has remained
437 largely unreported. Ranjbar et al. (2021) recently reported detecting a drainage-flow induced dust plume over (frozen) Lake
438 Hazen, Nunavut, Canada, using a variety of remote sensing techniques (Lake Hazen is the Arctic’s largest lake, by volume, at
439 81.8°N latitude in the northernmost portion of Ellesmere Island). Figure 6 shows a true-color georeferenced RGB MODIS-
440 Terra image acquired on 19 May 2014 at 19:50 UT (15:50 EDT) over Lake Hazen. The authors employed MISR stereoscopy,
441 CALIOP, and CloudSat vertical profiling, as well as MODIS thermal IR techniques, to identify and characterize the plume as
442 it crossed over a complex springtime terrain of snow, ice, and embedded dust. While limited by the lack of dedicated dust
443 remote sensing algorithms over snow and ice terrain, the plume characterization boded well for developing systematic,
444 satellite-based, high-latitude dust detection approaches using current and future generations of aerosol and cloud remote
445 sensing platforms.

446



447

448 **Figure 6. MODIS-Terra satellite image on 19 May 2014 at 19:50 UTC (a) True-color image: MODIS channels 1 (620–670nm), 3**
 449 **(459–479 nm), and 4 (545–565 nm) were loaded into the RGB channels of the display. The sub-image is a zoom of the most discernible**
 450 **part of the plume (outlined by the blue broken-line square).**

451 **3.4.3.2 Kluane Lake, Yukon**

452

453 Within the St. Elias Mountain range at the north end of the Pacific Coast Range on the continental side of the Yukon Territory
 454 lies the Kluane Lake region (KLR), which contains Łhù'àn Mân' (Kluane Lake) (no. 50 in Fig. 1). The lake is fed primarily
 455 from the meltwater of the Kaskawulsh glacier down the A'äy Chù (formally the Slims River) and snowmelt from the
 456 surrounding regions in the springtime. This seasonal discharge has, in recent history, been known to be highly variable as the
 457 glacier terminates at the fork of two distinct watersheds—one draining into the Bering Strait through the Yukon River and the
 458 other into the Gulf of Alaska—supplying the two watersheds' inconstant ratios. In 2016, most of the glacier's discharge was
 459 diverted to the Gulf of Alaska in an intense discharge event, dramatically decreasing the Łhù'àn Mân's water levels and
 460 increasing the dust emission potential from the A'äy Chù (Shugar et al., 2017). This drastic change makes the KLR an excellent
 461 natural laboratory for investigating the impact of pro-glacial hydrology on dust emission potential under past and future
 462 climates. Research was conducted in the early 1970s in this same valley as a comprehensive set of dust flux measurements as
 463 part of several publications (Nickling, 1978; Nickling and Brazel, 1985). Nickling (1978) concluded that there is a dynamic
 464 relationship between soil moisture (driven by precipitation and nighttime radiation insolation) and wind, resulting in periodicity
 465 of dust emissions from the valley in all but the mornings throughout the snow-free seasons. Within a more recent study by
 466 Bachelder et al. (2020), soil and aerosol samples were collected within the Ä'äy Chù delta, where air quality thresholds were
 467 exceeded, indicating a negative impact on local air quality throughout May. Notably, daily particle size distributions of PM10

468 were very fine (mode of 3.25 μm) compared to those measured at more well-characterized, low-latitude dust sources.
469 Moreover, mineralogy and elemental composition of ambient PM₁₀ were found to be enriched in trace elements (e.g., As and
470 Pb) compared to dust deposition, bulk soil samples, and fine soil fractions ($d < 53 \mu\text{m}$). Finally, through a comparison of the
471 elemental composition of PM₁₀, dust deposition, and fine and bulk soil fractions, as well as meteorological factors measured,
472 Bachelder et al. (2020) propose that the primary mechanisms for dust emissions from the Ä'äy Chù are the rupture of clay
473 coatings on particles and the release of resident fine particulate matter.

474 **3.4.4 Denmark and Sweden**

475 In Denmark, large areas with severe wind erosion have been documented (Kuhlman, 1960). Published literature on the activity
476 of dust sources in Denmark is rare; some documentation is only in Danish. On 23 April 2019, a dust plume from Denmark's
477 west coast, with dust plumes from Sweden 12 km long Mellbystrand around the mouth of the Lagan River (no. 51 in Fig. 1);
478 Poland could be observed in Meteosat-11 Dust RGB and Natural Colour images, 23 April 12:30 UTC. These dust plumes were
479 observed to travel to the North Sea (Meteosat, 2019). The source in Denmark appears to be from Holmsland Dunes (no. 15 in
480 Fig. 1). Other potential dust sources in Denmark include, e.g., the Råbjerg mile (no. 1 in Fig. 1), the largest moving dune in
481 Northern Europe with an area of around 2 km² (Doody et al., 2014), located between Skagen and Frederikshavn. Råbjerg Mile
482 moves at approximately 15 meters per year due to wind and has moved around 1.5 km further east in the last 110 years. The
483 drifting sand is not considered to be transported very far. In general, dust storms in Denmark are considered small, and locally
484 based dust storms can be expected when farmers prepare the arable soils in spring, creating dust in case of a very dry April
485 month. In Tilviden, flying sand took over (after King Frederik II cut the oak trees for building ships in 1600). Also, a regional
486 soil and sand event in Denmark, reportedly common in April, was recently documented between Mejrup and Holtebro on 6
487 April 2021 (Television Midtvest, 2021; not identified in Fig. 1; coordinates are estimated as 56°23'N, 8°41'E). This location
488 between Mejrup and Holtebro remains to be marked as a potential dust source for future observations. The event was observed
489 over roadways in several parts of the region, reducing visibility due to a long period without rain and with strong winds for >
490 24 hours, causing the soil to blow off the harrowed fields.

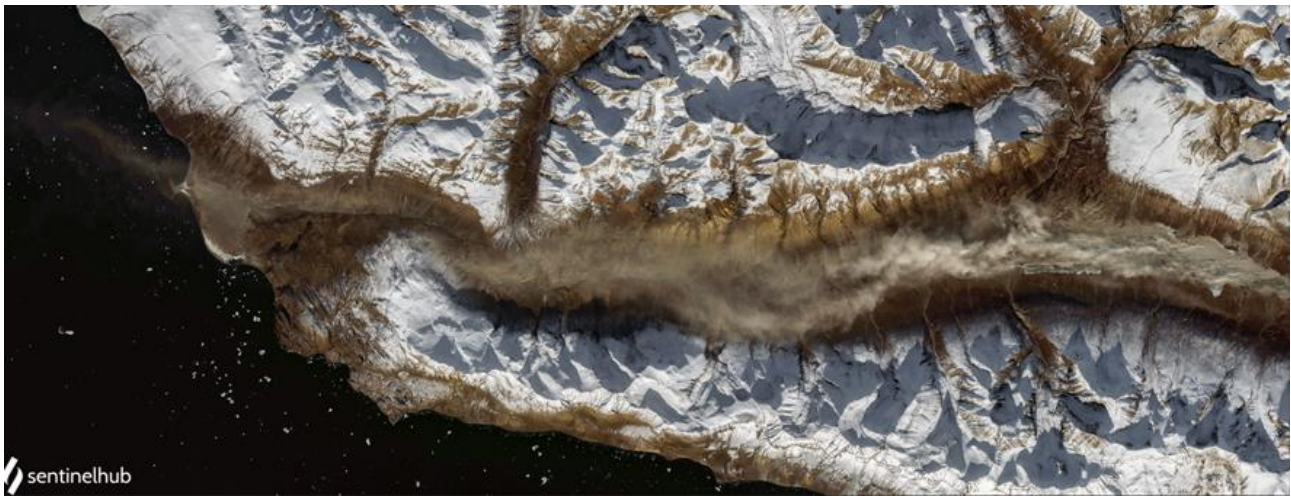
491 **3.4.5 Greenland**

492 Greenland's ice-free areas have long been identified as locally important dust sources (Hobbs, 1942), with dust storms
493 described as reaching >100 m high (Dijkmans and Törnqvist, 1991). These storms can cause the darkening of the Greenland
494 Ice Sheet by deposition, which may affect albedo and rates of ice melt (Wientjes et al., 2011; McCutcheon et al., 2021).
495 Potential dust source areas in Greenland are mapped in the recently issued global dust atlas by A. Vukovic (UNCCD, 2021).
496 Dust input to soils and lakes may also have substantial ecological impacts (Anderson et al., 2017). Bullard and Mockford
497 (2018) investigated the seasonal and decadal variability of dust emissions in southwest Greenland and presented the first long-
498 term assessment of dust emissions. Dust emissions occur all year but peak in spring and early autumn. The evidence linking
499 increased dust emissions to preceding jökulhlaup (a type of glacial outburst flood) events is inconclusive, requiring further

500 exploration. The decadal record confirmed that dust-storm magnitude may have increased from 1985 to the 1990s (Bullard
501 and Mockford, 2018). Amino et al. (2020) also showed that dust deposition on the southeastern dome in Greenland has
502 increased in recent decades. They link this increase to dust emissions in coastal Greenland, where snow cover is decreasing.
503 However, further work is needed to characterize the magnitude of dust events at the source and how their emissions are
504 changing. Bullard and Mockford (2018) also presented preferential dust-event pathways from Kangerlussuaq, indicating that
505 most events travel toward the Davis Strait and the Labrador Sea, where the dust might impact boundary layer of mixed-phase
506 clouds (Murray et al., 2021).

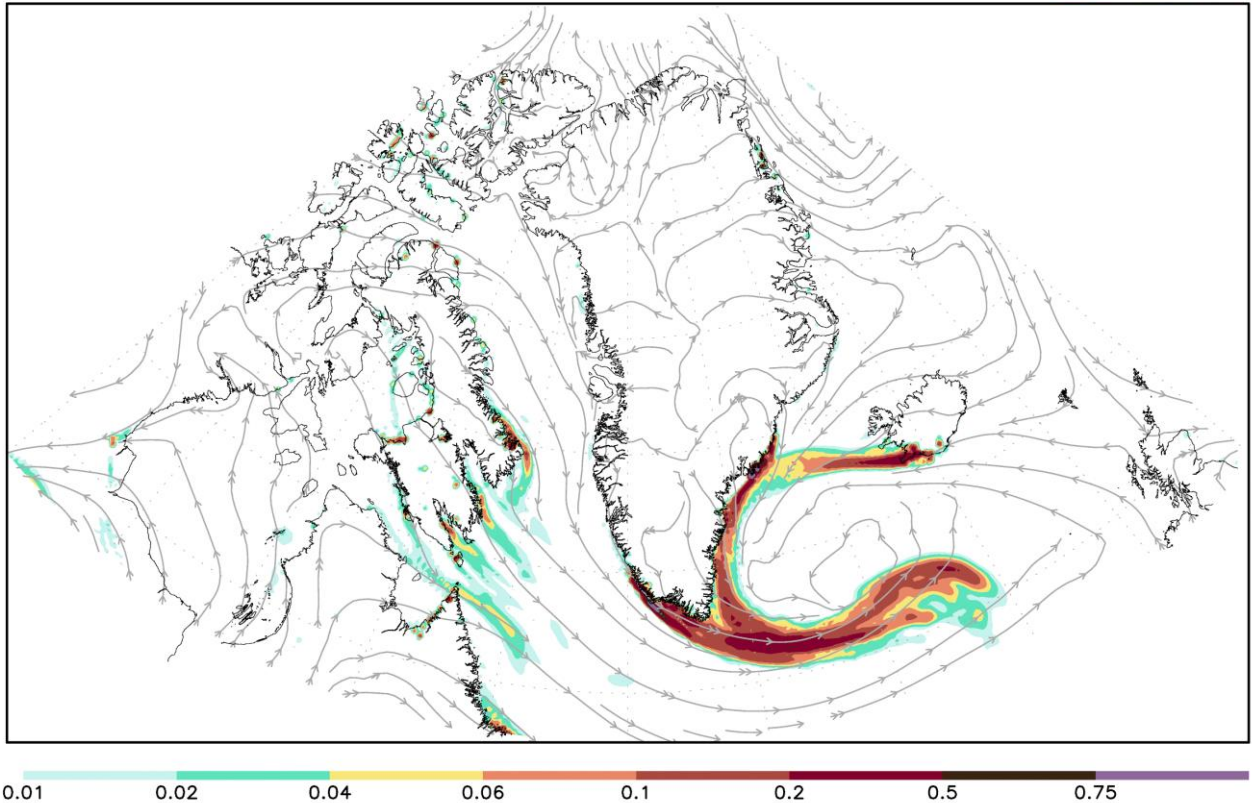
507 Modern satellite remote sensing methods can detect dust storm events in Greenland’s different valleys and coastal areas. The
508 new HLD sources identified in this study based on satellite observations are in Supplementary Table S3. Figure 7 illustrates
509 one such dust storm episode on the Nuussuaq Peninsula, Greenland, on 1 October 2020 (Markuse, 2020). One example of
510 DREAM regional-scale modeling of atmospheric transport of dust from Greenland potential dust sources is demonstrated in
511 Figure 8 (animation available in Supplementary), where the DREAM circumpolar prediction experiment example shows the
512 predicted surface dust concentration for 4 November 2013 and Icelandic volcanic desert dust to reach Greenland, as discussed,
513 e.g., in Meinander et al. (2016).

514



515

516 **Figure 7. High-latitude dust storm on the Nuussuaq Peninsula, Greenland – 1 October 2020 (Markuse, 2020; cc-by-2.0.2020)**



517

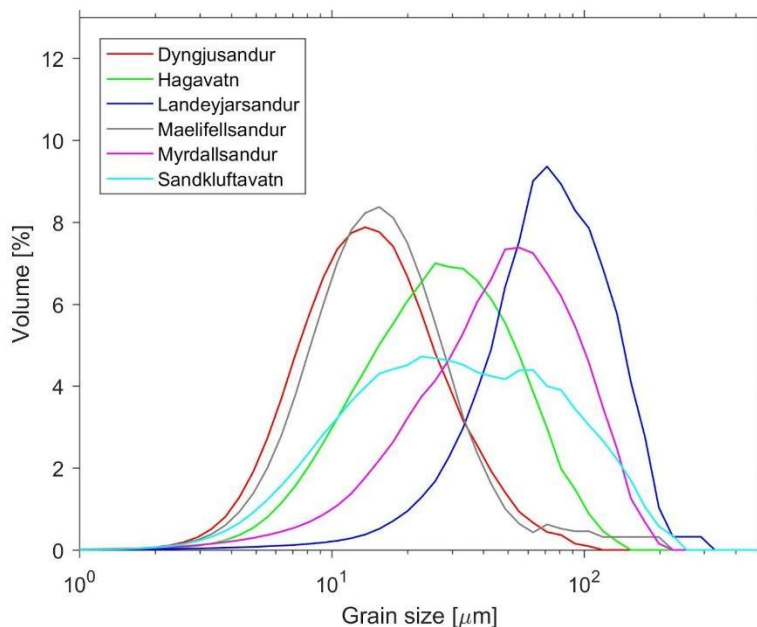
518 **Figure 8. DREAM model predicted dust load for 4 November 2013 (animation available in Supplementary).**

519

520 **3.4.6 Iceland**

521 Iceland has been recognized for a while as a potentially important dust source. In our collection, 13 new sources in Iceland
522 were included (Table S2), compared to previous sources, in which eight Icelandic dust hot spots were identified (Arnalds et
523 al., 2016). Sandkluftavatn, Kleifarvatn, Skafta jökulhlaup deposits and other areas have also been found to produce large
524 amounts of dust (Dagsson-Waldhauserová et al., 2019). In recent years, increased dust activity has been reported in Flosaskard
525 and Vonaskard (Gunnarsson et al., 2020). These dust hotspots cover almost 500 km^2 , while deserts are over $45\,000 \text{ km}^2$
526 (Arnalds et al., 2016). Most of the dust hotspots are near glaciers: glacial floodplains, old lakes, jökulhlaup (a type of glacial
527 outburst flood) deposit areas, or sandy beaches. Glacio-fluvial plains receive a massive amount of unconsolidated silty material
528 during the melting of nearby glacial regions.

529 New dust sources with the number of events are identified here and presented based on satellite image observations from 2002
530 to 2011 (Supplementary Table S2), suggesting that Iceland's entire southern coast could be considered one source. However,
531 previous results on Icelandic dust suggest that nearby locations may have different particle characteristics (Fig. 9). Therefore,
532 each source must be studied independently. For example, the grain size distribution curves of the samples from Dyngjúsandur,
533 Hagavatn, Landeyjarsandur, Maelifellsandur, Myrdallsandur, and Sandklúftavatn showed generally unimodal distributions
534 with a rather diverse character (average diameters ranging from 19.8 to 97.7 μm , Fig. 9). Richards-Thomas et al. (2021)
535 identified a range in particle diameter between 0.4 μm and 89 μm , with the medians (d_{50}) of the distributions from 12 to 25
536 μm). Some hotspot particles are bimodal with peaks at 2 μm and 30 μm and a more significant proportion of the sample within
537 the silt-size range.



538

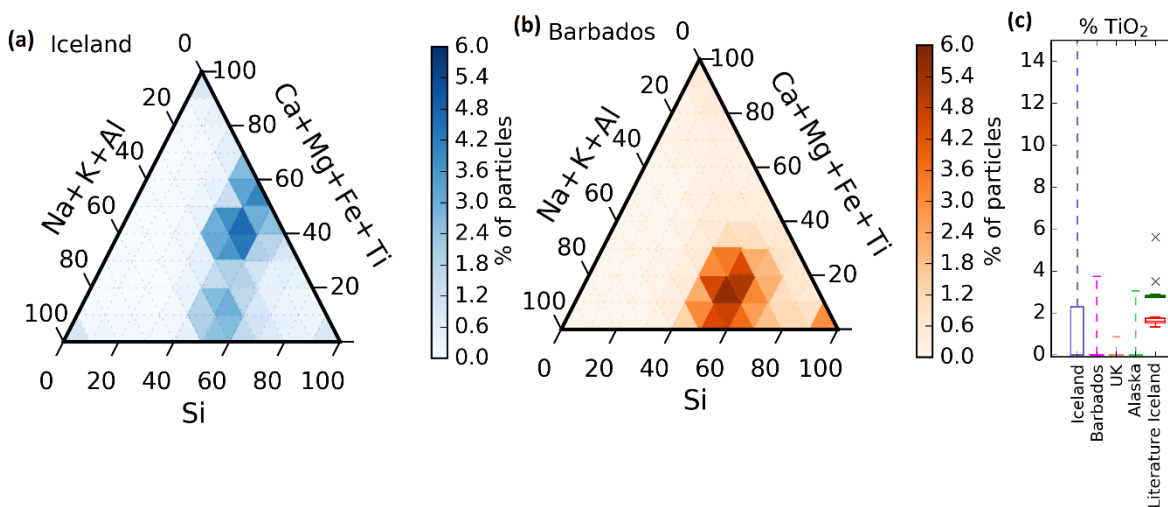
539 **Figure 9.** Grain size distributions of samples from Icelandic source areas (redrawn from Varga et al., 2021)

540 Icelandic dust particles have different shapes, lower densities, higher porosity, increased roughness, and darker colors than
541 other desert dust (Butwin et al., 2020; Richards-Thomas et al., 2021). Those greater than 20 μm retain the volcanic
542 morphological properties of fresh volcanic ash. Dust and fresh volcanic ash particles less than 20 μm are crystalline and blocky.
543 Icelandic dust particles contain amorphous glass, large internal voids, and copious dustcoats comprised of nano-scale flakes.
544 The amorphous basaltic material is mostly aluminosilicate glass ranging from 8 wt% (Hagavatn hotspot) to 60–90 wt%, with
545 relatively high total Fe with higher Fe solubility and magnetite fraction than low-latitude dust (10–13 wt%, Baldo et al., 2020).
546 PM10 concentrations measured during severe Icelandic dust storms well exceeded 7000 $\mu\text{g}\text{m}^{-3}$ (Dagsson-Waldhauserová et

547 al., 2014, 2015; Mockford et al., 2018). Submicron particles contribute with high proportions (> 50%) to PM10 mass
 548 concentrations and number concentrations (Dagsson-Waldhauserová et al., 2014, 2016, 2019). Aeolian transport of 11 t of
 549 dust over one meter transect was measured during the severe dust/ash storm in 2010, when grains > 2 mm were uplifted
 550 (Arnalds et al., 2013).

551 As well as differences in Icelandic dust sources, the chemical composition of the aircraft-collected Icelandic dust particles has
 552 a different chemical signature than, e.g., airborne Saharan dust particles transported to Barbados (Sanchez-Marroquin et al.,
 553 2020). This difference can be observed in Figs. 10a and 10b, where the chemical composition of most Icelandic dust particles
 554 falls in a different area of the chemical composition ternary diagram than the Saharan dust particles from Barbados. One of the
 555 most prominent differences between these types of dust is Ti's presence in ~ 30% of the Icelandic dust particles, while this
 556 element is almost absent in the Saharan dust particles and dust collected elsewhere, shown in Fig. 10c. Furthermore, the
 557 chemical composition of the aircraft-collected Icelandic dust is consistent with surface scooped samples of dust or volcanic
 558 ash from Iceland. Moreover, a droplet freezing-based assay confirmed that the sampled Icelandic dust has a high ice-nucleation
 559 ability and can influence the radiative and lifetime properties of clouds containing water and ice.

560



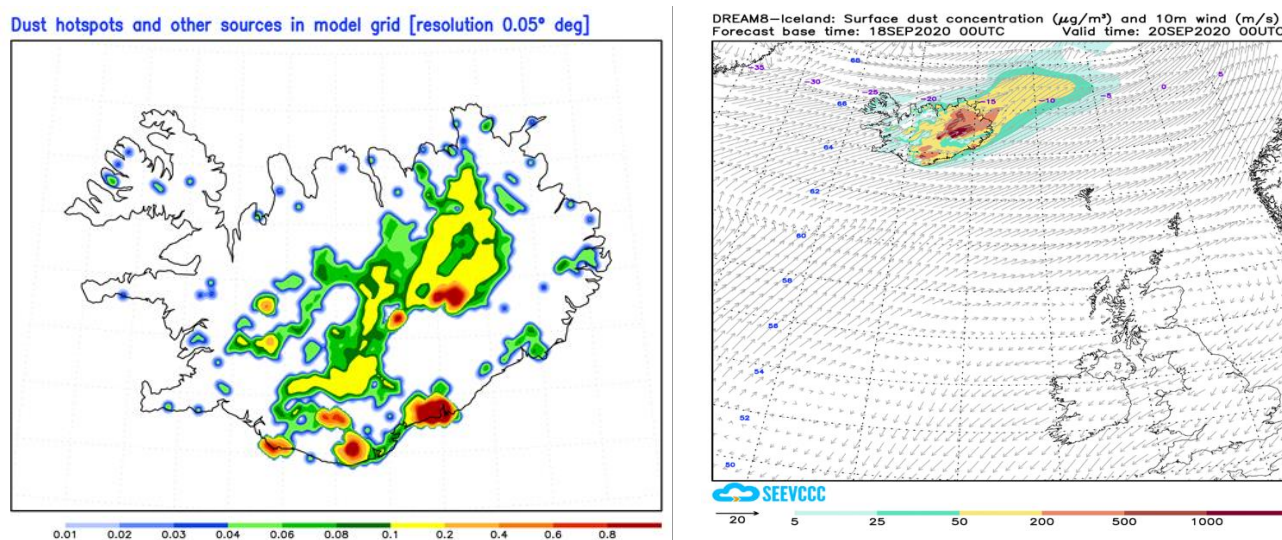
561

562 **Figure 10.** Ternary graphs of the chemical composition of Icelandic dust particles (a) and Saharan dust particles collected in
 563 Barbados (b). Each graph contains a heat map with the percentage of dust particles in each sample compositional bin. The chemical
 564 composition of each aerosol has been recalculated from the weight percentages given by the SEM software, excluding elements that
 565 are not Si, Al, Fe, Mg, Ca, Na, K, Ti, Mn, and P. (c) The box represents particles in the Q3 percentile of the percentage of the
 566 composition of Ti in all the dust particles in each sample (Icelandic dust, Saharan dust collected in Barbados, dust collected in the
 567 UK, and dust collected in Alaska). The whiskers represent the composition of all particles between the median plus and minus two

568 standard deviations. The data has been compared with the Ti weight percentage of different Icelandic dust and ash samples from
569 the literature. (Figure extracted from the Supplementary Material of Sanchez-Marroquin, 2020).

570 No direct observations or measurements of the new sources were available. Instead, two model computations are presented for
571 Iceland because of the lack of observations and complexity of the AOD interpretation in polar and subpolar regions. Without
572 high uncertainty of direct measurements, the importance of the HLD modeling rises; models validated over better-observed
573 regions may become an important or primary source of information. Results using the DREAM model, with a horizontal
574 resolution of ~3.5 km, were used here to resolve the heterogeneous and small-scale character of the Icelandic dust sources
575 (Fig. 11). As the first operational numerical HLD model, DREAM-ICELAND predicted the Icelandic dust for the example
576 case of 18 September 2020 (Fig. 11).

577
578



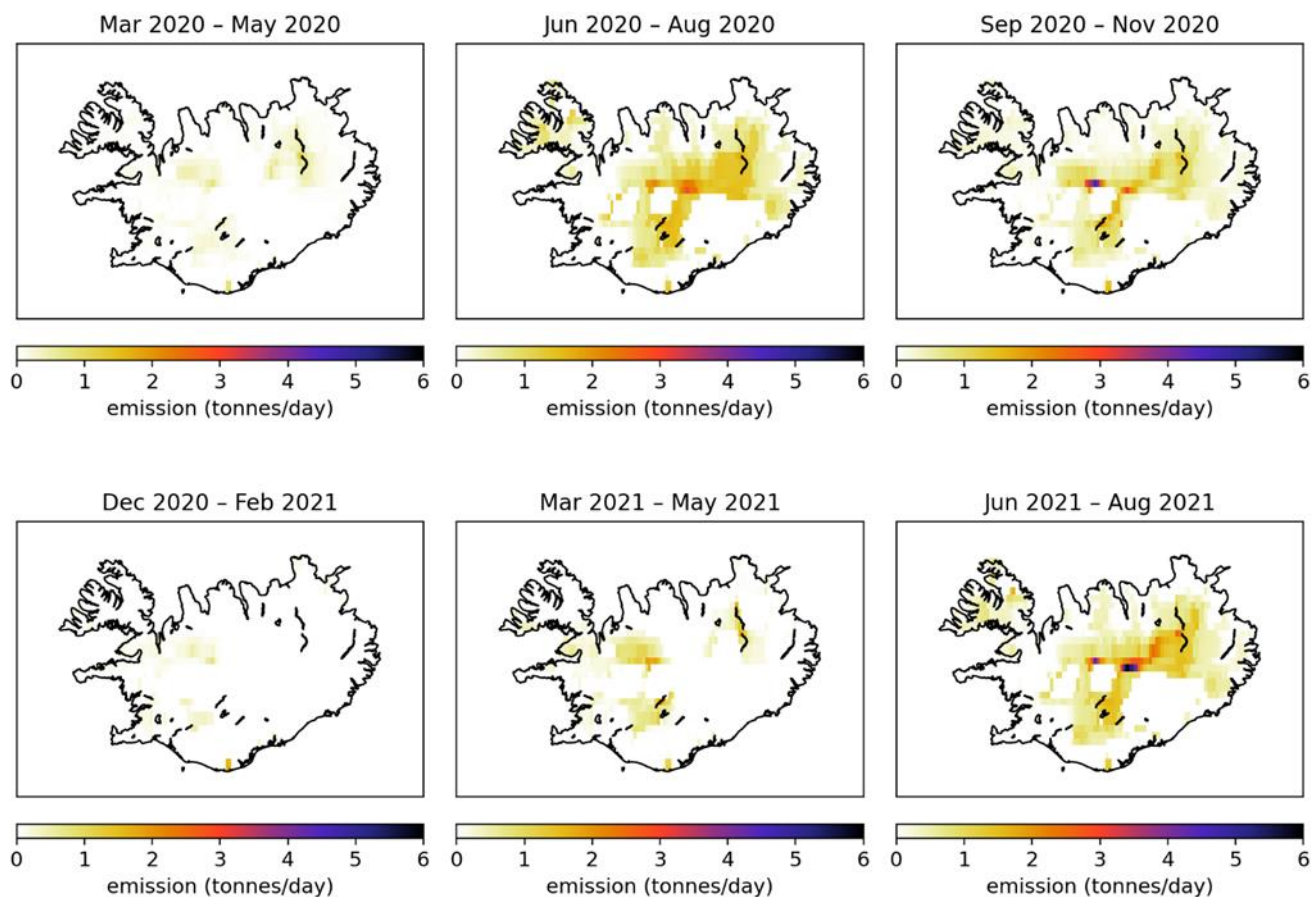
579

580 **Figure 11. Left panel: dust sources in DREAM-ICELAND model grid with areas vulnerable to erosion and containing hot spots**
581 **(Arnalds et al., 2016). Right panel: An example of the operational Icelandic dust surface concentration forecast for 18 September**
582 **2020 (available at the Republic Hydrometeorological Service of Serbia site, <http://www.seevccc.rs/?p=8>).**

583

584 In Figure 12, dust emissions in Iceland are presented in three-months periods for March 2020–August 2021. The modeled
585 results clearly show the seasonal nature of the dust sources. The summer season (June–August) appears to be the strongest
586 dust season. However, there are also dust emissions in wintertime with snow-covered land surfaces, according to observations
587 of dust events during snowfall (e.g., Dagsson-Waldhauserová et al., 2015). The 2021 summer season in these modeled emission

588 results appears in the same locations as summer 2020 but with more severe emissions in the highlands in 2021, agreeing with
589 the field observations in Vatnajökull national park during the HiLDA measurement campaign in the 2021 season
590 (<https://gomera.geo.tu-darmstadt.de/wordpress/>), where the most severe dust events were measured.



591
592 **Figure 12. SILAM modeled dust emissions (tonnes/day) in Iceland for three months periods in March 2020 – August**
593 **2021.**

594
595 **3.4.7 Russia**

596 The Russian Arctic and subarctic are the most relevant regions connected to the HLD sources. In these territories, atmospheric
597 dust is produced due to burning gas (Novy Urengoy is named the gas capital of Russia) and forest fires (especially in Siberia;
598 see MODIS or Sentinel images for Novy Urengoy on 3-8 August 2021), dusting of abandoned and non-reclaimed heaps).
599 Wind erosion is followed by vegetation destruction from gas and oil extraction, especially in Western Siberia. Some Russian

600 sources included in our collection (e.g., no. 7 and 8 of Fig. 1) could be identified as dust sources on the periphery of HLD and
 601 low-latitude source regions. Source no. 7 of Fig. 1 is the Altai Mountains. Some parts of these territories are covered by
 602 permafrost, where winter lasts for 5–6 months. From October, in lower mountains (less than 1000 m a.s.l.), and from
 603 September, in higher mountains (more than 1500 m a.s.l.), a stable snow cover persists. The mean daily air temperature during
 604 winter within the lower, middle, and higher mountains is -21°C , -29°C , and below -30°C , respectively. Source no. 8 is in
 605 Central Kazakhstan. From late December to early March, a stable snow cover from 5 cm to 30 cm occurs within plains and up
 606 to 50 cm within hollows. Periods of snow cover and thaw correspond to transitions of the mean daily temperature of air through
 607 0°C , which, on average, are the 7 November and 23 March plus/minus 10–12 days. From early January to late February, the
 608 air's mean daily temperature can be as low as -20°C . Soil Atlas of the Northern Circumpolar Region
 609 (<https://esdac.jrc.ec.europa.eu/content/soilatlas-northern-circumpolar-region>) covers all land surfaces in Eurasia and North
 610 America above the latitude of 50°N . Thus, these territories are considered high-latitude.

611 3.4.7.1 Western Siberia, Altai Mountains, and Central Kazakhstan

612 In the most widespread undisturbed soils (Gleysols, Phaeozems, Podzols, Retisols, and Stagnosols) in Western Siberia
 613 (Semenkov et al., 2015a, 2015b)—the vastest plain in the world—mineralogical and elemental composition (Supplementary
 614 Table S6) were studied using X-ray diffractometry, X-ray fluorescence spectrometry, ICP-MS, ICP-AES, and content of total
 615 organic carbon (TOC), as reported in detail in (Semenkov et al., 2019; Semenkov and Koroleva, 2019; Semenkov and
 616 Yakushev, 2019). At locations no.7 and no. 8 of Fig. 1 (Table 4), the concentration of N-containing substances, pH values,
 617 dust content and dust deposition rate were measured in snow in winter from 2009 to 2019 (Koroleva et al., 2016, 2017;
 618 Semenkov et al., 2021; Sharapova et al., 2020).

619 **Table 4. Major ions (mg/L), pH value, dust content (mg/m^2 in snow), and deposition rate ($\text{mg}/\text{m}^2/\text{d}$) during winter at HLD sources**
 620 **no. 7 and no. 8 in Fig. 1.**

HLD no	M	SD	Me	Min	Max	N
No. 7						
Dust content mg/m^2	316	439	112	0	1542	30
NH_4^+ mg/L	0.75	0.98	0.30	0	3.60	43
NO_2^- mg/L	0.015	0.019	0.008	0	0.08	107
NO_3^- mg/L	2.3	3.4	1.4	0	20.4	118
pH	6.6	0.8	6.7	4.1	8.4	129

No. 8						
Dust deposition rate mg/m ² /d	1.67	1.67	1.08	0.05	6.6	38
NH ₄ ⁺ mg/L	0.20	0.009	0.10	0	1.34	682
NO ₂ ⁻ mg/L	0.027	0.007	0	0	0.61	127
NO ₃ ⁻ mg/L	0.47	0.02	0.19	0	3.93	697
pH	6.1	0.02	6.1	4.6	8.0	585

621 M – mean, max – maximum, Me – median, min – minimum, N – number of observations, SD – standard deviation

622

623 3.4.7.2 Murmansk region: Apatity, Kirovsk, Kovdor

624 Large amounts of displaced rock have been breaking the balance of geological emissions of gas and dust from mining, dumps,
625 and tailing pits (e.g., Csavina, et al. 2012). Over 150 Mt of industrial wastes are disposed of in the Murmansk region annually,
626 achieving about 8 Gt (Supplementary Table S7). The dusting of processing tailing is one of the main sources of air pollution
627 resulting from suspended matters near the mining enterprises. About 30% of all suspended matter is released from the mining
628 enterprises into the atmosphere due to wind-induced dusting of beaches and slopes of tailings dumps. Elevated concentrations
629 of suspended matter are registered every summer in Apatity’s atmosphere. Dust storms from technogenic dust sources of the
630 mining industry on the Kola Peninsula are presented, e.g., in Baklanov and Rigma (1998), Baklanov et al., (2012), and Amosov
631 and Baklanov (2015).

632 3.4.7.3 Tiksi

633 Aerosol characterization was performed at the Hydrometeorological Observatory (HMO) Tiksi (71.36N; 128.53E) on the coast
634 of the Laptev Sea in Northern Siberia from 2014 to 2016 (Popovicheva et al., 2019). FTIR analyses of functionalities and ionic
635 and elemental components provided insight into the dust source-influenced and season-dependent composition of East Siberian
636 Arctic aerosols. Analysis of wind and aerosol pollutants roses, with long-range transport analysis, helped identify the dust
637 sources at Tiksi, demonstrating impacts from lower latitudes or local emissions from the adjacent urban Tiksi area. In warm
638 periods, Na⁺, Cl⁻, K⁺, and Mg²⁺ are found to be the major ions in the sea-salt aerosols, which are ubiquitous in the marine
639 boundary layer, significantly impacting the dust concentrations in the coastal region. However, Cl⁻ and K⁺ could also originate
640 from biomass burning during the warm period. Ammonium is mainly produced by the soil and emission from biota and the
641 ocean, commonly found in the form of (NH₄)₂SO₄ and NH₄Cl. Like sulfates, ammonium is influenced by regional sources of

642 secondary aerosol formation and transport. Bands of carbonates CO_3^{2-} (at 871 cm^{-1}) and ammonium NH_4^+ (3247 cm^{-1}) indicate
643 the dominance of dust carbonates in the natural inorganic aerosol. Also, S, Fe, Na, Al, Si, Ca, Cl, K, Ti, Mn, Co, Cu, Zn, Ga,
644 Sr, Ba, Hg, and Pb were detected in the background dust, with sulfur displaying the highest concentration, followed by Fe, Na,
645 and Al.

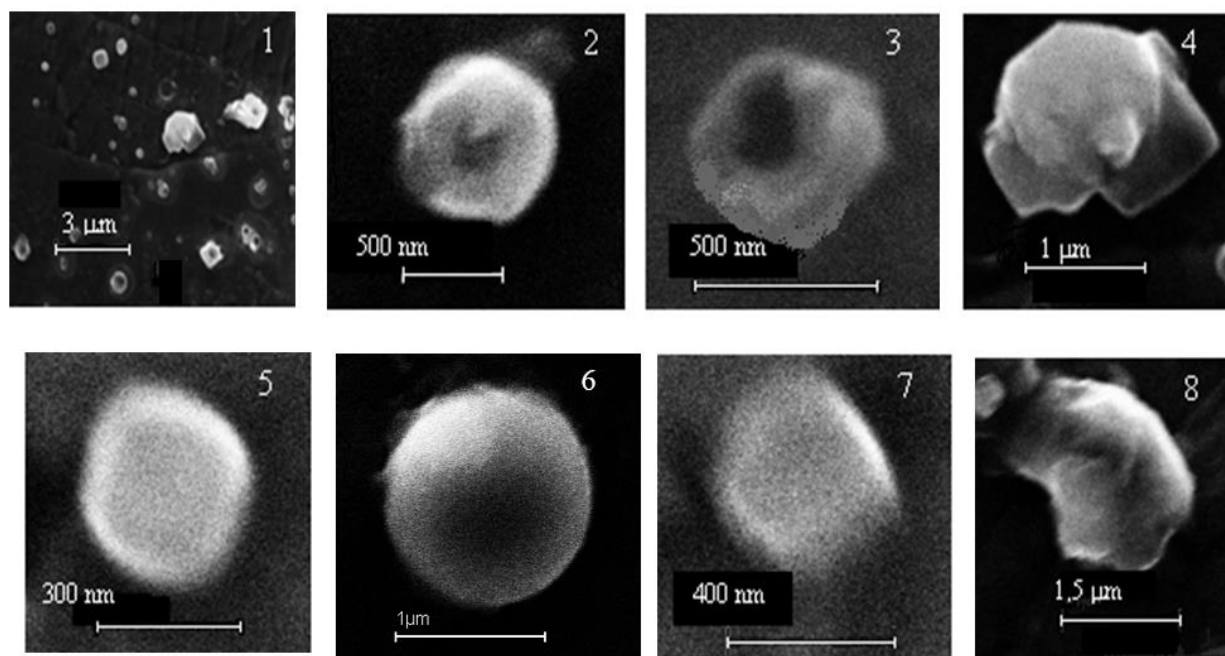
646 According to individual particle analyses by SEM-EDX, during the summer and autumn, when the wind comes from the
647 southwest and air masses arrive from the ocean, aerosol particles demonstrate a large variability in shapes, sizes, and
648 composition (Fig. 13.1). Elemental composition is characterized by a dominant weight percentage of C, K, Na, Cl, O, and Fe.
649 The distribution of elements over particles is heterogeneous, with greater amounts of Cl, K, and Na than C and O in around
650 50% of particles, indicating that background aerosols contain soil, salts, minerals, and carbonaceous compounds. Group Na-
651 rich with dominant Na and Cl is the most abundant at 32.5%, originating from sea spray near the ocean (Fig. 13.2). The other
652 particles contain small amounts of K, Ca, and Mg from seawater impurities, as well as S, gained through acid displacement.

653 The second most abundant group of individual particles is Group K-rich at 28.8%, dominated by K and Cl, which are not of
654 marine origin because the concentration of NSS K^+ ions significantly exceeds K's possible concentration in SSA. Instead,
655 Group K-rich particles are of natural mineral sylvite (KCl), transformed from genuine ones because the average weight ratio
656 of K/Cl was found to be equal to 3.3—significantly higher than 1.1—in sylvite (Fig. 13.3). KCl is water-soluble and may react
657 in a polluted atmosphere. The variation of wt% of K vs. Cl shows the lack of Cl compared to genuine sylvite and the formation
658 of complex chemical compounds K_xCl_y with various K and Cl atoms. A representative micrograph of particles in Group K-
659 rich demonstrates the reacted sylvite in Fig. 13.3, with slight damage by an electronic beam that can prove the presence of
660 nitrates that were easily evaporated during EDX analyses. A part of Group Na-rich and K-rich, 20% and 5%, respectively,
661 contains Na, Cl, and K and is assumed to be particles comprised of natural sylvite from alternative layers of halite and sylvite
662 ($n\text{NaCl} + m\text{KCl}$) (Fig. 13.4). They have distinctive mineral shapes and are stable regarding evaporation by an electron beam.
663 About 14.8% of individual particles composed of Group Organic made almost exclusively from C and O. These particles are
664 roughly spherical or liquid-like shaped (Fig. 13.5): Around half contain only C and O, being probably secondary organic
665 aerosol from the biogenic source; the other half come from the seawater of the Arctic Ocean, as demonstrated by trace amounts
666 of Na, Cl, and Mg. The oxidation of volatile organic compounds, humic-like substances (HULIS) in the marine environment,
667 perhaps contributes to observed organic matter.

668 Finally, a few biogenic particles such as pollen, spore, algae, bacteria, and plant or insect remnants are found in natural aerosols,
669 indicated by the specific shape and presence of K, S, Si, and Cl with C. The remaining groups—Fe-rich (14.4%), Ca-rich
670 (6.4%), and Al, Si-rich (3%)—are representative of atmospheric dust derived from the Earth's crustal surface. Dust particles
671 have solid irregular shapes of round and euhedral morphology. Analyses of the soil sample taken near the CAF showed stony
672 material with minimal fertile ground cover. EDX analyses demonstrated 27.7 and 9.8 wt% of Si and Al, 46 and 10.6 wt% of
673 O and Fe, respectively, and 3.5 w% of K in various Fe,K—aluminosilicates containing small additives (less than 1.7 wt%) of

674 Na and Mg. Since the tiny dust of stony soil may be easily dispersed into the atmosphere by wind, we assume that Group Al,
675 which is Si-rich, and around half of Group Fe-rich, is composed of Fe,K—aluminosilicates (Fig. 13.6). Group Fe-rich
676 containing Fe, Ni, Ca, and Si is composed of soil particles of iron-nickel ore (Fig. 13.7). Finally, Ca carbonates and sulfates
677 with Ca, C, S, and O are found in Group Ca-rich (Fig. 8.8), according to the observation of Ca^{2+} , CO_3^{2-} , and SO_4^{2-} ions described
678 above. With aluminosilicates, they are most likely windblown dust.

679
680



681

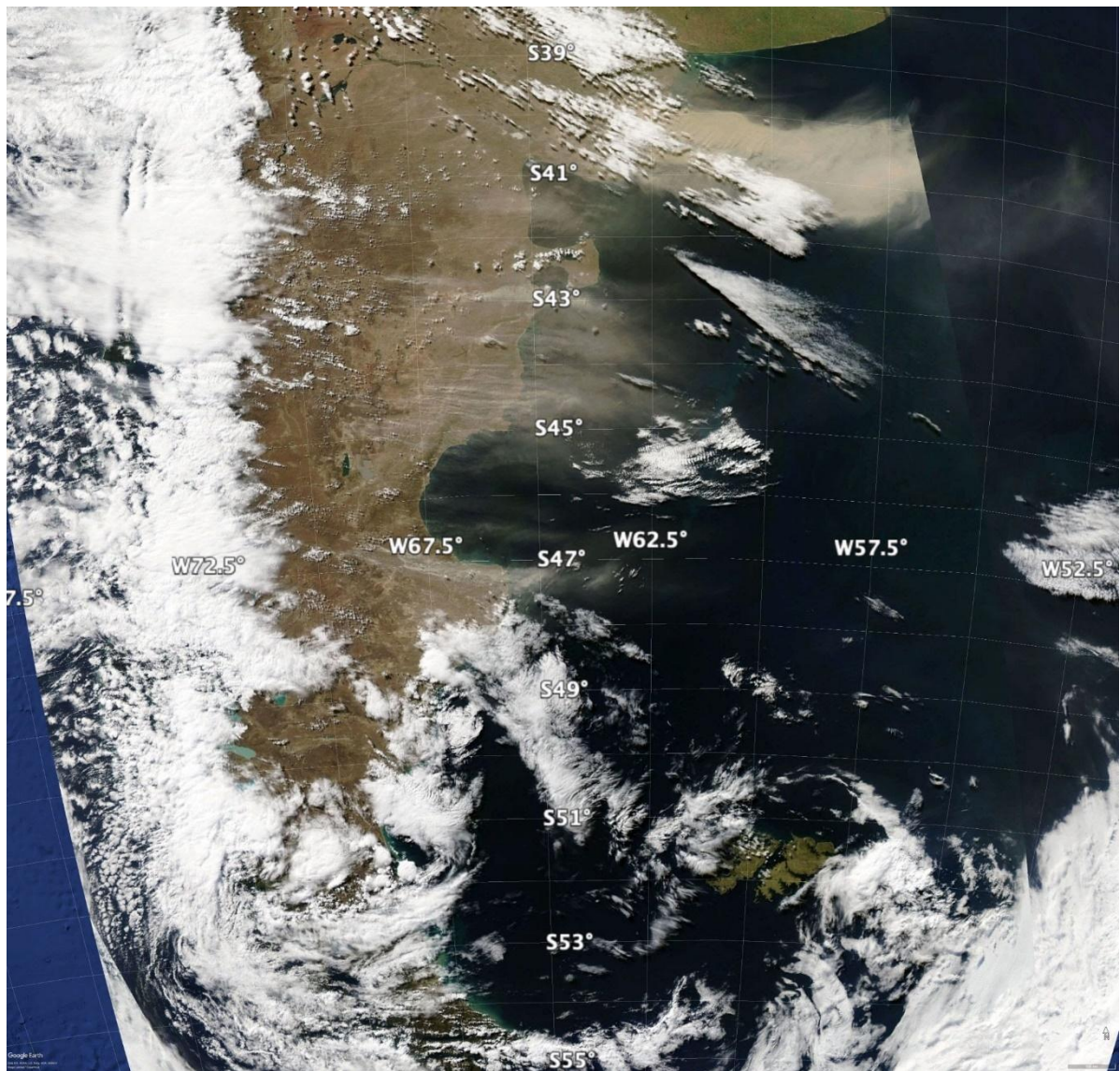
682 **Figure 13. 1. Panorama and representative micrographs of natural background aerosols at HMO Tiksi; 2. reacted sea salt NaCl in**
683 **Group Na-rich; 3. reacted sylvite KCl and 4. sylvinite (nNaCl + mKCl) in Group K-rich; 5. an organic particle in Group Organic;**
684 **6. Fe, Ca- aluminosilicate in Group Al, Si-rich; 7. Fe/Ni particle in Group Fe-rich and 8. CaCO₃ in Group Ca-rich of natural aerosols**
685 **on 27.09.2014. New unpublished results of Popovicheva et al. (2019) investigation.**

686

687 3.4.8 South America and Patagonia

688 Extending from 39°S to 54°S, with an area of 600 000 km², dust activity (Fig. 14) from this large desert remains largely
689 unknown. Some basic facts must be formally assessed, such as the location of sources and geomorphological features
690 associated with dust, as well as the seasonality and frequency of the dust's activity. To date, limited surveys of dust activity

691 (Crespi-Abril et al., 2017; Gaiero et al., 2003; Gassó and Torres, 2019) and case studies of individual sources exist (Gassó et
692 al., 2010; Gassó and Stein, 2007; Johnson et al., 2011). Recently, a list of dust activities and sources in Tierra del Fuego
693 (Cosentino et al., 2020) has been published. Generally, dust sources in Patagonia are at topographic lows, and the river valleys
694 (e.g., the Deseado and Santa Cruz rivers) (Coronato et al., 2017; Hernández et al., 2008) are associated with the late Holocene
695 para-glacial environments. The most active modern source of dust is the drying of Colhué Huapi Lake (CHL) in Central
696 Patagonia (45.5°S and 68°W) (Montes et al., 2017)—a shallow lake with variable water levels exposed to intense
697 evapotranspiration. An anthropogenic component appears to be linked to intense farming, oil prospection, and supplying water
698 to urban centers (Gaitán et al., 2009; Hernández et al., 2008; Mazzonia and Vazquez, 2009; Valle et al., 1998). CHL has been
699 steadily shrinking (Llanos et al., 2016) and was dried up by the summer of 2020. Consequently, dust activity originating in
700 CHL has increased with frequent blowouts large enough to be easily detected from space (Gassó and Torres, 2019).



701

702 **Figure 14. A dust event spanning the north and central sections of the Patagonian Desert (+1000 km) on March 28, 2009. Events this**
 703 **large occur about once every one to three years. This event is typical in that it was triggered by the passage of a powerful low-**
 704 **pressure center commonly found in these high latitudes. Also, this event is singular in that a large portion of it is cloudless, enabling**
 705 **a direct view from space (most dust activity in Patagonia occurs under cloudy conditions). The thick dust cloud in the upper right**
 706 **corner is from an area used for cattle farming, which was undergoing a drought, whereas the active sources further south can be**
 707 **considered more naturally occurring with less anthropogenic interference. Source: NASA's Worldview interface image processed**
 708 **with Google Earth.**

709

710 Overall, satellite detection in the Patagonia region remains challenging. There are several difficulties in surveying dust activity
711 in the area: obstructed views from space because of cloudiness, nighttime dust activity, and sparse population. Also, except
712 for a few sources, the lack of recurrence in dust emission is a general feature of the desert: Sources that were active during one
713 season do not reactivate until two or three seasons later. A comprehensive and dedicated survey combining surface and space-
714 based detection networks is needed for a better understanding.

715 **3.4.9 Svalbard**

716 Evidence of the presence and activity of dust sources in Svalbard is only recent and quite rare. Yet, for example, dust storms
717 in Longyearbyen are reported as a regular feature in autumn. Dörnbrack et al. (2010) documented and characterized a strong
718 dust storm in the Adventdalen valley—the center of Spitsbergen Island—in May 2004, using airborne lidar observations and
719 mesoscale numerical modeling. In the same area, near Longyearbyen, dust emissions from an active coal mine were
720 documented by Khan et al. (2017). Kandler et al. (2020) also reported Svalbard measurements in Longyearbyen in September
721 2017, with high iron and chlorite-like contributions in dust.

722 The accelerated ablation of Svalbard's glaciers (Schuler et al., 2020) and the increasing melt rate of permafrost are causing
723 accelerated growth in periglacial and proglacial areas. The significance of the morphogenetic processes of deflation,
724 denudation, and sediment transport on slopes and in river channels in glaciers' marginal zones is increasing (Zwolinski et al.,
725 2013). Thus, these areas have become potential sources of dust and, as such, have been investigated for the physical and
726 chemical properties of their sediments, regardless of the documented occurrences of the dust events these areas have
727 experienced.

728 Fluvial, glaciofluvial, and weathering deposits at five different sites on the coastal plains near the Ny-Ålesund Research Station
729 (78.92481°N, 11.92474°E), NW Spitsbergen were investigated (Moroni et al., 2018). The mineralogical assemblage is
730 characterized by dolomite, calcite, quartz, albite, and sheet silicates (vermiculite, muscovite, clinocllore) in variable amounts,
731 along with monazite, zircon, apatite, baryte, iron sulfate, Fe, Ti, Cu, and Zn ores as accessory minerals. With a weight fraction
732 of 4 to 53% of particles smaller than 100 µm, these deposits should be considered a valid dust source. However, the contribution
733 is influenced by the modest extension of bare soils (less than 4 km²) and the brief duration of the area's driest summer. The
734 composition of the aerosols collected at the Gruvebadet lab near Ny-Ålesund during the summer-fall period reveals the
735 presence of such a local dust component (Moroni et al., 2016; Moroni et al., 2018). Further evidence of local dust sources in
736 the Ny-Ålesund area and Brøgger Peninsula also results from the annual snowpack's chemical composition (Gallet et al., 2018,
737 Jacobi et al., 2019). The contribution of local dust sources on this site is of secondary importance compared to that of long-
738 range transport (Moroni et al., 2015; Moroni et al., 2016; Moroni et al., 2018, Conca et al., 2019).

739 A similar study was conducted on the loose sediment deposits in the neighborhood of the Polish Polar Station Hornsund
740 (77.00180°N, 15.54057°E), SW Spitsbergen, where a belt of nearshore plains consisting of marine terraces and nival moraine
741 bars, with bare surfaces available for mineral dust uplift from late spring, widely outcrop (Zwolinski et al., 2013). The
742 mineralogical assemblage consists of quartz, alkali feldspar, plagioclase, dark mica, and chlorite, with zircon, apatite,
743 monazite, iron sulfide, and Fe ore as accessory minerals. The same assemblage was found in the aerosols and snow cover
744 collected at the base station and the surrounding glaciers in the same period. This fact, along with the significant proportion of
745 particles smaller than 50 μm in the loose sediment deposits, supports the prevalence of the local dust source in the melting
746 season. Further evaluation of the impact of local dust sources was obtained from analyzing shallow and deep cores from
747 different glaciers in the Hornsund area (Lewandowski et al., 2020; Spolaor et al., 2020). The results suggest that for Spitsbergen
748 glaciers with the summit close (Ny-Ålesund) or below (Hornsund) the equilibrium line, the summer dust deposition from the
749 local sources is predominant, affecting the glacier ice's chemical composition. However, the dating of monazite grains and
750 presence of magnetite and iron sulfide (magnetic susceptibility and SEM data, Lewandowski et al., 2020) also suggest the
751 existence of regional wind transport from Nordaustlandet and Edgeøya, respectively. Further, a long-range component from
752 Northern Europe, Siberia, and, to a limited extent, Greenland, Iceland, and Alaska, was also evidenced (Moroni et al., 2018;
753 Crocchianti et al., 2021).

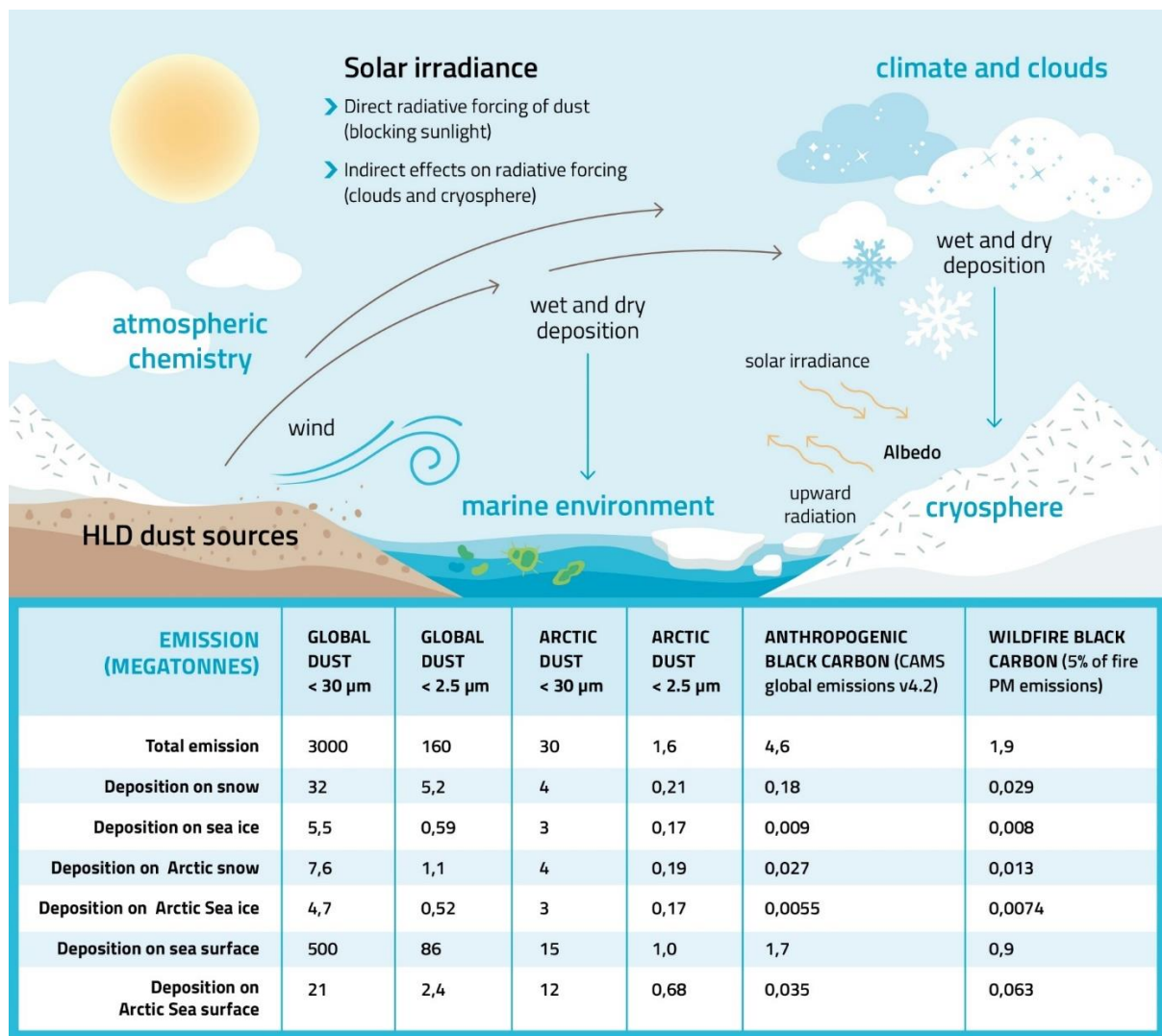
754 Recent estimations of dust load in Central and Southern Svalbard from different sources range from 4 g up to 4 – 5 kg m⁻²
755 (Rymer, 2018; Rymer et al. 2022), with the highest values in the Ebba Valley due to frequent dust storms in this area (Strzelecki
756 and Long, 2020). Kavan et al. (2020a) found a negative correlation between deposition rate and altitude at Pyramiden
757 (78.71060°N, 16.46059°E), the west coast of Petuniabukta, and Ariekammen (77.00035°N, 15.53674°E), and Hornsund area.
758 The pattern was clear up to the altitude of approximately 300 m a.s.l., suggesting the influence of local sources in the lower
759 levels of the atmosphere and long-range transport at higher altitudes. The lower values of the deposition rates found at
760 Ariekammen were ascribed due to the more frankly maritime climate of the Hornsund region.

761 **3.5 Climatic and environmental impacts of HLD**

762 Climatic and environmental impacts of HLD on clouds and climate feedback, atmospheric chemistry, marine environment and
763 cryosphere-atmosphere feedback (Fig. 15) were investigated with the help of topical literature surveys (Sections 3.5.1 - 3.5.4).
764 Direct radiative forcing of HLD dust (blocking sunlight) and comparison of dust and black carbon as SLCF in the cryosphere
765 are included in the cryosphere-atmosphere feedback section.

766
767 The amounts of dust emission and deposition (megatonnes) of annual global and Arctic dust (data for 2017), as compared to
768 anthropogenic and wildfire black carbon (Fig. 15), were studied using the SILAM model (Sofiev et al., 2015). The results of
769 black carbon emissions presented in Figure 15 were based on the Copernicus Atmosphere Monitoring Service (CAMS) global

770 emission inventory version 4.2 and black carbon originating from wildfires from the SILAM IS4FIRES fire emission model,
 771 equaling 5 % of the total primary fire PM emissions of the model. The IS4FIRES model is based on fires observed by the
 772 MODIS instrument onboard the Terra and Aqua satellites.
 773
 774



775
 776
 777 **Figure 15. Climatic and environmental impacts of high latitude dust include direct radiative forcing (blocking sunlight), indirect**
 778 **radiative forcing (clouds and cryosphere) as well as effects on atmospheric chemistry and marine environment. The amounts of dust**
 779 **emission and deposition (megatonnes) of global and Arctic dust, as compared to black carbon, were estimated using the SILAM**
 780 **model (Sofiev et al., 2015). The black carbon emissions are based on the CAM5 global anthropogenic emission dataset v4.2 and the**

781 wildfire black carbon emissions are based on the IS4FIRES fire emission model, equaling 5 % of the total primary fire PM emissions
782 of the model.

783 3.5.1 Impacts of HLD on atmospheric chemistry

784 Icelandic dust, a specific HLD of volcanic origin, is constantly resuspended from the deserts. Regarding atmospheric
785 chemistry, the most substantial impact comes from the particles in the 0.002 to 10 μm range, as they can be carried over more
786 considerable distances (Finlayson-Pitts, 1999). The Icelandic dust in the troposphere is not as addressed as the impact of desert
787 dust. This HLD is very likely a long-range transporting carrier for many species adsorbed on its surface, which can act as a
788 sink of trace gases and a subsequent platform for transferring taken-up species. Along with transport, adsorbed species may
789 undergo different heterogeneous reactions that can lead to secondary compound formation. Such processes can influence the
790 reactivity and balance of atmospheric species. Optical, hygroscopic, and, more generally, physicochemical properties of the
791 HLD can change due to surface processes, implying atmospheric trace gases due to heterogeneous interactions (Usher et al.,
792 2003). The consequences can be starkly different depending on the nature of atmospheric trace gases interacting with HLD.
793 This section aims to illustrate the diversity of interactions between HLD and atmospheric trace gases to emphasize the various
794 impacts of these aerosols on atmospheric physics and chemistry. In the case of ozone, if the direct heterogeneous interaction
795 with dust does not play a major role in the atmospheric concentration decrease of the primary compound, surface processes
796 are triggered, affecting the atmospheric budget of ozone. In the case of NO_2 , heterogeneous processes on dust can significantly
797 lead to HONO species forming, with direct impacts on gas-phase atmospheric reactivity. In the case of SO_2 , beyond a complex
798 reaction pathway, the heterogeneous process dually affects the budget of the taken-up species and the chemical and physical
799 properties of the dust surface.

800 If the heterogeneous reaction of NO_2 on various types of atmospheric particles, e.g., salts, soot, mineral dust, and proxies, was
801 addressed in the literature (George et al., 2015), the interaction of NO_2 with volcanic particles, typical HLD desert dust, under
802 atmospheric conditions, has only been studied by Romanias et al. (2020). They explore the possible formation of a short
803 lifetime key atmospheric species, considered a trigger of numerous atmospheric processes: HONO, a precursor of OH radicals
804 in the atmosphere. To that end, NO_2 uptake on Icelandic HLD is explored under various and contrasting atmospheric
805 conditions. Despite the relatively close volcanic regions where the selected samples originate, uptake coefficients of NO_2
806 contrasted significantly with the dust location due to magmatic and morphological differences among samples. This point
807 confirms that concerning heterogeneous atmospheric chemistry, sample behavior can dramatically deviate from one class of
808 dust to another, with physical and chemical characterizations of the samples remaining key intrinsic descriptors. Nonetheless,
809 volcanic dust appears as effective NO_2 scavengers from the atmosphere. The interaction of NO_2 with HLD is evidenced as a
810 source of NO and, more interestingly, HONO, with kinetics and formation yields highly dependent on relative humidity.
811 Higher HONO formation yields on volcanic samples are observed for RH values exceeding 30% RH. Heterogeneous
812 construction of HONO from NO_2 interaction with Icelandic dust is estimated as atmospherically significant under volcanic

813 eruptions or, more frequently in Iceland, during typical volcanic dust storms. Such leads to HONO formation rates up to 10
814 pptV/hr, which can significantly influence the regional atmosphere's oxidative capacity. The experimental determination of
815 NO₂ uptake coefficient γ allows including such processes in atmospheric modeling, improving their representativeness.

816 A transient uptake of SO₂ – an initially important uptake of SO₂ that is progressively reduced – leads to low steady-state uptake
817 coefficients of SO₂ after several hours of exposure in the range of 10⁻⁹ to 10⁻⁸. The surface coverages were in the range of
818 10¹⁴ molecule cm⁻² or 10¹⁶ molecule cm⁻² using the total surface area or the geometric surface area of aerosols, respectively
819 (Urupina et al., 2019). Zhu et al. (2020) estimated that around 43% more volcanic sulfur is removed from the stratosphere
820 within months due to SO₂ heterogeneous chemistry on volcanic particles than without. Concomitantly with SO₂ uptake, sulfites
821 and sulfates are monitored on the surface of volcanic dust, with sulfates being the final oxidation product, attesting to SO₂
822 surface reaction. Through surface hydroxyl groups, the dust surface's chemical composition plays a crucial role in converting
823 SO₂ to sulfites, as evidenced experimentally using lab scale but atmospheric relevant experimental setups (Urupina et al, 2019).
824 This provides original insights into the kinetics and mechanism of SO₂ uptake and the transformation on volcanic material
825 under simulated atmospheric conditions, bringing an accurate perspective on SO₂ heterogeneous sinks in the atmosphere on
826 the HLD surface. The model simulations of Zhu et al. (2020) suggested that the transformation of SO₂ on such particles plays
827 a key role in the stratosphere's sulfate content. Interestingly, this transformation and accumulation of sulfates on the surface
828 of particles could turn the unreactive ozone material into reactive, especially in the stratosphere, where volcanic particles have
829 longevity.

830 The case of SO₂ uptake points to the aging of the HLD surface with subsequent impacts on its chemical (e.g., hygroscopicity)
831 and physical (e.g., optical) properties. Changes in hygroscopic properties can correlate with HLD's erratic behavior to act as
832 cloud-or ice-nucleating particles, depending on their interactions with atmospheric gases. Similarly, sulfate and sulfuric acid's
833 high surface coverage for volcanic dust, as reported by Urupina et al. (2019), questions the variability of the HLD refractive
834 index and the impact on remote sensing of fresh vs. aged dust.

835 **3.5.2-Impacts of HLD on clouds and climate feedback**

836 Clouds across the mid- and high latitudes are of first-order importance. Climate and HLDs may play a first-order but highly
837 uncertain role in defining their properties through the initiation of ice formation. Clouds frequently persist in a supercooled
838 state. However, even a few droplets converting to ice crystals through heterogeneous freezing can lead to microphysical
839 processes that dramatically reduce a cloud's liquid water content, reducing its albedo and exposing the surface underneath
840 (Murray et al., 2021; Tan and Storelvmo, 2019). Only a small subset of atmospheric aerosol can nucleate ice; concentrations
841 of around only 1 INP per liter of air active at the cloud temperature can dramatically alter cloud albedo. In contrast, the
842 concentration of aerosol particles capable of serving as cloud condensation nuclei (CCN) are orders of magnitude larger.
843 Hence, dust particles in the high latitudes will rarely exist in high enough concentrations to dramatically impact cloud droplet

844 numbers by providing additional CCN. However, high-latitude dust has been shown to serve as an effective INP in sufficient
845 concentrations to potentially impact mixed-phase clouds (Sanchez-Marroquin, 2020). Ice formation's role in climate
846 projections depends on the clouds' location. In the following paragraphs, we discuss two distinct classes of clouds that may be
847 influenced by HLD particles serving as INPs.

848 For boundary layer clouds over oceans between approximately 45–70°, the amount of ice versus supercooled water, as well as
849 albedo, is critical for global climate (Vergara-Temprado et al., 2018; Bodas-Salcedo et al., 2014). These clouds are where
850 substantial solar insolation exists, and the contrast between a high albedo cloud and a dark ocean surface is significant. Hence,
851 these clouds are implicated in the cloud-phase feedback, where water replaces ice, increasing their albedo as the world warms
852 with increased carbon dioxide (Storelvmo et al., 2015). This feedback's uncertainty is very high, with the temperature rise
853 associated with a doubling of carbon dioxide, rising from around 4 K to well above 5 K, simply by increasing the amount of
854 supercooled water in clouds in the current climate (Frey and Kay, 2018). Hence, understanding the sources of ice-nucleating
855 particles in the high latitudes, including HLDs, is critical to understanding these climate-relevant issues (Murray et al., 2021).

856 The second group of clouds is those occurring at high latitudes. For example, in the central Arctic, mixed-phase clouds play a
857 critical role in the local Arctic climate and the phenomenon of Arctic amplification. In a corollary to the cloud-phase feedback,
858 water replacing ice leads to more downward longwave radiation, resulting in positive feedback (i.e., amplification) (Tan et al.,
859 2019). Hence, the phase of clouds and, therefore, the INP population in clouds in the present Arctic atmosphere are key for
860 defining this feedback's strength. Moreover, any changes in the INP population with a changing climate may also provide
861 feedback on cloud properties (Murray et al., 2021).

862 Given the apparent importance of INPs in defining cloud properties and climate feedback, surprisingly little is known about
863 the ice-nucleating properties of HLDs. Mineral dust is one of the most important types of atmospheric INPs in clouds below
864 approximately -15°C around the globe because of its relatively high ice-nucleating activity and abundance in the atmosphere
865 (Murray et al., 2012). A handful of papers have also identified HLDs as significant contributors to the Arctic's INP population
866 (Irish et al., 2019; Sanchez-Marroquin, 2020; Tobo et al., 2019; Šantl-Temkiv et al., 2019). HLDs may differ in their ice-
867 nucleating ability from LLDs for several reasons: Firstly, the HLDs from glacial valleys, for example, are often richer in
868 primary minerals (olivines, pyroxenes, feldspars, and amphiboles) and less rich in clays compared to LLDs. This is crucial
869 because K-rich feldspars are known for their exceptional ice-nucleating ability, whereas clays are much less active (Harrison
870 et al., 2019; Atkinson et al., 2013). Secondly, the most prominent LLD sources, like those in Africa, are abiotic (Price et al.,
871 2018), whereas it has been found that HLDs can be associated with highly effective biogenic ice-nucleating material (Tobo et
872 al., 2019; Šantl-Temkiv et al., 2019). The inclusion of biological ice-nucleating material, which can be ice-active at
873 temperatures much higher than -15 °C, may mean that these dust sources have a disproportionately greater impact on cloud
874 glaciation and climate than their low-latitude counterparts. Much more research is needed to define and understand the ice-
875 nucleating ability of these HLD sources.

876 3.5.3 Impacts of HLD on the marine environment

877 Mineral dust particles are a source of essential nutrients such as phosphorus (P) and iron (Fe) to the ocean ecosystems (e.g.,
878 Jickells et al., 2005; Mahowald et al., 2005; Stockdale et al., 2016). Dust deposition onto the ocean's surface can stimulate
879 primary productivity and enhance carbon uptake, indirectly affecting the climate (e.g., Jickells and Moore, 2015; Mahowald,
880 2011). The extent of these impacts primarily depends on the dust deposition fluxes, its chemical properties, and the nutrients
881 of (co)limitations patterns in the ocean waters (e.g., Boyd et al., 2007; Boyd et al., 2010; Kanakidou et al., 2018; Mahowald et
882 al., 2010; Mills et al., 2004; Moore et al., 2013; Shi et al., 2012; Stockdale et al., 2016). Arctic Ocean is often nitrogen-limited
883 (von Friesen and Riemann, 2020).

884 The aerosol fractional Fe solubility (%) is defined as the ratio of dissolved Fe (in the filtrate, which has passed through 0.2 or
885 0.45 μm pore size filters) to the total Fe in the bulk aerosol (e.g., Meskhidze et al., 2019; Shi et al., 2012). This is typically
886 used to indicate the fraction of Fe, which is likely to be bio-accessible for marine ecosystems (Meskhidze et al., 2019).

887 Sub-Arctic oceans are Fe-limited or seasonally Fe-limited. Fe limits primary productivity in the Sub-Arctic Pacific Ocean
888 (Martin and Fitzwater, 1988). The atmospheric Fe deposition in the Gulf of Alaska is dominated by dust transported from
889 glacial sediments from the Gulf of Alaska coastline (Crusius et al., 2011), with relatively high fractional Fe solubility—around
890 1.4% (Schroth et al., 2017). Although the upwelling of deep water is the major source of dissolved Fe, the atmospheric flux of
891 dissolved Fe to the Gulf of Alaska's surface water is comparable to the Fe flux from eddies of coastal origin (Crusius et al.,
892 2011). The magnitude of glacial dust's deposition to the Gulf of Alaska varies significantly depending on the regional weather
893 conditions. However, the extent of its impacts is still unclear (Schroth et al., 2017). Currently, the spatial resolution of global
894 dust models is too low to accurately reproduce Alaskan dust flux, generated by anomalous offshore winds and channeled
895 through mountains (Crusius, 2021). Recently, Crusius (2021) determined dissolved Fe inventories based on time series of
896 dissolved Fe and particulate Fe concentrations from the Ocean Station Papa in the central Gulf of Alaska, including
897 measurements from September 1997 to February 1999. The analysis showed 33%–70% increases in dissolved Fe inventories
898 between September and February of successive years. These increases were possibly linked to dust fluxes from the Alaskan
899 coastline—known to occur mostly in autumn (Crusius et al., 2011; Schroth et al., 2017). These new results support the
900 importance of atmospheric Fe's contribution, although more work is needed to confirm the sources of dissolved Fe in the Gulf
901 of Alaska.

902 The Sub-Arctic North Atlantic Ocean is seasonally Fe-limited (Nielsdottir et al., 2009; Ryan-Keogh et al., 2013). Natural dust
903 from Iceland largely contributes to the atmospheric dust deposition in the North Atlantic Ocean (Bullard, 2016). Icelandic dust
904 originates from volcanic sediments and has a relatively high total Fe content—about 10% (e.g., Arnalds et al., 2014, Baldo et
905 al., 2020). The estimated total Fe deposition from Icelandic dust to the ocean's surface is 0.56–1.38 Mt yr⁻¹ (Arnalds et al.,
906 2014). The initial Fe solubility observed in dust samples from Icelandic dust hotspots is from 0.08% to 0.6%—comparable to

907 that of mineral dust from low-latitude regions such as Northern Africa, while the fractional Fe solubility at low pH (i.e., 2) is
908 significantly higher than typical low-latitude dust (up to 30%) (Baldo et al., 2020). Achterberg et al. (2018) argued that deep-
909 water mixing is the dominant source of Fe in the Sub-Arctic North Atlantic Ocean's surface water, which is up to ten times
910 higher than the Fe supply by atmospheric Fe deposition. However, during the 2010 eruption of the Icelandic volcano
911 Eyjafjallajökull, Achterberg et al. (2013) observed elevated dissolved Fe concentration and nitrate depletion in the Iceland
912 Basin, followed by an early spring bloom. They measured an initial fractional Fe solubility of 0.04%–0.14% for Icelandic
913 ash, which is below or towards the lower end of the range of values estimated for Icelandic dust (0.08%–0.6%) (Baldo et al.,
914 2020). High deposition flux (Arnalds et al., 2016) and higher Fe solubility of Icelandic dust (Baldo et al., 2020) suggest that
915 they may impact Fe biogeochemistry and primary productivity in the surface ocean. However, more research is needed to
916 confirm this.

917 The Southern Ocean is known to be Fe-limited (Moore et al., 2013). Major atmospheric dust sources include, for example,
918 Australia, southern South America, and Southern Africa (e.g., Ito and Kok, 2017). Contribution from local sources in
919 Antarctica is also observed (e.g., Chewings et al., 2014; Winton et al., 2014; Winton et al., 2016). Winton et al. (2016) reported
920 a background fractional Fe solubility from Antarctic dust sources of 0.7%—similar to the upper limit of Fe solubilities observed
921 in Icelandic dust (Baldo et al., 2020). However, mineral dust originating from glacial sediments from the Gulf of Alaska
922 coastline showed higher Fe solubilities (1.4%) (Schroth et al., 2017)—likely due to the different mineralogy and Fe speciation
923 in the samples. The various methods used to determine the fractional Fe solubility in these studies may also contribute to this
924 difference (Perron et al., 2020).

925 Although the upwelling of deep water is a major source of dissolved Fe, the atmospheric deposition of dissolved Fe can locally
926 contribute to the phytoplankton bloom (Winton et al., 2014). However, evidence exists that increased dust flux enhanced
927 primary production in the Southern Ocean in the last glacial age (Martínez-García et al., 2014). The Ross Sea is a continental
928 shelf region around Antarctica and a highly biologically productive area in the Southern Ocean, which has important
929 implications for global carbon sequestration (e.g., Arrigo et al., 2008; Arrigo and Van Dijken, 2007). In the Ross Sea, an
930 additional Fe supply is required to sustain the intense phytoplankton bloom during the austral summer (Tagliabue and Arrigo,
931 2005). Measurements conducted on snow pits and surface snow samples showed that local Antarctic dust contributes to Fe
932 deposition. However, this contribution is only a minor component of the total Fe supply to the Ross Sea, with most being
933 supplied by the upwelling of deep water (Winton et al., 2014; Winton et al., 2016a,b).

934 In the Polar regions, atmospheric dust is mostly delivered to the sea ice, where melting and freezing cycles (ice processing)
935 can enhance the formation of relatively more soluble phases of Fe oxide-hydroxide minerals such as ferrihydrite. This
936 formation can increase the flux of atmospheric dissolved Fe to the ocean (Raiswell et al., 2016).

937 **3.5.4 HLD impacts on cryosphere and cryosphere-atmosphere feedback**

938 The cryosphere is the frozen water part of the Earth system, including sea, lake, and river ice; snow cover, glaciers, ice caps,
939 and ice sheets; permafrost and frozen ground. These components play a crucial role in the Earth's climate (IPCC, 2019).
940 Temperatures in fragile areas, such as the pristine polar regions, have been increasing at twice the global average; the highest
941 increase in the temperature on the coldest days—up to three times the rate of global warming—is projected for the Arctic
942 (IPCC, 2021). Warming in vulnerable cold climate land areas causes glacier retreat, permafrost thaw, and a decrease in snow
943 cover extent (IPCC, 2019). Consequently, potential HLD sources, such as glacial sediments, can increase (e.g., Nagatsuka et
944 al., 2021). When dust is long-range transported and wet- or dry-deposited or windblown from local dust sources, the ice and
945 snow albedo decrease and influences glacier melt (e.g., Boy et al., 2019) via the positive ice-albedo feedback mechanism
946 (AMAP, 2015; Flanner et al., 2007; Gardner and Sharp, 2010; IPCC, 2019). Cryospheric melt processes are controlled by
947 many environmental factors (IPCC, 2019), such as solar irradiance, ambient temperature, and precipitation (e.g., Meinander
948 et al., 2013, 2014; Mori et al., 2019). Kylling et al. (2018) used dust load estimates from Groot Zwaafink et al. (2016) (using
949 low-latitude dust complex refractive index for high-latitude dust) to quantify the mineral dust instantaneous radiative forcing
950 (IRF) in the Arctic for 2012. They found that the annual-mean top of the atmosphere IRF (0.225 W/m^2) had the largest
951 contributions from dust transported from Asia south of 60°N and Africa; high-latitude ($>60^\circ\text{N}$) dust sources contributed about
952 39% to the top of the atmosphere IRF. However, HLD had a larger impact (1 to 2 orders of magnitude) on IRF per emitted
953 kilogram of dust than low-latitude sources. They also reported that mineral dust deposited on snow accounted for nearly all
954 the bottom of the atmosphere IRF (0.135 W/m^2), with over half caused by dust from high-latitude sources north of 60°N .

955 For snow and ice (glacier) surface radiation balance, the net energy flux E_N is due to differences between downward (\downarrow) and
956 upward (\uparrow) non-thermal shortwave (SW) and thermal longwave (LW) radiative fluxes. Such is most critically influenced by
957 the surface characteristics of the bi-hemispherical reflectance (BHR), i.e., albedo (Manninen et al., 2021). Therefore, melt is
958 also controlled by dark impurities in snow and ice (IPCC, 2019). Black carbon (BC) is, climactically, the most significant and
959 best-studied dark light-absorbing aerosol particle in snow (e.g., Bond et al., 2013; Dang et al., 2017; Evangeliou et al., 2018;
960 Flanner et al., 2007; Forsström et al., 2013; Mori et al., 2019; Meinander et al., 2020a,b). Radiation-transfer (RT) calculations
961 indicate that seemingly small amounts of black carbon (BC) in snow, in the order of 10–100 parts per billion by mass (ppb),
962 decrease its albedo by 1–5% (Hadley and Kirchtetter, 2012). BC has been shown to enhance snowmelt (AMAP, 2015; Bond
963 et al., 2013; IPCC, 2019). Other light-absorbing particles include organic carbon (OC, including brown carbon BrC) and dust.
964 Also, blooms of pigmented glacier ice algae can lower ice albedo and accelerate surface melting (McCutcheon et al., 2021),
965 showing a direct link between mineral phosphorus in surface ice and glacier ice algae biomass. They say nutrients from mineral
966 dust likely drive glacier ice algal growth, identifying mineral dust as a secondary control on ice sheet melting. Some Icelandic
967 dust sources have particles almost as black as black carbon by the reflectivity properties when measured as bulk material or
968 on snow and ice surfaces (Peltoniemi et al., 2015). Unlike black carbon, Icelandic dust has been shown to melt snow quicker
969 in small amounts and insulate and prevent melt in larger amounts (e.g., Dragosics et al., 2015; Möller et al., 2016; Boy et al.,

970 2019). Changes related to permafrost thaw and snow and ice melt, including disappearing glaciers, rising sea levels, and
971 drinking water shortages, are among the most serious global threats (IPCC, 2019). Water availability is vital in regions where
972 crops depend most on snowmelt water resources (Qin et al., 2020). Snow is also essential in the catchment areas (i.e., areas
973 supplying watercourses) and for many snow-dependent organisms, including plants, animals, and microbes (Zhu et al., 2019).
974 Melt can also run hydroelectric power plants that supply electricity (e.g., Lappalainen et al., 2022). This all highlights the
975 importance of investigations and continuous assessment of the temporal and spatial significance and contribution of different
976 light-absorbing impurities in enhancing or initiating cryospheric melt in the changing climate.

977 **3.6 Understanding the HLD sources**

978 The HLD results are further discussed from the perspective of HLD source intensity values; comparison with available HLD
979 information on the various regions; geological perspective on sources, focusing on a gap identified in HLD observations for
980 the Central part of the East European Plain and dust particle properties; and local HLD sources and long-range transport of
981 dust with the focus on results from the observations in Svalbard and Antarctica.

982 **3.6.1 Source intensity values**

983 Most of the HLD study sites agree with UNCCD G-SDS-SBM source intensity (SI) values of the highest dust productive areas,
984 identifying an environment from a given location within a distance $\leq 0.1^\circ$. Surfaces with higher maximum SI include a
985 significant portion of the land surface in HLD regions. In the south HLD region, an annual change of SI exists. However,
986 approximately half the dust productive surface stays exposed to wind erosion during the year. In the north HLD region, SI
987 intensity varies significantly with the weather. High values of SI may not always coincide with high surface winds, meaning
988 high values may exist but not necessarily result in a dust storm. In case emissions occur, dust may remain undetected because
989 of the absence of ground observations over most of the HLD region and frequent cloud cover over airborne dust, obscuring
990 remotely sensed imagery.

991 Based on the SI values, the East Greenland sources in this study (no. 58–64 in Fig. 1) are seasonal, meaning their SI minimum
992 value is zero. Conversely, the West Greenland sources are not necessarily seasonal since their SI minimum values are
993 somewhat reduced (but not to zero). However, the term “seasonal” regarding the SI values means the soil surface conditions
994 are suitable for dust emissions, although that doesn’t mean emissions will happen. Similarly, the seasonality of all sources in
995 this collection can be further studied.

996 When the newly identified sources are close together, such might indicate they are part of the larger dust source area, like
997 South Iceland, West Greenland, or East Greenland. The discovered sources could be considered to represent the hot spot
998 locations, i.e., the most emissive or active locations, of those dust-productive areas. Simultaneously, however, the land surface

999 and soil composition can be very complex and spatially variable, and the identification of single sources justified until the
1000 source characteristics and particle properties have been characterized in more detail. For example, Icelandic sources have
1001 shown that each source, even proximate ones, may have different particle size distributions and optical properties. The results
1002 (Fig. 2) suggest two northern high-latitude dust belts. The first HLD belt would extend at 50–58°N in Eurasia and 50–55°N in
1003 Canada, and the second dust belt at >60°N in Eurasia and >58°N in Canada, with a “no dust” belt between the HLD and LLD
1004 dust belts (except for British Columbia).

1005 Uncertainties about the detected locations of the HLD sources and G-SDS-SBM source intensity values arise from the
1006 methodology for determining HLD source locations. These locations are ad-hoc location sources from satellite images of dust
1007 plumes; other kinds of airborne dust observations may introduce some errors in location estimation compared to on-site land
1008 surface monitoring and the precision of available data locations. The resolution of G-SDS-SBM may be too coarse for small-
1009 scale source areas (in this case, the representative grid point value shows reduced source intensity value since it represents the
1010 whole grid box). However, the in-point (at location) values are also given maximum values in the area around the given
1011 location (one point distance: 30 arcsec, 0.1°, 0.5°, and 1° distance). Values of source intensity above 0.9 have topsoil potential
1012 for SDS production in the top 10% of grid boxes with some emission potential in G-SDS-SBM (or in the top 10% of most
1013 dust-productive surfaces globally in case of favorable weather conditions), above 0.8 in the top 20%, above 0.7 in the top 30%,
1014 and so forth. Factors reducing source function value or topsoil dust productivity are sparse vegetation, coarser soil texture,
1015 higher moisture, and temperatures near the freezing point. Uncertainties in methodology for deriving G-SDS-SBM arise from
1016 the quality and resolution of available global datasets and the determination of thresholds for EVI in defining bare land fraction
1017 (primarily for brown grassland, which may appear as potential dust sources but with lower productivity). Surfaces with low SI
1018 values in favorable conditions for dust emission, in case of high winds, may produce some blowing dust events; sources with
1019 higher values of SI may generate dust storms. Real dust production from sources depends on high winds occurring while SI is
1020 high.

1021 Forty-nine locations were in the north HLD region (except for two: no. 8 and no. 48, with latitudes 43.7°N and 43.6°N,
1022 respectively), while 15 were in the south HLD region, including four south of 60°S, where the values of SI are not provided.
1023 In the north HLD region, higher dust productive potential (SI 0.5) has 17 of 49 marked locations at the HLD source marks
1024 exact location. Also, 38 sites are where a distance from a mark point (D) is equal to or less than 0.1° (Supplementary Table
1025 S4). Very high dust productivity, with SI 0.7, has 33 locations within D 0.1°, and 42 and 46 within 0.5° and 1°, respectively.
1026 The highest dust productive potential, with SI 0.9°, has 27 locations within D 0.1°, and 39 and 44 within 0.5° and 1°,
1027 respectively. One point has the highest SI value, with less than 0.5° and five less than 0.9° away, when considering the largest
1028 environment of the HLD source mark. Three HLD source region marks are in the sea, so their source values are marked as -
1029 99 (undefined). In the south HLD region, 11 locations are considered (situated between 40°S and 60°S). Seven sources have
1030 very high dust productivity with SI 0.7 where the HLD source marker is; three more have SI 0.7° in the area of the source

1031 marker with D 0.1°. The highest dust productive potential, with SI 0.9°, has seven sources in the area with the source marker
1032 with D 0.1°, and three more in the area with D 0.5°. The source maximum and minimum intensities in these south HLD regions
1033 differ much less than in the north HLD region.

1034 As a summary, our modeling results on the spatial distribution of the dust sources (Fig. 2) showed evidence supporting a
1035 northern High Latitude Dust (HLD) belt, defined as the area north of 50°N, where we distinguish the following HLD-source
1036 areas: (a) “transitional HLD-source area,” which extends at latitudes 50–58°N in Eurasia and 50–55°N in Canada, and (b)
1037 “cold HLD-source area,” which includes areas north of 60°N in Eurasia and north of 58°N in Canada, with currently “no dust
1038 source” area between the HLD and LLD dust belts (except for British Columbia).

1039 **3.6.2 Comparison of various regions**

1040 For the HLD sources identified and included in our collection, the available information varied from detailed characterizations
1041 to the first satellite observations, waiting to be complemented with measurement data. Model output of dust transport can
1042 provide valuable additional information. The sources are in the northern and southern high latitudes and include a variety of
1043 environments. Particle properties, such as particle size distributions, have been determined for only some of the identified
1044 HLD sources. For example, our study’s many Iceland south coast sources have not had any characterization done. Previous
1045 results on the known sources in Iceland’s south coast region show that the particle size distributions vary substantially from
1046 location to location. No assumptions can be made based on characterization in one place.

1047 For Iceland seasonality, the correlation of SILAM modeled and measured PM10 and PM2.5 total aerosol concentration in
1048 Iceland is low, especially in 2018, which can mainly be explained by the measurement locations being far from the source
1049 locations and showing the effects of road dust rather than long-range transported dust. Also, the Reykjavik and Akureyri dust
1050 inventories are unrepresentative due to the challenge of fitting the modeled long-range transported dust emissions 695 to the
1051 measurement data within the 0.1 degrees model resolution. Near Reykjavik, dust emissions, e.g., from Landeyjasandur, may
1052 contribute to the measured dust concentrations. However, the 0.1 degrees resolution of the model is too scarce to simulate
1053 them.

1054 The end of summer and autumn (October) are the seasons for dust activity in Greenland. For example, on 19 October 2021,
1055 there was significant dust activity in western Greenland; several glacial valleys emitted dust along the 700-km coast. During
1056 that dust event was a good Sentinel overpass showing a long narrow valley with a great deal of haze(dust) suspended (appearing
1057 as fuzziness in the image) (Gassó, 2021b). As far as we know, no previous observations for this source exist. Greenland’s HLD
1058 sources (no. 53–58 of Fig. 1) from its west coast are considered new and identified here using satellite observations. Currently,
1059 further knowledge on the recurrency and area of the emission source is lacking. It is probable that these Greenland HLD
1060 sources from the west coast have been unidentified due to frequent cloudy conditions. The representation of dust sources in

1061 modeling approaches requires information on the location, soil characteristics, and temporal changes. A detailed specification
1062 of the geographic distribution of potential dust sources and their physical (e.g., particle size distribution, optics) and
1063 mineralogical/chemical (mineral fractions, chemical composition, etc.) properties is critical to accurately parameterize dust
1064 emission's potential in numerical dust models. Various methods exist to detect new sources; remote sensing is one of the most
1065 powerful tools, as demonstrated in Iceland's southern coast and Greenland's west and east coasts.

1066 The central part of the East European Plain, with the wide occurrence of silty soils derived from loess-like sediments and
1067 reduced natural vegetation, is a potential aeolian dust source (Bullard et al., 2011; Sweeney and Manson, 2013). However, this
1068 region currently lacks observations on dust lifting and transport. Therefore, this region was not included in our collection of
1069 HLD sources. The gap for observations in the central part of the East European Plain for potential HLD source updates is filled
1070 here with new data in the Supplement Figures S1–S4 on the partitioning of elements among the five particle-size fractions
1071 separated from the natural soils of a rural area 100 km southwest of Moscow (Fig. S1). The study area (55°12–13'N, 36°21–
1072 22'E) belongs to the southeastern part of the Smolensk-Moscow Upland (314 m a.s.l.), representing a marginal area of the
1073 Middle Pleistocene (MIS 6) glaciation with moraine topography modified by post-glacial erosional and fluvial processes. The
1074 major soil reference group is Retisol (IUSS Working Group WRB, 2015), developed on the loess-like loam. About 50% of the
1075 soils in the interfluvial area were subjected to arable farming. A new and unpublished independent dataset on 33 elements in
1076 topsoil horizons was obtained with a higher accuracy ICP-MS/AES analysis (compared to the DC-ARC-AES data set of
1077 Samonova and Aseyeva, 2020).

1078 Additional dust sources with massive dust storms causing severe traffic disruption have been documented outside the dust belt
1079 in higher latitudes. These sources were mainly arable fields, such as those in Germany and Poland, as well as Montana and
1080 Washington state (in the US) (Hojan et al., 2019).

1081 **3.6.3 A geological perspective on HLD sources and particle properties**

1082 Dust sources involve very different formations and geological environments, each leaving its own imprint on the sediments.
1083 Thus, the geomorphological, sedimentological, petrological, and geochemical study of the loose sedimentary formations in the
1084 source areas provides information on the origin and provenance of dust when it is transported out or far away. These types of
1085 studies—quite typical for Saharan dust—are not so well-established in the case of HLD sources. These territories are not all
1086 easily accessible. Even when they are, the time may not coincide with the dust production and/or dust emission period, which
1087 may be one reason for this missing source area characterization.

1088 Geomorphological studies cover a wide range of subjects and topics, from characterizing specific dust sources (e.g., Arnalds
1089 et al., 2016; Bullard and Mockford, 2018; Bertran et al., 2021) to analyzing processes (e.g., Bullard and Austin, 2011; Hedding
1090 et al., 2015; Wolfe, 2020) to landform evolution (Heindel et al., 2017). Sedimentological studies on dust sources focus on the
1091 particles' morphological characteristics and textural details of the loose sediment formations. The size, shape, and surface

1092 characteristics of the particles result from morphogenetic processes. As such, these particles say a great deal about the source
1093 areas. Furthermore, the particles' size and shape influence their lifting and transport capacity and, finally, the distance they
1094 can reach from their site of origin. Such applies to the studies of the properties of volcanoclastic dust sources in Iceland (e.g.,
1095 Butwin et al., 2020; Richard-Thomas et al., 2021). From the petrological and geochemical perspective, the panorama is even
1096 wider and more varied. Save a few (e.g., Baratoux et al., 2011; Moroni et al., 2018), most studies are not aimed at studying
1097 dust sources but comprise different targets involving the parental soils (e.g., Antcibor et al., 2014; Brédoire et al., 2015).
1098 Although providing information on the (possible) source areas for dust, these latter studies are not explicitly aimed at studying
1099 dust sources, so they are not functional for that purpose. Specific survey and sampling activities by a team of experts would
1100 be required to address all aspects of dust sources and properties adequately. Thus, obtaining a database as rich and articulated
1101 as possible on the particles' physico-chemical properties within dust would be feasible, providing the ability to predict dust
1102 behavior within the aerosols and understand medium and long-range transport phenomena is present. A further aspect
1103 regarding dust sources and properties is the evolution of the particles' physico-chemical properties due to the lifting and
1104 transport mechanisms. The aerosols must be sampled in different places at different distances from the source. However, this
1105 approach is complicated by the air masses mixing during transport, requiring a deep investigation of air mass back trajectories.
1106 Conversely, treating the soils in the lab by re-suspending and sampling them using impactors at well-defined cut-off size ranges
1107 can be very advantageous. Such work has been carried out on Australian soils and southern African soils (Gili et al, 2021) to
1108 study the dust sources in Antarctica, which is now underway in Iceland (Moroni, 2021, personal communication).

1109 **3.6.4 Local HLD sources versus long-range transported dust: discussing Svalbard and Antarctica**

1110 The same areas of dust lifting can also be deposition sites when particles leaving their respective source regions are deposited
1111 there after prolonged transport pathways. The extent of the contribution of local and long-range sources may vary during the
1112 year depending on the type of atmospheric circulation and state of the exposed surfaces, particularly the presence of bare
1113 deglaciated soils. Such is the case of Svalbard, where the local dust sources prevail over the long-range ones, especially in
1114 summer; the contrary occurs the rest of the year (Moroni et al., 2016; Spolaor et al., 2021). Conversely, and always in
1115 Spitsbergen, the type of contributions—local and long-range—may also depend on the altitude due to the stratified structure
1116 of the lower atmosphere frequently found at high latitudes (e.g., Moroni et al., 2015; Kavan et al., 2020a).

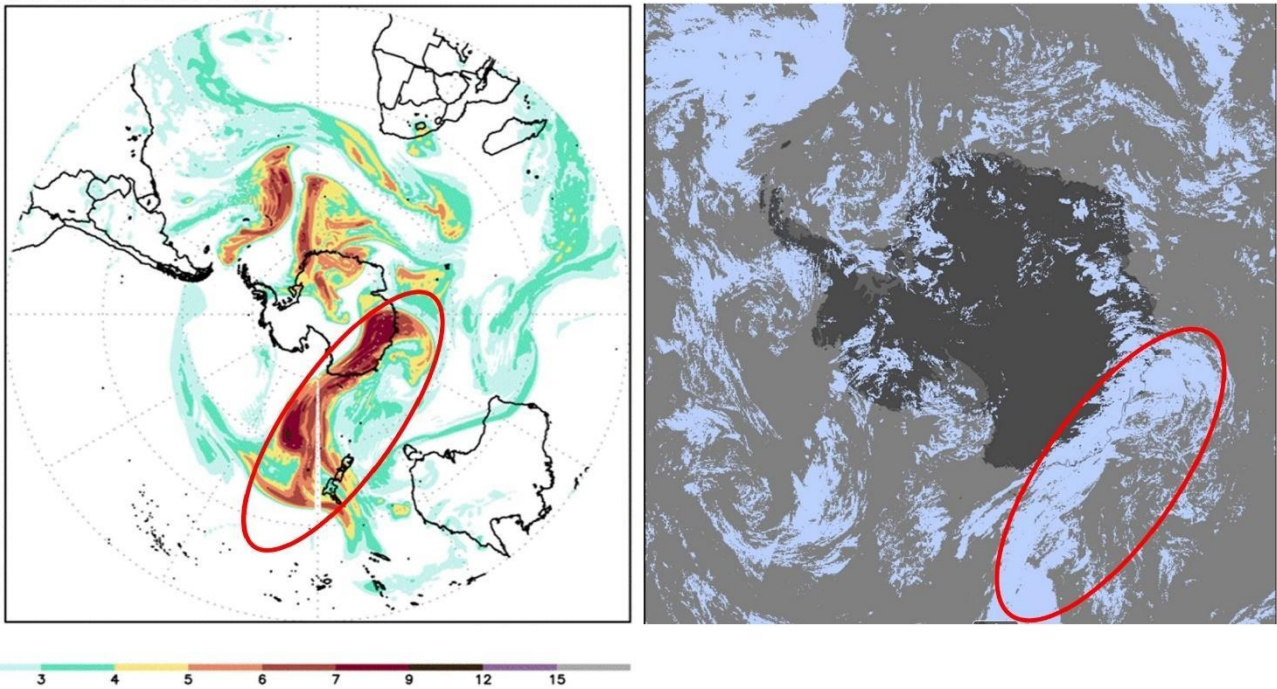
1117 Investigating the physico-chemical properties, and possibly estimating their contributions at different times of the year, is key
1118 to identifying the source regions of dust. For example, in Spitsbergen's case, the potential Source Contribution Function
1119 (PSCF) analysis of aerosol samples taken in Ny-Alesund clearly identified four different HLD sources in Eurasia, Greenland,
1120 Arctic-Alaska, and Iceland (Crocchianti et al., 2021). Conversely, chemical-mineralogical investigation and single-particle
1121 analysis recognized and estimated Icelandic dust's contribution to Ny-Alesund (Moroni et al., 2018).

1122 Kandler et al. (2020) collected dry dust deposition near sources in Northwestern Africa, Central Asia, on Svalbard, and at three
1123 locations of the African outflow region, and studied particle sizes and composition. Their results showed low temporal variation
1124 in estimated optical properties for each site but considerable differences among the African, Central Asian, and Arctic regions.
1125 An insignificant difference was found between the K-feldspar relative abundances, indicating comparable ice-nucleation
1126 abilities. The mixing state between calcium and iron compounds differed for near-source and transport regimes, potentially
1127 and partially due to size-sorting effects. Thus, in certain situations (high acid availability, limited time), atmospheric processing
1128 of the dust is expected to lead to less iron solubility for near-source dust (for Central Asian ones) than for transported ones
1129 (particularly those of Sahelian origin).

1130 In the southern part, under certain meteorological conditions, dust from lower latitudes can be transported far toward polar
1131 regions. Such was the case when a massive dust storm formed over Australia on 22 January 2020. Two days later, dust moved
1132 southward, covering a large part of Antarctica's eastern coast. The RHMSS global version of the DREAM model with
1133 incorporated ice nucleation parameterization due to dust (Nickovic et al., 2016) predicted the formation of cold clouds over
1134 the Antarctic. This ice cloud phase was also documented by NASA satellite observations (Fig. 16). The simulation was part of
1135 a WMO SDS-WAS initiative to include dust impacts on high latitudes in its agenda to better understand the role of mineral
1136 dust as a climate factor at high latitudes.

1137

NMME–DREAM forecast: $\log_{10}(\text{IN})$ (IN #/lit) Ullrich
Valid time: 24JAN2020 21UTC



1138

1139 **Figure 16. Global NMME DREAM model experiments over Australia and the South Pole. Model dust load 22 January 2020; B)**
1140 **Model \log_{10} (vertical load of ice nuclei number) (left). NASA MODIS ice cloud phase for 24 January 2020 (right).**

1141

1142 The McMurdo Dry Valleys (MDV) were previously assumed to be a significant regional source of dust (e.g., Bullard, 2016).
1143 New observations show otherwise. Instead, the McMurdo Ice Shelf's (sometimes called the McMurdo debris bands) debris-
1144 covered surface is the major dust source. In this study, more details are provided to underline the importance and estimates of
1145 the size of the areas. The MDV (4 800 km²) was estimated to fit Category 3 best. Despite active local aeolian sediment transport
1146 with many annual occurrences, they are an insignificant source or exporter of dust regionally, thus having only a small but
1147 poorly known climatic or environmental significance. The MDV are changing quickly with increased ablation, meltwater, and
1148 permafrost incision, so their importance regarding dust generation may change in the near future. The McMurdo Ice shelf
1149 "debris bands" fit Category 2 best. Although it is only about 1500 km², the McMurdo Ice shelf is clearly the region's largest
1150 and most important dust source—active with a continuous supply of new sediment for export and exposed to frequent strong
1151 winds (with many events during the year), although few have been documented. The aeolian sediment impacts sea ice albedo
1152 (not directly measured) and marine sedimentation, contributing enough dissolved Fe to potentially support up to 15% of
1153 primary productivity in the SW Ross Sea (Winton et al., 2014).

1154 Ice core studies from Antarctica ice sheets show that Antarctica receives long-range dust transport from Australia, South
1155 America, South Africa, and New Zealand (e.g., Bullard, 2016). However, several studies around coastal areas have shown that
1156 locally, Antarctic sourced dust accumulation rates are at least two orders of magnitude higher than that recorded from the polar
1157 plateau or global dust models (Chewings et al., 2014; Winton et al., 2014).

1158 **4 Conclusions and outlook**

1159 This study aimed to identify new HLD sources with the focus on their potential climatic and environmental impacts. A
1160 literature survey on impacts and model calculations on emission, transport and deposition were made to investigate the local,
1161 regional, and global significance of the HLD sources. We identified 64 new HLD sources. We estimated that in the high
1162 latitudes, the land area with higher ($SI \geq 0.5$), very high ($SI \geq 0.7$), and the highest potential ($SI \geq 0.9$) for dust emission cover >1
1163 $670\,000\text{ km}^2$, $>560\,000\text{ km}^2$, and $>240\,000\text{ km}^2$, respectively. These estimations agree with the first HLD sources' estimate of
1164 an area $>500\,000\text{ km}^2$ by Bullard et al. (2016), which mainly included the sources with a very high potential for dust emission,
1165 as classified in this study. Our study shows that active sources cover a significantly larger area, confirmed by over 60 new
1166 HLD sources with evidence of their dust activity, which is not limited to dry areas. The potential HLD emission areas need
1167 proof of observed and identified HLD emission sources.

1168 Our modeling results on spatial distribution of the dust sources showed evidence supporting a northern High Latitude Dust
1169 (HLD) belt, defined as the area north of 50°N , with a "transitional HLD-source area," extending at latitudes $50\text{--}58^\circ\text{N}$ in
1170 Eurasia, $50\text{--}55^\circ\text{N}$ in Canada, and a "cold HLD-source area," including areas north of 60°N in Eurasia and north of 58°N in
1171 Canada, with currently "no dust source" area between the HLD and LLD dust belt, except for British Columbia. Using the
1172 global atmospheric transport model SILAM, we estimated that 1.0% of the global dust emission originated from the high-
1173 latitude regions. About 57% of the dust deposition on snow and the ice-covered Arctic regions came from HLD sources.

1174 Our update provides crucial information on the extent of active HLD sources and their locations. Active HLD sources as
1175 essential sources of aerosols that directly and indirectly affect climate and the environment in remote regions are often poorly
1176 understood and predicted. HLD is likely a significant source of atmospheric iron deposition in the Southern Ocean encircling
1177 Antarctica. More research is needed to quantify the deposition flux of HLD and nutrient (Fe, P, and trace metals such as Co)
1178 content and solubility, which can then be fed to ocean biogeochemical models to quantify their impact on ocean
1179 biogeochemistry. HLD is also an active ice-nucleating particle changing cloud properties, which has severe consequences
1180 when deposited within the cryosphere. However, more studies are needed for HLD from different regions. For example,
1181 Northern Asia HLD sources are assumed to be numerous but are difficult to access and gain information from. Such points to
1182 the following main action items for monitoring dust in high latitudes:

1183 · Firstly, the work on HLD sources needs a multidisciplinary combination of field, laboratory, and experimental work;
1184 remote sensing; and emission, transport and deposition modeling. An increase in observational and modeling studies
1185 improves HLD monitoring and predicting.

1186 · Secondly, the activity of the currently identified active sources should be followed and reevaluated in the coming
1187 years and decades.

1188 · Thirdly, research gaps and future research directions essentially include finding, identifying, and characterizing new
1189 dust sources. As soon as there is evidence of finding a new HLD source, it should be included in the list of dust sources
1190 and subject to further study.

1191 · Fourthly, the role of different types of road dust in the Arctic could be separately assessed using a standard
1192 methodology.

1193 Namely, in Arctic communities, road dust as a signature of non-exhaust traffic dust formed via the abrasion and wearing down
1194 of pavement, traction control materials, vehicle brakes, and tires is a common concern (e.g., Kupiainen et al., 2016; Nordic
1195 Council of Ministers, 2017). This paper excluded this type of road dust and only included significant anthropogenic road dust
1196 sources where unpaved roads are a substantial dust source. Unpaved areas of parking lots, storage areas, road shoulders,
1197 roadside lawn dust, and winter's effects could be considered, too. During winter's cold and wet conditions, dust accumulates
1198 in snow and ice and the humid road surface texture. As snow and ice melt and street surfaces dry up in spring, high amounts
1199 of dust become available for suspension. For example, in Finland, north of 60°N, a major anthropogenic dust source comes
1200 from sand and gravel uptake for building purposes from ridges formed during the Ice Age. These nonrenewable ridges cover
1201 1.5 million ha. Since 1960, it has been estimated that approximately 40 million tons per year have been utilized (Fig. 211 of
1202 Wahlström et al., 1996). These open-sand areas are visible in aircraft photos and satellite images. In Finland, long-range
1203 transported low latitude dust contributes to the dust amounts, too (e.g., Meinander et al., 2021). Another health-significant
1204 anthropogenic springtime dust source is wintertime pavement traction sanding (Kuhns et al., 2010; Kupiainen, 2007;
1205 Stojiljkovic et al., 2019). These springtime dust events are annual but local throughout the country. In comparison, the Moscow
1206 metropolitan area (55°45'N, 37°37'E) is one of the most significant sources of dust at latitudes above 50° N, where dust's
1207 impact can extend over several hundred kilometers (Adzhiev et al., 2017). Moscow's road dust is mainly generated on paved
1208 roads, but roadside soils also contribute (Kasimov et al., 2020). Most often, unsealed soils are covered with lawns and are
1209 widespread in parks and recreational and industrial zones, characterized by heavy pollution, mixed upper horizon, and a high
1210 degree of soil cover heterogeneity.

1211 This paper aimed to contribute beyond the state-of-the-art of HLD sources by focusing on collecting and providing information
1212 on the geographical distribution of dust-productive soils and potential dust sources. This is some of the most important

1213 information that is currently lacking but is necessary to perform successful long-range transport and deposition modeling. The
1214 information on the geographical distribution of dust-productive soils needs evidence and verification on detected dust events
1215 and is insufficient alone. Therefore, the paper focused on identifying new dust sources, clarifying their climatic and
1216 environmental importance, and using emission, long-range transport and deposition modeling to study where the potential
1217 impact areas of the HLD sources are.

1218 Icelandic sources have shown that each source, even if nearby, may have different particle size distributions and optical
1219 properties. A detailed specification of the geographic distribution of potential dust productive soils, verified dust sources, and
1220 their physical (e.g., particle size distribution, optics, etc.) and mineralogical/chemical (e.g., mineral fractions, chemical
1221 composition, etc.) properties can contribute to the various topics: predicting dust forecasts (e.g., health protection warnings
1222 during extreme events); long-range emission, transport and deposition modeling; dust monitoring control; understanding
1223 extreme and rare events; Arctic protection; aviation control; health; tourist boards; assessing climate, environment, and air
1224 quality (e.g., Arctic Council Arctic Monitoring and Assessment Program AMAP, and Intergovernmental Panel on Climate
1225 Change IPCC reports); and implementing HLD in calculations on direct and indirect radiative forcing, including cloud
1226 formation, cryospheric effects, and modeling the impacts. The new observations in this study improved the representation of
1227 HLD sources for various approaches and applications related to the observed current, previous, and future environmental
1228 changes at high latitudes.

1229 In summary, establishing continuous monitoring of HLD sources and their future changes is key to understanding the climatic
1230 and environmental effects at high latitudes, especially in the Arctic. Climate change causes permafrost thaw, decreases snow
1231 cover duration, and increases drought, glacial melt, and heatwave intensity and frequency – all leading to increasing the
1232 frequency of topsoil conditions favorable for dust emission (increasing soil's exposure to wind erosion) and the probability of
1233 dust storms. Although dust originates from natural soils, dust sources are also influenced by human activities, e.g., when
1234 deforestation and land management in cold regions leads to ecosystem collapse and desertification (Prospero et al., 2012;
1235 Arnalds, 2015). Dust storms from agricultural fields (as reported, e.g., in Poland) can reach distances over 300 km, drastically
1236 reducing visibility and resulting in hundreds of car accidents and fatalities (Hojan et al., 2019). Whether natural or
1237 anthropogenic, wildfires can result from new dust sources also (Miller et al., 2012). Hence, human actions can positively and
1238 negatively influence HLD and its effects. To understand and assess the temporal activity changes in HLD sources and the
1239 multiple impacts of high-latitude dust on the Earth systems over time, continuous monitoring and regular updates on location,
1240 particle properties, and activities of current and new HLD sources are needed.

1241

1242

1243

1244 **Competing interests.** The authors declare they have no conflict of interest.

1245 **Special issue statement.** This article is part of the special issue “Arctic climate, air quality, and health impacts from short-
1246 lived climate forcers (SLCFs): contributions from the AMAP Expert Group (ACP/BG inter-journal SI)”. It is not associated
1247 with a conference.

1248 **Acknowledgements**

1249 This paper was developed as part of the Arctic Monitoring and Assessment Programme (AMAP), AMAP 2021 assessment:
1250 Arctic climate, air quality, and health impacts from short-lived climate forcers (SLCFs). Kaarle Kupiainen, Johanna
1251 Ikävalko, and Terhikki Manninen are gratefully acknowledged. The staff’s help regarding the stations is highly appreciated.

1252 **Financial support**

1253 This research has been supported by the Ministry for Foreign Affairs of Finland (IBA-project No. PC0TQ4BT-25). The study
1254 of dust composition in Moscow and Tiksi was supported by the Russian Science Foundation (No. 19-77-30004). Firn cores
1255 collection on southern Spitsbergen, Svalbard, has been co-funded by the Research Council of Norway, Arctic Field Grant 2018
1256 (No. 282538), funds of the Leading National Research Centre (KNOW) received by the Centre for Polar Studies of the
1257 University of Silesia, and statutory activities No. 3841/E-41/S/2018 of the Ministry of Science and Higher Education of Poland.
1258 The Czech Science Foundation projects 20-06168Y, GA20-20240S, and the Ministry of Education, Youth and Sports of the
1259 Czech Republic projects No. LM2015078 and CZ.02.1.01/0.0/0.0/16_013/0001708 are acknowledged. The support of the
1260 EPOS-PL project (No. POIR.04.02.00-14-A003/16), co-financed by the European Union from the funds of the European
1261 Regional Development Fund (ERDF) to the laboratory facilities at IG PAS used in the study, is also acknowledged. European
1262 Union COST Action InDust is acknowledged. The preparation of this paper was partially funded by the Icelandic Research
1263 Fund (Rannis) Grant No. 207057-051. O. Meinander acknowledges funding from the Academy of Finland (ACCC Flagship
1264 funding grant No. 337552 and BBrCAC No. 341271), H2020 EU-Interact (No. 730938), International Arctic Science
1265 Committee (IASC Cross-Cutting grant), and the Ministry for Foreign Affairs of Finland (IBA-project No. PC0TQ4BT-20). D.
1266 Frolov is thankful to Lomonosov Moscow State University (state topic “Danger and risk of natural processes and phenomena”
1267 No. 121051300175-4). K. Kandler was funded by the Deutsche Forschungsgemeinschaft (DFG, German Research Foundation
1268 No. 264912134, 416816480, 417012665N). J. King acknowledges NSERC Discovery 2016-05417, CFI 36564, and the CMN
1269 RES00044975. B. Murray, A. Sanchez-Marroquin, and S. Barr thank the European Research Council (648661 MarineIce) and
1270 the Natural Environment Research Council (NE/T00648X/1; NE/R006687/1). O. Möhler and N.S. Umo acknowledge the
1271 funding support from Helmholtz Association of German Research Centres through its ‘Changing Earth — Sustaining our
1272 Future’ Programme. M. Kulmala, N.S. Kasimov, and O. Popovicheva acknowledge funding from the Russian Ministry of
1273 Education and Science (075-15-2021-574). K. Ranjbar and N.T. O’Neill acknowledge the PAHA project (NSERC-CCAR

1274 program; RGPCC-433842-2012), the SACIA project (CSA-ESSDA program; 16UASACIA), and the NSERC DG grants of
1275 O’Neill (RGPIN-05002-2014). I. Semenov, O. Popovicheva, and N. Kasimov acknowledge funding from the M.V.
1276 Lomonosov Moscow State University (the Interdisciplinary Scientific and Educational School «Future Planet and Global
1277 Environmental Change» and project No. 121051400083-1). Z. Shi and C. Baldo are funded by the UK Natural Environment
1278 Research Council (NE/L002493/1; NE/S00579X).

1279

1280 **Supplement**

1281 The supplement related to this article is available online at:

1282

1283 **Data availability**

1284 Data are mostly included in this article or available on request via personal communication.

1285

1286 **Author contribution**

1287 The paper was initiated and lead by O. Meinander. P. Dagsson-Waldhauserová co-coordinated and edited. HLD SI and area
1288 calculations were by A. Vukovic and B. Cvetkovic. New HLD sources were identified as follows: Alaska, Canada: S. Barr, P.
1289 Dagsson-Waldhauserová, P., S. Gassó, J. King, B.J. Murray, J.B. McQuaid, N.T. O’Neill, K. Ranjbar. Antarctica: P. Dagsson-
1290 Waldhauserová, J. Kavan, K. Láska, O. Meinander, E. Shevnina. Denmark and Sweden: O. Meinander. Greenland: A.
1291 Baklanov, L.G. Benning, P. Dagsson-Waldhauserová, S. Gassó. Iceland: T. Thorsteinsson. Russia: P. Amosov, A. Baklanov,
1292 P. Enchilik, T. Koroleva, V. Krupskaya, O. Popovicheva, A. Sharapova, I. Semenov, M. Timofeev. Svalbard: B. Barzycka,
1293 M. Kusiak, M. Laska, M. Lewandowski, B. Luks, A. Nawrot, T. Werner, K. Kandler, N. S. Umo, B.J. Murray, J.B. McQuaid,
1294 A. Sánchez-Marroquín, O. Möhler. South America, Argentina, and Patagonia: S. Gassó. DREAM model: B. Cvetkovic, S.
1295 Nickovic. SILAM model: A. Uppstu and M. Sofiev. N. Kasimov, E. Aseyeva, and O. Samonova contributed supplementary
1296 material on the central part of European Russia (potential dust source). Dust and clouds: B.J. Murray and A. Sánchez-
1297 Marroquín. Dust and ocean biogeochemistry: Z. Shi and C. Baldo. Dust and atmospheric chemistry: F. Thevenet, M.N.
1298 Romanias, J.Lasne, D. Urupina. Dust and cryosphere: O. Meinander. All authors contributed significantly to preparing the
1299 manuscript.

1300

1301 **References**

1302 Abbatt, J. P. D., Leaitch, W. R., Aliabadi, A. A., Bertram, A. K., Blanchet, J.-P., Boivin-Rioux, A., Bozem, H., Burkart, J.,
1303 Chang, R. Y. W., Charette, J., Chaubey, J. P., Christensen, R. J., Cirisan, A., Collins, D. B., Croft, B., Dionne, J., Evans, G. J.,
1304 Fletcher, C. G., Galí, M., Ghahremaninezhad, R., Girard, E., Gong, W., Gosselin, M., Gourdal, M., Hanna, S. J., Hayashida,

1305 H., Herber, A. B., Hesaraki, S., Hoor, P., Huang, L., Husserr, R., Irish, V. E., Keita, S. A., Kodros, J. K., Köllner, F., Kolonjari,
1306 F., Kunkel, D., Ladino, L. A., Law, K., Levasseur, M., Libois, Q., Liggio, J., Lizotte, M., Macdonald, K. M., Mahmood, R.,
1307 Martin, R. V., Mason, R. H., Miller, L. A., Moravek, A., Mortenson, E., Mungall, E. L., Murphy, J. G., Namazi, M., Norman,
1308 A.-L., O'Neill, N. T., Pierce, J. R., Russell, L. M., Schneider, J., Schulz, H., Sharma, S., Si, M., Staebler, R. M., Steiner, N. S.,
1309 Thomas, J. L., von Salzen, K., Wentzell, J. J. B., Willis, M. D., Wentworth, G. R., Xu, J.-W., and Yakobi-Hancock, J. D.:
1310 Overview paper: New insights into aerosol and climate in the Arctic, *Atmos. Chem. Phys.*, 19, 2527–2560, doi:10.5194/acp-
1311 19-2527-2019, 2019.

1312 Achterberg, E. P., Moore, C. M., Henson, S. A., Steigenberger, S., Stohl, A., Eckhardt, S., Avendano, L. C., Cassidy, M.,
1313 Hembury, D., Klar, J. K., Lucas, M. I., Macey, A. I., Marsay, C. M., and Ryan-Keogh, T. J.: Natural iron fertilization by the
1314 Eyjafjallajökull volcanic eruption, *Geophysical Research Letters*, 40, 921-926, doi: 10.1002/grl.50221, 2013.

1315 Achterberg, E. P., Steigenberger, S., Marsay, C. M., LeMoigne, F. A. C., Painter, S. C., Baker, A. R., Connelly, D. P., Moore,
1316 C. M., Tagliabue, A., and Tanhua, T.: Iron Biogeochemistry in the High Latitude North Atlantic Ocean, *Scientific Reports*, 8,
1317 doi: 10.1038/s41598-018-19472-1, 2018.

1318 Adzhiev, A. H., Bartalyov, S. A., Bekkiev, M. Y., Biryukov, M. V., Biryukova, O. N., Bitjukova, V. R., Bobilev, S. N.,
1319 Bogdanova, M. D., Bozhilina, E. A., Bronnikova, V. K., et al.: Ecological atlas of Russia, Feoria, Moscow, 510 p., 2017.

1320 AMAP: Black Carbon and Ozone as Arctic Climate Forcers. Arctic Monitoring and Assessment Programme (AMAP), Oslo,
1321 116, 2015.

1322 Amino, T., Y. Iizuka, S. Matoba, R. Shimada, N. Oshima, T. Suzuki, T. Ando, T. Aoki, and K. Fujita: Increasing dust emission
1323 from ice free terrain in southeastern Greenland since 2000, *Polar Science*, 100599, doi:10.1016/j.polar.2020.100599, 2020.

1324 Amosov P.V. and Baklanov A.A.: Assessment of dusting intensity on ANOF-2 tailing by using a Westphal D.L. dependency
1325 // Proceedings of the X International Symposium on Recycling Technologies and Sustainable Development, 4-7 November
1326 2015, Bor, Serbia. – Bor: University of Belgrade, Technical Faculty, 39-43, 2015.

1327 Anderson, N. J., J. E. Saros, J. E. Bullard, S. M. P. Cahoon, S. McGowan, E. A. Bagshaw, C. D. Barry, R. Bindler, B. T.
1328 Burpee, J. L. Carrivick, et al.: The Arctic in the twenty-first century: Changing biogeochemical linkages across a paraglacial
1329 landscape of Greenland. *BioScience*, 67, 118–133, doi:10.1093/biosci/biw158, 2017.

1330 Antcibor, I., Eschenbach, A., Zubrzycki, S., Kutzbach, L. et al: Trace metal distribution in pristine permafrost-affected soils
1331 of the Lena River delta and its hinterland, northern Siberia, Russia. *Biogeosciences* 11:1–15, 2014.

- 1332 Arnalds O.: *The Soils of Iceland*. World Soils Book Series, Springer, Dordrecht, The Netherlands, 2015.
- 1333 Arnalds, O., Thorarinsdottir, E.F., Thorsson, J., Dagsson-Waldhauserová, P., Agustsdottir, A.M.: An extreme wind erosion
1334 event of the fresh Eyjafjallajökull 2010 volcanic ash. *Nature Scientific Reports* 3, 1257, 2013.
- 1335 Arnalds, O., Olafsson, H., and Dagsson-Waldhauserová, P.: Quantification of iron-rich volcanogenic dust emissions and
1336 deposition over the ocean from Icelandic dust sources, *Biogeosciences*, 11, 6623-6632, doi: 10.5194/bg-11-6623-2014, 2014.
- 1337 Arnalds, O., Dagsson-Waldhauserová, P., and Olafsson, H.: The Icelandic volcanic aeolian environment: Processes and
1338 impacts — A review, *Aeolian Res.*, 20, 176-195, doi: 10.1016/j.aeolia.2016.01.004, 2016.
- 1339 Arrigo, K. R., and Van Dijken, G. L.: Interannual variation in air-sea CO₂ flux in the Ross Sea, Antarctica: A model analysis,
1340 *Journal of Geophysical Research-Oceans*, 112, doi: 10.1029/2006jc003492, 2007.
- 1341 Arrigo, K. R., van Dijken, G., and Long, M.: Coastal Southern Ocean: A strong anthropogenic CO₂ sink, *Geophysical Research*
1342 *Letters*, 35, doi: 10.1029/2008gl035624, 2008.
- 1343 Atkins, C.B., and Dunbar, G. B. Aeolian sediment flux from sea ice into Southern McMurdo Sound, Antarctica, *Global and*
1344 *Planetary Change*, 69, 133-141, 2009.
- 1345 Atkinson, J. D., B. J. Murray, M. T. Woodhouse, T. F. Whale, K. J. Baustian, K. S. Carslaw, S. Dobbie, D. O’Sullivan, and T.
1346 L. Malkin, The importance of feldspar for ice nucleation by mineral dust in mixed-phase clouds, *Nature*, 498, 7454, 355-358,
1347 doi:10.1038/nature12278, 2013.
- 1348 Aun, M., Lakkala, K., Sanchez,R., Asmi, E., Nollas, F., Meinander, O., Sogacheva, L., De Bock, V., Arola, A., de Leeuw, G.,
1349 Aaltonen, V., Bolsée, D., Cizkova, K, Mangold, A., Metelka,L., Jakobson, E., Svendby,T., Gillotay, D., and Van Opstal, B.:
1350 Solar UV radiation measurements in Marambio, Antarctica, during years 2017–2019, *Atmos. Chem. Phys.*, 20, 6037–6054,
1351 doi:10.5194/acp-20-6037-2020, 2020.
- 1352 Ayling, B. F. and McGowan, H.A.: Niveo-eolian sediment deposits in coastal South Victoria Land, Antarctica: Indicators of
1353 regional variability in weather and climate, *Arc. Antarct. Alp. Res.*, 38, 3, 313–324, 2006.
- 1354 Bachelder, J., Cadieux, M., Liu-Kang, C., Lambert, P., Filoche, A., Aparecida Galhardi, J., Hadioui, M., Chaput, A., Bastien-
1355 Thibault, M.-P., Wilkinson, K.J., King, J., and Hayes, P.J.: Chemical and microphysical properties of wind-blown dust near
1356 an actively retreating glacier in Yukon, Canada. *Aerosol Science and Technology* 54:1, 2-20, doi:
1357 10.1080/02786826.2019.1676394, 2020.

- 1358 Baddock, M., Mockford, T., Bullard, J.E., and Thorsteinsson, Th.: Pathways of high-latitude dust in the North Atlantic. *Earth*
1359 *and Planetary Science Letters*, 459: 170 – 182. doi: 10.1016/j.epsl.2016.11.034, 2017.
- 1360 Baklanov A. and Rigina O. Environmental modeling of dusting from the mining and concentration sites in the Kola Peninsula,
1361 Northwest Russia. The XI World Clear Air and Environment Congress, 14-18 September 1998, Durban, South Africa,
1362 IUAPPA-NACA. Durban, v. 1, 4F-3, 1-18, 1998.
- 1363 Baklanov, A., A. Mahura, L. Nazarenko, N. Tausnev, A Kuchin, and O. Rigina: Modelling of atmospheric Pollution and
1364 Climate Change in Northern Latitudes. Russian Academy of Sciences, Apatity, Russia, 106 p. Book in Russian,
1365 <https://search.rsl.ru/ru/record/01006534167>, 2012.
- 1366 Baldo, C., Formenti, P., Nowak, S., Chevaillier, S., Cazaunau, M., Pangui, E., Di Biagio, C., Doussin, J.-F., Ignatyev, K.,
1367 Dagsson-Waldhauserová, P., Arnalds, O., MacKenzie, A. R., and Shi, Z.: Distinct chemical and mineralogical composition of
1368 Icelandic dust compared to northern African and Asian dust, *Atmos. Chem. Phys.*, 20, 13521–13539, doi:10.5194/acp-20-
1369 13521-2020, 2020.
- 1370 Baratoux, D., Mangold, N., Arnalds, O., Bardintzeff, J.-M., Platevoët, B., Grégoire, M. and Pinet, P.: Volcanic sands of Iceland
1371 - Diverse origins of aeolian sand deposits revealed at Dyngjúsandur and Lambhraun. *EARTH SURFACE PROCESSES AND*
1372 *LANDFORMS Earth Surf. Process. Landforms*, doi: 10.1002/esp.2201, 2011.
- 1373 Beckett, F., Kylling, A., Sigurðardóttir, G., von Löwis, S., and Witham, C.: Quantifying the mass loading of particles in an ash
1374 cloud remobilized from tephra deposits on Iceland, *Atmos. Chem. Phys.*, 17, 4401-4418, 2017.
- 1375 Bertran P, Bosq, M., Quentin Borderie, Coussot, C., Coutard, S., Deschodt, L., Franc, O., Gardère, P., Liard, M., and Wuscher,
1376 P.: Revised map of European aeolian deposits derived from soil texture data, *Quaternary Science Reviews*, 266, 107085,
1377 doi:10.1016/j.quascirev.2021.107085, 2021.
- 1378 Bhattachan, A., L. Wang, M. F. Miller, K. J. Licht, and P. D’Odorico: Antarctica’s Dry Valleys: A potential source of soluble
1379 iron to the Southern Ocean?, *Geophys. Res. Lett.*, 42, 1912–1918, doi:[10.1002/2015GL063419](https://doi.org/10.1002/2015GL063419), 2015.
- 1380 Bishop, J. K. B., Davis, R. E., and Sherman, J. T.: Robotic observations of dust storm enhancement of carbon biomass in the
1381 North Pacific. *Science*, doi:[10.1126/science.1074961](https://doi.org/10.1126/science.1074961), 2002.
- 1382 Bodas-Salcedo, A., K. D. Williams, M. A. Ringer, I. Beau, J. N. S. Cole, J. L. Dufresne, T. Koshiro, B. Stevens, Z. Wang, and
1383 T. Yokohata: Origins of the Solar Radiation Biases over the Southern Ocean in CFMIP2 Models, *J. Clim.*, 27, 1, 41-56,
1384 doi:10.1175/jcli-d-13-00169.1, 2014.

1385 Bond, T. C., Doherty, S. J., Fahey, D. W., Forster, P. M., Bernsten, T., DeAngelo, B. J., et al.: Bounding the role of black
1386 carbon in the climate system: a scientific assessment. *J. Geophys. Res. Atmos.* 188, 5380–5552, doi: 10.1002/jgrd.50171,
1387 2013.

1388 Boy, M., Thomson, E. S., Acosta Navarro, J.-C., Arnalds, O., Batchvarova, E., Bäck, J., Berninger, F., Bilde, M., Brasseur,
1389 Z., Dagsson-Waldhauserová, P., Castarède, D., Dalirian, M., de Leeuw, G., Dragosics, M., Duplissy, E.-M., Duplissy, J.,
1390 Ekman, A. M. L., Fang, K., Gallet, J.-C., Glasius, M., Gryning, S.-E., Grythe, H., Hansson, H.-C., Hansson, M., Isaksson, E.,
1391 Iversen, T., Jonsdottir, I., Kasurinen, V., Kirkevåg, A., Korhola, A., Krejci, R., Kristjansson, J. E., Lappalainen, H. K., Lauri,
1392 A., Leppäranta, M., Lihavainen, H., Makkonen, R., Massling, A., Meinander, O., Nilsson, E. D., Olafsson, H., Pettersson, J.
1393 B. C., Prisle, N. L., Riipinen, I., Roldin, P., Ruppel, M., Salter, M., Sand, M., Seland, Ø., Seppä, H., Skov, H., Soares, J., Stohl,
1394 A., Ström, J., Svensson, J., Swietlicki, E., Tabakova, K., Thorsteinsson, T., Virkkula, A., Weyhenmeyer, G. A., Wu, Y., Zieger,
1395 P., and Kulmala, M.: Interactions between the atmosphere, cryosphere, and ecosystems at northern high latitudes, *Atmos.*
1396 *Chem. Phys.*, 19, 2015–2061, <https://doi.org/10.5194/acp-19-2015-2019>, 2019.

1397 Boyd, P. W., Jickells, T., Law, C. S., Blain, S., Boyle, E. A., Buesseler, K. O., Coale, K. H., Cullen, J. J., de Baar, H. J. W.,
1398 Follows, M., Harvey, M., Lancelot, C., Levasseur, M., Owens, N. P. J., Pollard, R., Rivkin, R. B., Sarmiento, J., Schoemann,
1399 V., Smetacek, V., Takeda, S., Tsuda, A., Turner, S., and Watson, A. J.: Mesoscale Iron Enrichment Experiments 1993-2005:
1400 Synthesis and Future Directions, *Science*, 315, 612-617, doi: 10.1126/science.1131669, 2007.

1401 Boyd, P. W., Mackie, D. S., and Hunter, K. A.: Aerosol iron deposition to the surface ocean - Modes of iron supply and
1402 biological responses, *Mar. Chem.*, 120, 128-143, doi: 10.1016/j.marchem.2009.01.008, 2010.

1403 Brabets, T P.: Geomorphology of the lower Copper River, Alaska I by Timothy P. Brabets, U.S. Geological Survey
1404 professional paper, 1581, <https://pubs.usgs.gov/pp/1581/report.pdf>, 1997.

1405 Brédoire, F., Bakker, M.R., Augusto, L., Barsukov, P.A., Derrien, D., Nikitich, P., Rusalimova, O., Zeller, B., Acha, D.L.:
1406 What is the P value of Siberian soils? *Biogeosci Discuss* 12:19819–19859, 2015.

1407 Bullard, J. E.: The distribution and biogeochemical importance of high-latitude dust in the Arctic and Southern Ocean-
1408 Antarctic regions, *Journal of Geophysical Research-Atmospheres*, 122, 3098-3103, doi: 10.1002/2016jd026363, 2016.

1409 Bullard J. and Austin, M.J.: Dust generation on a proglacial floodplain, West Greenland Article in *Aeolian Research* · June
1410 2011, doi: 10.1016/j.aeolia.2011.01.002, 2011.

- 1411 Bullard, J.E. and Mockford, T.: Seasonal and decadal variability of dust observations in the Kangerlussuaq area, west
1412 Greenland, Arctic, Antarctic, and Alpine Research, 50:1, S100011, doi: 10.1080/15230430.2017.1415854, 2018.
- 1413 Bullard, J.E., Harrison, S.P., Baddock, M.C., Drake, N., Gill, T.E., McTainsh, G. and Sun, Y.: Preferential dust sources: A
1414 geomorphological classification designed for use in global dust-cycle models. Journal of Geophysical Research 116, doi:
1415 10.1029/2011JF002061, issn: 0148-0227, 2011.
- 1416 Bullard, J. E., Baddock, M., Bradwell, T., Crusius, J., Darlington, E., Gaiero, D., ... McCulloch, R.: High-latitude dust in the
1417 Earth system. Reviews of Geophysics, 54, 2, 447–485, 2016.
- 1418 Butwin, M.K., Pfeffer, M.A., von Löwis, S., Støren, E., W.N., Bali, E. and Thorsteinsson, T.: Properties of dust source material
1419 and volcanic ash in Iceland, Sedimentology, 67, 6, 3067-3087, doi:10.1111/sed.12734, 2020.
- 1420 Chewings, J., Atkins, C, Dunbar, G., and Golledge, N.: Aeolian sediment transport and deposition in a modern high latitude
1421 glacial marine environment. Sedimentology, v. 61, 6, 1485–1882, doi: 10.1111/sed.12108, 2014.
- 1422 Conca, E., Abollino, O., Giacomino, A., Buoso, S., Traversi, R., Becagli, S., Grotti, M., and Malandrino, M.: Source
1423 identification and temporal evolution of trace elements in PM10 collected near to Ny-Ålesund (Norwegian Arctic), Atmos.
1424 Environ., 203, 153–165, doi:10.1016/j.atmosenv.2019.02.001, 2019.
- 1425 Coronato, A., Mazzoni, E., Vázquez, M., and Coronato, F.: PATAGONIA Una síntesis de su Geografía Física (Ediciones).
1426 Río Gallegos, Argentina: Universidad Nacional de la Patagonia Austral. Retrieved from
1427 [http://www.unpa.edu.ar/sites/default/files/publicaciones_adjuntos/PATAGONIA_una_sintesis_de_su_geografia_fisica](http://www.unpa.edu.ar/sites/default/files/publicaciones_adjuntos/PATAGONIA_una_sintesis_de_su_geografia_fisica_web_0.pdf)
1428 [web_0.pdf](http://www.unpa.edu.ar/sites/default/files/publicaciones_adjuntos/PATAGONIA_una_sintesis_de_su_geografia_fisica_web_0.pdf), 2017.
- 1429 Cosentino, N. J., Ruiz-Etcheverry, L. A., Bia, G. L., Simonella, L. E., Coppo, R., Torre, G., et al. Does Satellite Chlorophyll-
1430 a Respond to Southernmost Patagonian Dust? A Multi-year, Event-Based Approach. Journal of Geophysical Research:
1431 Biogeosciences, 125, 12, doi:10.1029/2020JG006073, 2020.
- 1432 Creamean, J.M., Suski, K.J., Rosenfeld, D., Cazorla, A., DeMott, P.J., Sullivan, R.C., White, A.B., Ralph, F.M., Minnis, P.,
1433 Comstock, J.M., Tomlinson, J.M., Prather, K.A.: Dust and biological aerosols from the Sahara and Asia influence precipitation
1434 in the Western U.S., Science, 339, 6127, 1572-1578, doi:10.1126/science.1227279, 2013.
- 1435 Crespi-Abril, A. C., Soria, G., De Cian, A., and López-Moreno, C.: Roaring forties: An analysis of a decadal series of data of
1436 dust in Northern Patagonia. Atmospheric Environment, doi:10.1016/j.atmosenv.2017.11.019, 2017.

- 1437 Crocchianti,S.; Moroni,B.; Waldhauserová, P.D.; Becagli, S.; Severi, M.; Traversi, R.; Cappelletti, D. Potential Source
1438 Contribution Function Analysis of High Latitude Dust Sources over the Arctic: Preliminary Results and Prospects. *Atmosphere*
1439 2021, 12, 347, doi:10.3390/atmos12030347, 2021.
- 1440 Crusius, J.: Dissolved Fe Supply to the Central Gulf of Alaska Is Inferred to Be Derived From Alaskan Glacial Dust That Is
1441 Not Resolved by Dust Transport Models. *Journal of Geophysical Research: Biogeosciences*, 126, 6, e2021JG006323,
1442 doi:10.1029/2021JG006323, 2021.
- 1443 Crusius, J., Schroth, A. W., Gassó, S., Moy, C. M., Levy, R. C., and Gatica, M.: Glacial flour dust storms in the Gulf of Alaska:
1444 Hydrologic and meteorological controls and their importance as a source of bioavailable iron, *Geophysical Research Letters*,
1445 38, doi: 10.1029/2010gl046573, 2011.
- 1446 Crusius, J., Schroth, A. W., Resing, J. A., Cullen, J., and Campbell, R. W. Seasonal and spatial variabilities in northern Gulf
1447 of Alaska surface water iron concentrations driven by shelf sediment resuspension, glacial meltwater, a Yakutat eddy, and
1448 dust. *Global Biogeochemical Cycles*, 31, 6, 942–960, doi:10.1002/2016GB005493, 2017.
- 1449 Csavina, J., Field, J., Taylor, M.P., Gao, S., Landázuri, A., Betterton, E.A., Sáez, A.E.: A review on the importance of metals
1450 and metalloids in atmospheric dust and aerosol from mining operations, *Science of The Total Environment*, 433, 58-73,
1451 doi:10.1016/j.scitotenv.2012.06.013, 2012.
- 1452 Cvetkovic, et al., 2021: Fully dynamic numerical prediction model for dispersion of Icelandic mineral dust (submitted), 2021.
- 1453 Dagsson-Waldhauserová P. and Meinander O.: Editorial: Atmosphere - cryosphere interaction in the Arctic, at high latitudes
1454 and mountains with focus on transport, deposition and effects of dust, black carbon, and other aerosols. *Front. Earth Sci.*, 18
1455 December 2019, <https://doi.org/10.3389/feart.2019.00337>, 2019.
- 1456 Dagsson-Waldhauserová, P. and Meinander, O. (eds.): Atmosphere – Cryosphere Interaction in the Arctic, at High Latitudes
1457 and Mountains With Focus on Transport, Deposition and Effects of Dust, Black Carbon, and Other Aerosols. Lausanne:
1458 Frontiers Media SA. ISSN 1664-8714, ISBN 978-2-88963-504-7, doi: 10.3389/978-2-88963-504-7, e-book, 2020.
- 1459 Dagsson-Waldhauserová, P., O. Arnalds, H. Ólafsson, L. Skrabalova, G. Sigurðardóttir, M. Branis, J. Hladil, R. Skala, T.
1460 Navratil, L. Chadimova, S. Löwis, T. Thorsteinsson, H. Carlsen, I. Jónsdóttir, Physical properties of suspended dust during
1461 moist and low wind conditions in Iceland. *Icelandic Agricultural Sciences* 27, 25-39, 2014.
- 1462 Dagsson-Waldhauserová, P., O. Arnalds, H. Olafsson, J. Hladil, R. Skala, T. Navratil, L. Chadimova, O. Meinander: Snow–
1463 Dust Storm: Unique case study from Iceland, March 6–7, 2013. *Aeolian Res* 16, 69-74, 2015.

- 1464 Dagsson-Waldhauserová P, Magnúsdóttir AÖ, Ólafsson H, Arnalds O: The spatial variation of dust particulate matter
1465 concentrations during two Icelandic dust storms in 2015. *Atmosphere*, 7, 77, 2016.
- 1466 Dagsson-Waldhauserová, P., Renard, J.-B., Ólafsson, H., Vignelles, D., Berthet, G., Verdier, N., Duverger, V.: Vertical
1467 distribution of aerosols in dust storms during the Arctic winter. *Scientific Reports* 6, 1-11, 2019.
- 1468 Dang, C., Warren, S. G., Fu, Q., Doherty, S. J., Sturm, M., and Su, J.: Measurements of light-absorbing particles in snow
1469 across the Arctic, North America, and China: Effects on surface albedo, *J. Geophys. Res. Atmos.*, 122, 10,149– 10,168,
1470 doi:10.1002/2017JD027070, 2017.
- 1471 Diaz, M.A., Welch, S.A., Sheets, J.M., Welch, K.A., Khan, A.L., Adams, B.J., McKnight, D.M., Cary, S.C, W.B, Lyons:
1472 Geochemistry of aeolian material from the McMurdo Dry Valleys, Antarctica: Insights into Southern Hemisphere dust sources.
1473 *Earth and Planetary Science Letters*, 547, doi:10.1016/j.epsl.2020.116460, 2020.
- 1474 Dijkmans, J. W. A., and Törnqvist, T.E.: Modern periglacial eolian deposits and landforms in the Søndre Strømfjord area,
1475 West Greenland and their palaeoenvironmental implications. *Meddelelser Om Grønland Geoscience*, 25, 3–39, 1991.
- 1476 Doody, J.P., Ferreira, M., Lombardo, S., Lucius, I., Misdorp, R., Niesing, H., Salman, A., and Smallegange, M. (eds): Living
1477 with coastal erosion in Europe – sediment and space for sustainability. Results from the EUROSION study, European
1478 Commission, Office for Official Publications of the European Communities. Available at:
1479 http://www.euroSION.org/project/euroSION_en.pdf (last accessed 19 November 2021), 2004.
- 1480 Đorđević Dragana, Tošić Ivana, Sakan Sanja, Petrović Srđan, Đuričić-Milanković Jelena, Finger David C., Dagsson-
1481 Waldhauserová P.: Can Volcanic Dust Suspended From Surface Soil and Deserts of Iceland Be Transferred to Central Balkan
1482 Similarly to African Dust (Sahara)? *Frontiers in Earth Science*, 7, doi:10.3389/feart.2019.00142, 2019.
- 1483 Dragosics, M., Meinander, O., Jonsdóttir, T. et al. Insulation effects of Icelandic dust and volcanic ash on snow and ice,
1484 *Arabian Journal of Geosciences* Volume: 9 Issue: 2, Dust special issue, DOI: 10.1007/s12517-015-2224-6, 2016.
- 1485 Dörnbrack, A., Stachlewska, I. S., Ritter, C., and Neuber, R.: Aerosol distribution around Svalbard during intense easterly
1486 winds, *Atmos. Chem. Phys.*, 10, 1473–1490, <https://doi.org/10.5194/acp-10-1473-2010>, 2010.
- 1487 Evangelidou, N., Shevchenko, V. P., Yttri, K. E., Eckhardt, S., Sollum, E., Pokrovsky, O. S., Kobelev, V. O., Korobov, V. B.,
1488 Lobanov, A. A., Starodymova, D. P., Vorobiev, S. N., Thompson, R. L., and Stohl, A.: Origin of elemental carbon in snow
1489 from western Siberia and northwestern European Russia during winter–spring 2014, 2015 and 2016, *Atmos. Chem. Phys.*, 18,
1490 963–977, <https://doi.org/10.5194/acp-18-963-2018>, 2018.

- 1491 Finlayson-Pitts, B.J. and Pitts, J.N. Jr., Chemistry of the upper and lower atmosphere: theory, experiments, and applications,
1492 Elsevier, 969 p., 1999.
- 1493 Flanner, M. G., Zender, C. S., Randerson, J. T., and Rasch, P. T.: Present day climate forcing and response from black carbon
1494 in snow. *J. Geophys. Res.* 112:D11202. doi: 10.1029/2006JD008003, 2007.
- 1495 Foroutan, H., et al. Development and evaluation of a physics-based windblown dust emission scheme implemented in the
1496 CMAQ modeling system, *J Adv Model Earth Syst.*,9, 1, 585–608, 2017.
- 1497 Forsström, S., Isaksson, E., Skeie, R. B., Ström, J., Pedersen, C. A., Hudson, S. R., Berntsen, T. K., Lihavainen, H.,
1498 Godtlielsen, F. and Gerland, S.: Elemental carbon measurements in European Arctic snow packs, *J. Geophys. Res. Atmos.*,
1499 118, 13,614–13,627, 2013.
- 1500 Fountain, A.G., Levy, J.S., Gooseff, M.N., Van Horn, D: The McMurdo Dry Valleys: A landscape on the threshold of change
1501 (2014). *Geomorphology* 225, 15, P, 25-35, doi:/10.1016/j.geomorph.2014.03.044, 2014.
- 1502 Fox, T. A., Barchyn, T. E. and Hugenholtz, C. H.: Successes of soil conservation in the Canadian Prairies highlighted by a
1503 historical decline in blowing dust, *Environ. Res. Lett.*, 7, 1, doi:10.1088/1748-9326/7/1/014008, 2012.
- 1504 Frey, W. R., and J. E. Kay: The influence of extratropical cloud phase and amount feedbacks on climate sensitivity, *Climate*
1505 *Dynamics*, 50, 7, 3097-3116, doi:10.1007/s00382-017-3796-5, 2018.
- 1506 Gaiero, D. M., Probst, J.-L., Depetris, P. J., Bidart, S. M., and Leleyter, L.: Iron and other transition metals in Patagonian
1507 riverborne and windborne materials: geochemical control and transport to the southern South Atlantic Ocean. *Geochimica et*
1508 *Cosmochimica Acta*, 67, 19, 3603–3623, doi:10.1016/S0016-7037(03)00211-4, 2003.
- 1509 Gaitán, J. J., López, C. R., and Bran, D.: Efectos del pastoreo sobre el suelo y la vegetación en la estepa patagónica. *Ci. Suelo*
1510 (Argentina), 27, 2, 261–270, 2009.
- 1511 Gallet, J.-C., Björkman, M. P., Larose, C., Luks, B., Martma, T., and Zdanowicz, C.: Protocols and recommendations for the
1512 measurement of snow physical properties, and sampling of snow for black carbon, water isotopes, major ions and
1513 microorganisms, *Norsk Polarinstitut*, 27 p., 2018.
- 1514 Gardner, A. S. and Sharp, M. J.: A review of snow and ice albedo and the development of a new physically based broadband
1515 albedo parameterization, *J. Geophys. Res.*, 115, F01009, doi: 10.1029/2009JF001444, 2010.

1516 Gassó, S., twitter.com/SanGassó, 2 Gassó, Santiago (@SanGassó). "Sunrise in Alaska and more #highlatitudedust is visible
1517 in Larsen Bay, just downwind from the Ten Thousand Smokes Valley in @KatmaiNPS, visible in webcams and early GOES17
1518 image." Nov 2, 2020 , Tweet, <https://twitter.com/SanGassó/status/1323716227793997824?>, 2020a.

1519 Gassó, Santiago (@SanGassó). "More #highlatitudedust today in #Alaska , 3 active sources identified in #NOAA20. Surface
1520 webcams confirm dust presence." Nov 2, 2020 , Twitter. <https://twitter.com/SanGassó/status/1323384615344640000>, 2020b.

1521 Gassó, Santiago (@SanGassó). "#highlatitudedust in SE Alaska yesterday several plumes are visible in the spots where there
1522 is little snow " Jan, 27, 2021. Twitter. <https://twitter.com/SanGassó/status/1354548215186644993021>, 2021a.

1523 Gassó, S., twitter.com/SanGassó, 2 Gassó, Santiago (@SanGassó), "A very nice example of #highlatitudedust activity in
1524 western #Greenland", Oct 19, 2021, <https://twitter.com/SanGassó/status/1450468551379329029>, 2021b.

1525 Gassó, S., and Stein, A. F.: Does dust from Patagonia reach the sub-Antarctic Atlantic Ocean? *Geophysical Research Letters*,
1526 34, 1, L01801. <https://doi.org/10.1029/2006GL027693>, 2007.

1527 Gassó, S., and Torres, O.: Temporal Characterization of Dust Activity in the Central Patagonia Desert (Years 1964–2017).
1528 *Journal of Geophysical Research: Atmospheres*, 124, 6, 3417–3434, [doi:10.1029/2018JD030209](https://doi.org/10.1029/2018JD030209), 2019.

1529 Gassó, S., Stein, A., Marino, F., Castellano, E., Udisti, R., and Ceratto, J.: A combined observational and modeling approach
1530 to study modern dust transport from the Patagonia desert to East Antarctica. *Atmospheric Chemistry and Physics*, 10, 17,
1531 8287–8303, [doi:10.5194/acp-10-8287-2010](https://doi.org/10.5194/acp-10-8287-2010), 2010.

1532 George, C., Ammann, M., D'Anna, B., Donaldson, D. J., Nizkorodov, S A.: Heterogeneous Photochemistry in the Atmosphere.
1533 *Chem. Rev.* 115, 4218-4258, doi: 10.1021/cr500648z, 2015.

1534 Gili, S., Vanderstraeten, A., Chaput, A., King, J., Gaiero, D., Delmonte, B., Vallelonga, P., Formenti, P., Di Biagio, C.,
1535 Cazanau, M. and Pangui, E.: Southern Africa: The Missing Piece To The Dust Provenance Puzzle of East Antarctica?
1536 *Communications Earth & Environment*, doi: 10.21203/rs.3.rs-923449/v1, 2021.

1537 Gillies, J. A., W. G. Nickling, and M. Tilson: Frequency, magnitude and characteristics of aeolian sediment transport:
1538 McMurdo Dry Valleys, Antarctica, *J. Geophys. Res. Earth Surf.*, 118, 461–479, doi:[10.1002/jgrf.20007](https://doi.org/10.1002/jgrf.20007).2013.

1539 Ginoux, P., J. M. Prospero, T. E. Gill, N. C. Hsu, M. Zhao: Global-scale attribution of anthropogenic and natural dust
1540 sources and their emission rates based on MODIS Deep Blue aerosol products. *Rev. Geophys.* 50, RG3005, 2012.

- 1541 Groot Zwaaftink, C. D., Grythe, H., Skov, H., and Stohl, A.: Substantial contribution of northern high-latitude sources to
1542 mineral dust in the Arctic, *Journal of Geophysical Research-Atmospheres*, 121, 13678-13697, doi: 10.1002/2016jd025482,
1543 2016.
- 1544 Groot Zwaaftink, C. D., Arnalds, O., Dagsson-Waldhauserová, P., Eckhardt, S., Prospero, J. M., and Stohl, A.: Temporal and
1545 spatial variability of Icelandic dust emission and atmospheric transport, *Atmos. Chem. Phys.*, 17, 10865-10878, 2017.
- 1546 Gunnarsson, A., Gardarsson, S. M., Pálsson, F., Jóhannesson, T., and Sveinsson, Ó. G. B.: Annual and interannual variability
1547 and trends of albedo for Icelandic glaciers. *The Cryosphere* 15, 547–570, 2020.
- 1548 Hadley, D., G. L. Hufford, and J. J. Simpson: Resuspension of relic volcanic ash and dust from Katmai: Still an aviation
1549 hazard, *Weather Forecast.*, 19, 5, 829–840, doi:10.1175/1520-0434(2004)019<0829:RORVAA>2.0.CO;2, 2004.
- 1550 Hadley, O., and Kirchstetter, T.: Black-Carbon reduction of snow albedo. *Nat. Clim. Change* 2, 437–440. doi:
1551 10.1038/nclimate1433, 2012.
- 1552 Hardy M. and Cornu S. Location of natural trace elements in silty soils using particle-size fractionation. *Geoderma*, 133, 295-
1553 308, doi:10.1016/j.geoderma.2005.07.015, 2006.
- 1554 Harrison, A. D., K. Lever, A. Sanchez-Marroquin, M. A. Holden, T. F. Whale, M. D. Tarn, J. B. McQuaid, and B. J. Murray:
1555 The ice-nucleating ability of quartz immersed in water and its atmospheric importance compared to K-feldspar, *Atmos. Chem.*
1556 *Phys.*, 19, 17, 11343-11361, doi:10.5194/acp-19-11343-2019, 2019.
- 1557 Hedding DW, Werner Nel, Ryan L. Anderson, Aeolian processes and landforms in the sub-Antarctic: preliminary observations
1558 from Marion Island, *Polar Research*, 34, 1, 26365, doi:10.3402/polar.v34.26365, 2015.
- 1559 Heindel RC, Lauren E Culler, Ross A Virginia, Rates and processes of aeolian soil erosion in West Greenland, *The Holocene*,
1560 27,9, 1281-1290, doi:10.1177/0959683616687381, 2017.
- 1561 Hernández, M. A., González, N., and Hernández, L.: Late Cenozoic Geohydrology of Extra-Andean Patagonia, Argentina. In
1562 J. Rabassa (Ed.), *The Late Cenozoic of Patagonia and Tierra del Fuego*, Vol. 11, 497–509, Elsevier, doi:10.1016/S1571-
1563 0866(07)10024-5, 2008.
- 1564 Hobbs, W. H.: Wind: The dominant transportation agent within extramarginal zones to continental glaciers. *The Journal of*
1565 *Geology*, 50, 5, 556–59, doi:10.1086/625072, 1942.

1566 Hojan, M., Rurek, M., Więclaw, M., and Krupa, A.: Effects of Extreme Dust Storm in Agricultural Areas (Poland, the Greater
1567 Lowland). *Geosciences*, 9, 106, doi:10.3390/geosciences9030106, 2019.

1568 Hugenholtz, C. H. and Wolfe, S. A.: Rates and environmental controls of aeolian dust accumulation, Athabasca River
1569 Valley, Canadian Rocky Mountains, *Geomorphology*, 121, 3, 274–282, doi:10.1016/j.geomorph.2010.04.024, 2010.

1570 IPCC, 2013: *Climate Change 2013: The Physical Science Basis. Contribution of Working Group I to the Fifth Assessment*
1571 *Report of the Intergovernmental Panel on Climate Change* [Stocker, T.F., D. Qin, G.-K. Plattner, M. Tignor, S.K. Allen, J.
1572 Boschung, A. Nauels, Y. Xia, V. Bex and P.M. Midgley (eds.)]. Cambridge University Press, Cambridge, United Kingdom
1573 and New York, NY, USA, 1535 p., 2013.

1574 IPCC, 2019: *IPCC Special Report on the Ocean and Cryosphere in a Changing Climate* [H.-O. Pörtner, D.C. Roberts, V.
1575 Masson-Delmotte, P. Zhai, M. Tignor, E. Poloczanska, K. Mintenbeck, A. Alegria, M. Nicolai, A. Okem, J. Petzold, B. Rama,
1576 N.M. Weyer (eds.)]. In press. (last accessed 19 November 2021), 2019.

1577 IPCC, 2021: *Climate Change 2021: The Physical Science Basis. Contribution of Working Group I to the Sixth Assessment*
1578 *Report of the Intergovernmental Panel on Climate Change* [Masson-Delmotte, V., P. Zhai, A. Pirani, S.L. Connors, C. Péan,
1579 S. Berger, N. Caud, Y. Chen, L. Goldfarb, M.I. Gomis, M. Huang, K. Leitzell, E. Lonnoy, J.B.R. Matthews, T.K. Maycock,
1580 T. Waterfield, O. Yelekçi, R. Yu, and B. Zhou (eds.)]. Cambridge University Press. In Press, (last accessed 19 November
1581 2021), 2021.

1582 Irish, V. E., et al.: Ice nucleating particles in the marine boundary layer in the Canadian Arctic during summer 2014, *Atmos.*
1583 *Chem. Phys.*, 19, 2, 1027-1039, doi:10.5194/acp-19-1027-2019, 2019.

1584 Ito, A., and Kok, J. F.: Do dust emissions from sparsely vegetated regions dominate atmospheric iron supply to the Southern
1585 Ocean?, *Journal of Geophysical Research-Atmospheres*, 122, 3987-4002, doi: 10.1002/2016jd025939, 2017.

1586 IUSS Working Group WRB: *World Reference Base for Soil Resources 2014, update 2015 International soil classification*
1587 *system for naming soils and creating legends for soil maps. World Soil Resources Reports No. 106. FAO, Rome, 2015.*

1588 Jacobi, H.-W., Obleitner, F., Da Costa, S., Ginot, P., Eleftheriadis, K., Aas, W., and Zanatta, M.: Deposition of ionic species
1589 and black carbon to the Arctic snowpack: combining snow pit observations with modeling, *Atmos. Chem. Phys.*, 19, 10361–
1590 10377, <https://doi.org/10.5194/acp-19-10361-2019>, 2019.

1591 Janjic Z. I., J. P. Gerrity, Jr. and S. Nickovic: An Alternative Approach to Nonhydrostatic Modeling, *Mon. Wea. Rev.*, 129,
1592 1164-1178, 2001.

- 1593 Jickells, T., and Moore, C. M.: The importance of Atmospheric Deposition for Ocean Productivity, *Annu. Rev. Ecol. Evol.*
1594 *Syst.*, 46, 481-501, doi: 10.1146/annurev-ecolsys-112414-054118, 2015.
- 1595 Jickells, T. D., An, Z. S., Andersen, K. K., Baker, A. R., Bergametti, G., Brooks, N., Cao, J. J., Boyd, P. W., Duce, R. A.,
1596 Hunter, K. A., Kawahata, H., Kubilay, N., laRoche, J., Liss, P. S., Mahowald, N., Prospero, J. M., Ridgwell, A. J., Tegen, I.,
1597 and Torres, R.: Global iron connections between desert dust, ocean biogeochemistry, and climate, *Science*, 308, 67-71, doi:
1598 10.1126/science.1105959, 2005.
- 1599 Johnson, M. S., Meskhidze, N., Kiliyanpilakkil, V. P., and Gassó, S.: Understanding the transport of Patagonian dust and its
1600 influence on marine biological activity in the South Atlantic Ocean. *Atmospheric Chemistry and Physics*, 11, 6, 2487–2502,
1601 2011.
- 1602 Kanakidou, M., Myriokefalitakis, S., and Tsigaridis, K.: Aerosols in atmospheric chemistry and biogeochemical cycles of
1603 nutrients, *Environmental Research Letters*, 13, doi: 10.1088/1748-9326/aabcbd, 2018.
- 1604 Kandler, K.; Schneiders, K.; Heuser, J.; Waza, A.; Aryasree, S.; Althausen, D.; Hofer, J.; Abdullaev, S.F.; Makhmudov, A.N.
1605 Differences and Similarities of Central Asian, African, and Arctic Dust Composition from a Single Particle Perspective.
1606 *Atmosphere* 2020, 11, 269. [doi:10.3390/atmos11030269](https://doi.org/10.3390/atmos11030269), 2020.
- 1607 Kasimov, N. S., Vlasov, D. V., and Kosheleva, N. E.: Enrichment of road dust particles and adjacent environments with metals
1608 and metalloids in eastern Moscow, *Urban Clim.*, 32, 100638, doi:10.1016/j.uclim.2020.100638, 2020.
- 1609 Kavan, J., Ondruch J, Nývlt D, Hrbáček F, Carrivick JL, Láska K.: Seasonal hydrological and suspended sediment transport
1610 dynamics in proglacial streams, James Ross Island, Antarctica. *Geografiska Annaler: Series A, Physical Geography* 99, 38-
1611 55, doi: 10.1080/04353676.2016.1257914, 2017.
- 1612 Kavan, J., Dagsson-Waldhauserová P, Renard JB, Láska K, Ambrožová, K.: Aerosol concentrations in relationship to local
1613 atmospheric conditions on James Ross Island, Antarctica. *Frontiers in Earth Science* 6: DOI: 10.3389/feart.2018.00207, 2018.
- 1614 Kavan, J., Kamil Láska K, Adam Nawrot A, and Tomasz Wawrzyniak T.: High Latitude Dust Transport Altitude Pattern
1615 Revealed from Deposition on Snow, Svalbard. *Atmosphere* 2020, 11, 1318; doi:10.3390/atmos11121318., 2020a.
- 1616 Kavan, J, Nývlt D, Láska K, Engel Z, Kňázková M.: High latitude dust deposition in snow on glaciers of James Ross Island,
1617 Antarctica. *Earth Surface Processes and Landforms*. DOI: 10.1002/esp.4831, 2020b.

- 1618 Khan, A. L., Dierssen, H., Schwarz, J. P., Schmitt, C., Chlus, A., Hermanson, M., Painter, T. H., and McKnight, D. M.: Impacts
1619 of coal dust from an active mine on the spectral reflectance of Arctic surface snow in Svalbard, Norway, *J. Geophys. Res.*,
1620 122, 1767–1778, doi:10.1002/2016jd025757, 2017.
- 1621 Kňažková, M., Hrbáček, F., Kavan, J., Nývlt, D. Effect of hyaloclastite breccia boulders on meso-scale periglacial-aeolian
1622 landsystem in semi-arid Antarctic environment, James Ross Island, Antarctic Peninsula. *Cuadernos de Investigación*
1623 *Geográfica*. doi: 10.18172/cig.3800, 2020.
- 1624 Koroleva, T. V., Krechetov, P. P., Semenov, I. N., Sharapova, A. V. and Kondrat'ev, A. D.: Transformation of chemical
1625 composition of snow in the impact areas of the first stage of the expandable launch system Proton in Central Kazakhstan, *Russ.*
1626 *Meteorol. Hydrol.*, 41(8), 585–591, doi:10.3103/S1068373916080094, 2016.
- 1627 Koroleva, T. V., Sharapova, A. V. and Krechetov, P. P.: A chemical composition of snow on areas exposed to space-rocket
1628 activities pollution (Altai republic), *Gig. i Sanit.*, doi:10.1882/0016-9900-2017-96-5-432-437, 2017.
- 1629 Kuhlman, H.: Den potentielle jordfygning på danske marker. Teoretiske beregninger vedrørende jordmaterialets
1630 vindbevægelighed. *Geografisk Tidsskrift - Danish Journal of Geography*, 59. Retrieved from
1631 <https://tidsskrift.dk/geografisktidskrift/article/view/46533>, 1960.
- 1632 Kuhns, H., Gillies, J., Etyemezian, V., Nikolich, G., King, J., Zhu, D., Uppapalli, S., Engelbrecht, J., and Kohl, S.: Effect of
1633 Soil Type and Momentum on Unpaved Road Particulate Matter Emissions from Wheeled and Tracked Vehicles. *Aerosol*
1634 *Science and Technology - AEROSOL SCI TECH.*, 44, 187-196, doi:10.1080/02786820903516844, 2010.
- 1635 Kupiainen K.: Road dust from pavement wear and traction sanding. *Monographs of the Boreal Environment Research*,
1636 No. 26, [Mono_26.indd \(helsinki.fi\)](#), 2007.
- 1637 Kupiainen, K., Ritola, R., Stojiljkovic, A., Pirjola, L., Malinen, A., and Niemi, J. Contribution of mineral dust sources to street
1638 side ambient and suspension PM10 samples. *Atmospheric Environment*, 147, 178-189. doi:10.1016/j.atmosenv.2016.09.059,
1639 2016.
- 1640 Kylling A., Groot Zwaaftink, C. D., and Stohl, A.: Mineral dust instantaneous radiative forcing in the Arctic. *Geophysical*
1641 *Research Letters*, 45, 4290–4298. doi:10.1029/2018GL077346, 2018.
- 1642 Lamy, F., Gersonde, R., Winckler, G., Esper, O., Jaeschke, A., Kuhn, G., Ullermann, J., Martinez-Garcia, A., Lambert, F.,
1643 Kilian, R.: Increased dust deposition in the Pacific Southern Ocean during glacial periods. *Science*, 343, 403–407, 2014.

- 1644 Lancaster, N., Nickling, W.G. and Gillies, J.A.: Sand transport by wind on complex surfaces: field studies in the McMurdo
1645 Dry Valleys, Antarctica. *J. Geophys. Res.*, 115, F03027, 2010.
- 1646 Lappalainen, H. K., Petäjä, T., Vihma, T., Räisänen, J., Baklanov, A., Chalov, S., Esau, I., Ezhova, E., Leppäranta, M.,
1647 Pozdnyakov, D., Pumpanen, J., Andreae, M. O., Arshinov, M., Asmi, E., Bai, J., Bashmachnikov, I., Belan, B., Bianchi, F.,
1648 Biskaborn, B., Boy, M., Bäck, J., Cheng, B., Chubarova, N., Duplissy, J., Dyukarev, E., Eleftheriadis, K., Forsius, M.,
1649 Heimann, M., Juhola, S., Konovalov, V., Konovalov, I., Konstantinov, P., Köster, K., Lapshina, E., Lintunen, A., Mahura, A.,
1650 Makkonen, R., Malkhazova, S., Mammarella, I., Mammola, S., Buenrostro Mazon, S., Meinander, O., Mikhailov, E., Miles,
1651 V., Myslenkov, S., Orlov, D., Paris, J.-D., Pirazzini, R., Popovicheva, O., Pulliainen, J., Rautiainen, K., Sachs, T., Shevchenko,
1652 V., Skorokhod, A., Stohl, A., Suhonen, E., Thomson, E. S., Tsidilina, M., Tynkkynen, V.-P., Uotila, P., Virkkula, A., Voropay,
1653 N., Wolf, T., Yasunaka, S., Zhang, J., Qiu, Y., Ding, A., Guo, H., Bondur, V., Kasimov, N., Zilitinkevich, S., Kerminen, V.-
1654 M., and Kulmala, M.: Overview: Recent advances in the understanding of the northern Eurasian environments and of the urban
1655 air quality in China – a Pan-Eurasian Experiment (PEEX) programme perspective, *Atmos. Chem. Phys.*, 22, 4413–4469,
1656 doi:10.5194/acp-22-4413-2022, 2022.
- 1657 Lewandowski, M., Kusiak, M.A., Werner, T., Nawrot, A., Barzycka, B., Laska, M., Luks, B.: Seeking the Sources of Dust:
1658 Geochemical and Magnetic Studies on “Cryodust” in Glacial Cores from Southern Spitsbergen (Svalbard, Norway).
1659 *Atmosphere* 2020, 11, 1325, doi:[10.3390/atmos11121325](https://doi.org/10.3390/atmos11121325), 2020.
- 1660 Llanos, M. E., Behr, S. J., Gonzalez, J. H., Colombani, E. N., Buono, G. G., and Escobar, J. M.: Informe de las Variaciones
1661 del Lago Colhue Huapi mediante sensores remotos y su relación con las precipitaciones. Retrieved January 5, 2018, from
1662 [https://inta.gob.ar/documentos/informe-de-las-variaciones-del-lago-colhue-huapi-mediante-sensores-remotos-y-su-relacion-](https://inta.gob.ar/documentos/informe-de-las-variaciones-del-lago-colhue-huapi-mediante-sensores-remotos-y-su-relacion-con-las-precipitaciones)
1663 [con-las-precipitaciones](https://inta.gob.ar/documentos/informe-de-las-variaciones-del-lago-colhue-huapi-mediante-sensores-remotos-y-su-relacion-con-las-precipitaciones), 2016.
- 1664 Lutz, S., Anesio, A., Raiswell, R. et al.: The biogeography of red snow microbiomes and their role in melting Arctic glaciers,
1665 *Nat. Commun.* 7, 11968, 2016.
- 1666 Mahowald, N.: Aerosol Indirect Effect on Biogeochemical Cycles and Climate, *Science*, 334, 794-796, doi:
1667 10.1126/science.1207374, 2011.
- 1668 Mahowald, N. M., Baker, A. R., Bergametti, G., Brooks, N., Duce, R. A., Jickells, T. D., Kubilay, N., Prospero, J. M., and
1669 Tegen, I.: Atmospheric global dust cycle and iron inputs to the ocean, *Global Biogeochem. Cy.*, 19, doi:
1670 10.1029/2004gb002402, 2005.

- 1671 Mahowald, N. M., Kloster, S., Engelstaedter, S., Moore, J. K., Mukhopadhyay, S., McConnell, J. R., Albani, S., Doney, S. C.,
1672 Bhattacharya, A., Curran, M. A. J., Flanner, M. G., Hoffman, F. M., Lawrence, D. M., Lindsay, K., Mayewski, P. A., Neff, J.,
1673 Rothenberg, D., Thomas, E., Thornton, P. E., and Zender, C. S.: Observed 20th century desert dust variability: impact on
1674 climate and biogeochemistry, *Atmos. Chem. Phys.*, 10, 10875-10893, doi: 10.5194/acp-10-10875-2010, 2010.
- 1675 Manninen, T., Anttila, K., Jääskeläinen, E., Riihelä, A., Peltoniemi, J., Räisänen, P., Lahtinen, P., Siljamo, N., Thölix, L.,
1676 Meinander, O., Kontu, A., Suokanerva, H., Pirazzini, R., Suomalainen, J., Hakala, T., Kaasalainen, S., Kaartinen, H., Kukko,
1677 A., Hautecoeur, O., and Roujean, J.-L.: Effect of small-scale snow surface roughness on snow albedo and reflectance, *The*
1678 *Cryosphere*, 15, 793–820, doi:10.5194/tc-15-793-2021, 2021.
- 1679 Markuse, Pierre: High latitude dust storm (silt), Nuussuaq Peninsula, Greenland - October 1st, 2020,
1680 https://www.flickr.com/photos/pierre_markuse/50447335522/, contains modified Copernicus Sentinel data [2020], processed
1681 by Pierre Markuse, originally posted to Flickr by Pierre Markuse at [https://flickr.com/photos/24998770@N07/50447335522.](https://flickr.com/photos/24998770@N07/50447335522),
1682 reviewed on 25 October 2020 by FlickrreviewR 2, licensed under the terms of the cc-by-2.0.2020, 2020.
- 1683 Martin, J. H., and Fitzwater, S. E.: Iron deficiency limits phytoplankton growth in the north-east Pacific sub Arctic, *Nature*,
1684 331, 341-343, 1988.
- 1685 Martínez-García, A., Sigman, D. M., Ren, H., Anderson, R. F., Straub, M., Hodell, D. A., Jaccard, S. L., Eglinton, T. I., and
1686 Haug, G. H.: Iron fertilization of the Sub-Antarctic Ocean during the last ice age, *Science*, 343, 1347-1350, 2014.
- 1687 Mazzonia, E., and Vazquez, M.: Desertification in Patagonia. In E. M. Latrubesse (Ed.), *Natural Hazards and Human-*
1688 *Exacerbated Disasters in Latin America*, Vol. 13, 351–377, Elsevier, doi:10.1016/S0928-2025(08)10017-7, 2009.
- 1689 McCutcheon, J., Lutz, S., Williamson, C. et al.: Mineral phosphorus drives glacier algal blooms on the Greenland Ice Sheet.
1690 *Nat. Commun.* 12, 570, doi:10.1038/s41467-020-20627-w, 2021.
- 1691 Meinander, O., Kazadzis, S., Arola, A., Riihelä, A., Räisänen, P., Kivi, R., Kontu, A., Kouznetsov, R., Sofiev, M., Svensson,
1692 J., Suokanerva, H., Aaltonen, V., Manninen, T., Roujean, J.-L., and Hautecoeur, O.: Spectral albedo of seasonal snow during
1693 intensive melt period at Sodankylä, beyond the Arctic Circle, *Atmos. Chem. Phys.*, 13, 3793–3810, doi:10.5194/acp-13-3793-
1694 2013, 2013.
- 1695 Meinander, O.; Kontu, A.; Virkkula, A.; et al., Brief communication: Light-absorbing impurities can reduce the density of
1696 melting snow, *Cryosphere*, Volume: 8 Issue: 3 Pages: 991-995, doi: 10.5194/tc-8-991-2014, 2014.

- 1697 Meinander, O., Dagsson-Waldhauserová, P., and Arnalds, O.: Icelandic volcanic dust can have a significant influence on the
1698 cryosphere in Greenland and elsewhere, *Polar Research Volume*: 35, doi: 10.3402/polar.v35.31313, 2016.
- 1699 Meinander O., Backman, L., Saranko, O., Asmi, E., Rodriguez, E. and Sanchez, R.: Effects of high latitude dust on snow UV
1700 albedo and solar UV irradiance measured at Marambio during 2013-2017 with comparison to simulated UV irradiances,
1701 *Geophysical Research Abstracts Vol. 20, EGU2018-2007*, 2018 EGU General Assembly 2018, available at
1702 <https://meetingorganizer.copernicus.org/EGU2018/EGU2018-2007.pdf>, 2018.
- 1703 Meinander, O., S. Chalov, H. Lappalainen, J. Ekman, K. Eleftheriadis, D. Frolov, A. Hyvärinen, V. Ivanov, N. Karvosenoja,
1704 K. Kupiainen, O. Popovicheva, I. Semenov, L. Sogacheva, and The MSU Workshop Participants: About Black Carbon in the
1705 Arctic and Significance Compared to High-Latitude Dust Sources (Finnish-Russian Workshop at the Lomonosov Moscow
1706 State University, 17-18 September 2019, in Co-operation with MSU, INAR, PEEEX, MFA/IBA and FMI), In: Tiia Laurila,
1707 Anna Lintunen, Markku Kulmala (eds.), *Proceedings of The Center of Excellence in Atmospheric Science (CoE ATM) Annual
1708 Seminar 2019, Report series in aerosol science*, available at: [http://www.faar.fi/wp-
1709 content/uploads/2019/11/CoE_proceedings_2019-compressed.pdf](http://www.faar.fi/wp-content/uploads/2019/11/CoE_proceedings_2019-compressed.pdf), p. 457-465, 2019a.
- 1710 Meinander O., Dagsson-Waldhauserová P., Björnsson H., Petersen G.N., Moore K., Larsen J.N. and Heininen L.: Report of
1711 the IASC Workshop on Effects and Extremes of High Latitude Dust, 13-14 FEB 2019, in co-operation with the IceDust Aerosol
1712 Association, IBA-FIN-BCDUST-project of MFA of Finland and EU COST InDust Action. Available at
1713 <https://iasc.info/news/iasc-news/472-workshop-report-iasc-workshop-on-effects-and-extremes-of-high-latitude-dust>, last
1714 accessed 3 June 2021, 2019b.
- 1715 Meinander, O.; Heikkinen, E.; Aurela, M.; Hyvärinen, A.: Sampling, Filtering, and Analysis Protocols to Detect Black Carbon,
1716 Organic Carbon, and Total Carbon in Seasonal Surface Snow in an Urban Background and Arctic Finland (>60°N).
1717 *Atmosphere*, 11, 923, doi:10.3390/atmos11090923, 2020a.
- 1718 Meinander O., Kontu A., Kouznetsov R., Sofiev M.: Snow Samples Combined With Long-Range Transport Modeling to
1719 Reveal the Origin and Temporal Variability of Black Carbon in Seasonal Snow in Sodankylä (67°N). *Front. Earth Sci.* 12 June
1720 2020, doi:10.3389/feart.2020.00153, 2020b.
- 1721 Meinander, O., Piedehierro, A., Welti, A., Kouznetsov, R., Heinonen, A., Viisanen, Y. and Laaksonen, A.: Saharan dust
1722 transported and deposited in Finland on February 23rd, 2021. EAC 2021 August 30-September 3 2021, Abstract AAS 19-2
1723 Paper ID 399, abstract available at:
1724 https://www.conftool.com/eac2021/index.php?page=browseSessions&form_session=206#paperID399; talk available at:
1725 <https://www.youtube.com/watch?v=ssJ6k8sT0so>. Book of abstracts for the 2021 European Aerosol Conference, A live virtual
1726 event, hosted by The Aerosol Society, <https://eac2021.co.uk/book-of-abstracts>, 2021, 2021.

1727 Meskhidze, N., Volker, C., Al-Abadleh, H. A., Barbeau, K., Bressac, M., Buck, C., Bundy, R. M., Croot, P., Feng, Y., Ito, A.,
1728 Johansen, A. M., Landing, W. M., Mao, J. Q., Myriokefalitakis, S., Ohnemus, D., Pasquier, B., and Ye, Y.: Perspective on
1729 identifying and characterizing the processes controlling iron speciation and residence time at the atmosphere-ocean interface,
1730 *Mar. Chem.*, 217, 103704, doi: 10.1016/j.marchem.2019.103704, 2019.

1731 Meteosat 2019: Two dust clouds, one from northern Africa and one from Central Europe, travelled north towards Iceland and
1732 Greenland in late April 2019. Dust over Europe 22 April 2019 12:00 UTC, 23 April 06:00–12:30 UTC, 24 April 06:00 UTC,
1733 by Jochen Kerkmann and Vesa Nietosvaara (EUMETSAT), Ivan Smiljanicv (SCISYS), Izabela Zablocka (IMGW), Mike
1734 Fromm (US Naval Research Laboratory, Published on 22 April 2019, available at: <https://www.eumetsat.int/dust-over-europe>,
1735 2019.

1736 Miller, M.E., Bowker, M.A., Reynolds, R.L. and Goldstein, H.L.: Post-fire land treatments and wind erosion – lessons from
1737 the Milford Flat Fire, UT, USA. *Aeolian Research*, 7, 29– 44, 2012.

1738 Mills, M. M., Ridame, C., Davey, M., La Roche, J., and Geider, R. J.: Iron and phosphorus co-limit nitrogen fixation in the
1739 eastern tropical North Atlantic, *Nature*, 429, 292-294, doi: 10.1038/nature02550, 2004.

1740 Mockford, T., Bullard, J., Thorsteinsson, T.: The dynamic effects of sediment availability on the relationship between wind
1741 speed and dust concentration. *Earth Surface Processes and Landforms*, 43, 11, 2484–2492, 2018.

1742 Montes, A., Rodríguez, S. S., and Domínguez, C. E.: Geomorphology context and characterization of dunefields developed by
1743 the southern westerlies at drying Colhué Huapi shallow lake, Patagonia Argentina. *Aeolian Research*, 28, Supplement C, 58–
1744 70, doi:10.1016/j.aeolia.2017.08.001, 2017.

1745 Moore, C. M., Mills, M. M., Arrigo, K. R., Berman-Frank, I., Bopp, L., Boyd, P. W., Galbraith, E. D., Geider, R. J., Guieu,
1746 C., Jaccard, S. L., Jickells, T. D., La Roche, J., Lenton, T. M., Mahowald, N. M., Maranon, E., Marinov, I., Moore, J. K.,
1747 Nakatsuka, T., Oeschies, A., Saito, M. A., Thingstad, T. F., Tsuda, A., and Ulloa, O.: Processes and patterns of oceanic nutrient
1748 limitation, *Nat. Geosci.*, 6, 701-710, doi: 10.1038/ngeo1765, 2013.

1749 Mori, Tatsuhiro, Goto-Azuma, Kumiko, Kondo, Yutaka, Ogawa-Tsukagawa, Yoshimi, Miura, Kazuhiko, Hirabayashi,
1750 Motohiro, Oshima, Naga, Koike, M., Kupiainen, Kaarle, Moteki, Nobuhiro, Ohata, Sho, Sinha, P.R., Sugiura, Konosuke, Aoki,
1751 Teruo, Schneebeli, Martin, Steffen, Konrad, Sato, Atsushi, Tsushima, A., Makarov, V., Nagatsuka, N.: Black Carbon and
1752 Inorganic Aerosols in Arctic Snowpack, *Journal of Geophysical Research: Atmospheres*. 124, doi:10.1029/2019JD030623,
1753 2019.

- 1754 Moroni B., Becagli S., Bolzacchini E., Busetto M., Cappelletti D., Crocchianti S., Ferrero L., Frosini D., Lanconelli C., Lupi
1755 A., Maturilli M., Mazzola M., Perrone G., Sangiorgi G., Traversi R., Udisti R., Viola A. and Vitale V.: Vertical profiles and
1756 chemical properties of aerosol particles upon Ny-Ålesund (Svalbard Islands). *Advances in Meteorology*,
1757 doi:10.1155/2015/292081.2015, 2015.
- 1758 Moroni B., Cappelletti D., Ferrero L., Crocchianti S., Busetto M., Mazzola M., Becagli S., Traversi R. and Udisti R.: Local
1759 vs. long-range sources of aerosol particles upon Ny-Ålesund (Svalbard Islands): mineral chemistry and geochemical records.
1760 *Rendiconti Lincei. Scienze Fisiche e Naturali*, doi: 10.1007/s12210-016-0533-7, 2016.
- 1761 Moroni B., Arnalds O., Dagsson-Waldhauserová P., Crocchianti S., Vivani R. and Cappelletti D. Mineralogical and Chemical
1762 Records of Icelandic Dust Sources Upon Ny-Ålesund (Svalbard Islands). *Front. Earth Sci.* 6:187, doi:
1763 10.3389/feart.2018.00187, 2018.
- 1764 Murray, B. J., D. O’Sullivan, J. D. Atkinson, and M. E. Webb: Ice nucleation by particles immersed in supercooled cloud
1765 droplets, *Chem. Soc. Rev.*, 41, 19, 6519-6554, doi:10.1039/c2cs35200a, 2012.
- 1766 Murray, K.T., Miller, M.F. and Bowser, S.S.: Depositional processes beneath coastal multi-year sea ice. *Sedimentology*, 60,
1767 391–410, 2013.
- 1768 Murray, B. J., K. S. Carslaw, and P. R. Field: Opinion: Cloud-phase climate feedback and the importance of ice-nucleating
1769 particles, *Atmos. Chem. Phys.*, 21, 2, 665-679, doi:10.5194/acp-21-665-2021, 2021.
- 1770 Möller, R., Möller, M., Kukla, P. A., and Schneider, C.: Impact of supraglacial deposits of tephra from Grimsvötn volcano,
1771 Iceland, on glacier ablation. *J. Glaciol.* 62, 933–943, doi: 10.1017/jog.2016.82, 2016.
- 1772 Nagatsuka, Naoko, Goto-Azuma, Kumiko, Tsushima, Akane, Fujita, Koji , Matoba, Sumito, Onuma, Yukihiro, Dallmayr,
1773 Remi, Kadota, Moe , Hirabayashi, Motohiro, Ogata, Jun, Ogawa-Tsukagawa, Yoshimi, Kitamura, Kyotaro, Minowa,
1774 Masahiro, Komuro, Yuki , Motoyama, Hideaki , Aoki, Teruo: Variations in mineralogy of dust in an ice core obtained from
1775 northwestern Greenland over the past 100 years. *Climate of the Past*, 17, 1341-1362, doi: 10.5194/cp-17-1341-2021, 2021.
- 1776 Nemuc, A., Basart, S., Tobias, A., Nickovic, S., Barnaba, F., Kazadzis, S., Mona, L., Amiridis, V., Vukovic, A., Christel, I.,
1777 Dagsson-Waldhauserová, P., Monteiro, A.: International Network to Encourage the Use of Monitoring and Forecasting Dust
1778 Products (InDust). *European Review*, 1-13, doi:10.1017/S1062798720000733, 2020.
- 1779
- 1780 Neuman, C. M.: Observations of winter aeolian transport and niveo-aeolian deposition at crater lake, pagnirtung pass,
1781 N.W.T., Canada, *Permafr. Periglac. Process.*, 1, 3–4, 235–247, doi:10.1002/ppp.3430010304, 1990.

- 1782 Nickling, W.: Eolian sediment transport during dust storms: Slims River valley, Yukon Territory. *Canadian Journal of Earth*
1783 *Science*, 15, 1069-1084, 1978.
- 1784 Nickling, W. G., and Brazel, A. J.: Surface wind characteristics along the icefield ranges, Yukon Territory, Canada. *Arctic and*
1785 *Alpine Research*, 17, 125–134. doi:10.2307/1550842, 1985.
- 1786 Nickovic, S., Cvetkovic, B., Madonna, F., Rosoldi, M., Pejanovic, G., Petkovic, S., and Nikolic, J.: Cloud ice caused by
1787 atmospheric mineral dust – Part 1: Parameterization of ice nuclei concentration in the NMME-DREAM model, *Atmos. Chem.*
1788 *Phys.*, 16, 11367-11378, doi:10.5194/acp-16-11367-2016, 2016.
- 1789 Nielsdottir, M. C., Moore, C. M., Sanders, R., Hinz, D. J., and Achterberg, E. P.: Iron limitation of the postbloom
1790 phytoplankton communities in the Iceland Basin, *Global Biogeochemical Cycles*, 23, doi: 10.1029/2008gb003410, 2009.
- 1791 Nordic Council of Ministers. Road dust and PM10 in the Nordic countries. Measures to Reduce Road Dust Emissions from
1792 Traffic. Publication number 2016:790. Publish date 27.01.17, available at: [https://www.norden.org/en/publication/road-dust-](https://www.norden.org/en/publication/road-dust-and-pm10-nordic-countries)
1793 [and-pm10-nordic-countries](https://www.norden.org/en/publication/road-dust-and-pm10-nordic-countries) (last accessed 4.11.2021), 2017.
- 1794 Ovadnevaite, J., Ceburnis, D., Plauskaite-Sukiene, K., Modini, R., Dupuy, R., Rimselyte, I., Ramonet, R., Kvietkus, K.,
1795 Ristovski, Z., Berresheim, H., and O'Dowd, C.D.: Volcanic sulphate and Arctic dust plumes over the North Atlantic Ocean.
1796 *Atmospheric Environment* 43, 4968-4974, 2009.
- 1797 Pejanovic, G., S. Nickovic, M. Vujadinovic, A. Vukovic, V. Djurdjevic, M. Dacic: Atmospheric deposition of minerals in dust
1798 over the open ocean and possible consequences on climate. WCRP OSC Climate Research in Service to Society, 24-28 October
1799 2011, Denver, CO, USA, 2011.
- 1800 Peltoniemi, J. I., Gritsevich, M., Hakala, T., Dagsson-Waldhauserová, P., Arnalds, Ó., Anttila, K., Hannula, H.-R., Kivekäs,
1801 N., Lihavainen, H., Meinander, O., Svensson, J., Virkkula, A., and de Leeuw, G.: Soot on Snow experiment: bidirectional
1802 reflectance factor measurements of contaminated snow, *The Cryosphere*, 9, 2323-2337, doi:10.5194/tc-9-2323-2015, 2015.
- 1803 Perron, M. M. G., Strzelec, M., Gault-Ringold, M., Proernse, B. C., Boyd, P. W., and Bowie, A. R.: Assessment of leaching
1804 protocols to determine the solubility of trace metals in aerosols, *Talanta*, 208, doi: 10.1016/j.talanta.2019.120377, 2020.
- 1805 Popovicheva, O., Diapouli, E., Makshtas, A., Shonija, N., Manousakas, M., Saraga, D., Uttal, T., and Eleftheriadis K.: East
1806 Siberian Arctic background and black carbon polluted aerosols at HMO Tiksi. *Science of the Total Environment*, 655, 924-
1807 938, doi.org/10.1016/j.scitotenv.2018.11.165, 2019.

- 1808 Price, H. C., et al.: Atmospheric Ice-Nucleating Particles in the Dusty Tropical Atlantic, *J. Geophys. Res.*, 123, 4, 2175-2193,
1809 doi:10.1002/2017JD027560, 2018.
- 1810 Prospero, J. M., Ginoux, P., Torres, O., Nicholson, S. E., and Gill, T. E., ENVIRONMENTAL CHARACTERIZATION OF
1811 GLOBAL SOURCES OF ATMOSPHERIC SOIL DUST IDENTIFIED WITH THE NIMBUS 7 TOTAL OZONE MAPPING
1812 SPECTROMETER (TOMS) ABSORBING AEROSOL PRODUCT, *Rev. Geophys.*, 40, 1, 1002,
1813 doi:10.1029/2000RG000095, 2002.
- 1814 Prospero, J.M., Bullard, J.E., Hodgkins, R.: High-latitude dust over the North Atlantic: inputs from Icelandic proglacial dust
1815 storms. *Science* 335, 1078–1082, 2012.
- 1816 Qin, Y., Abatzoglou, J.T., Siebert, S. et al.: Agricultural risks from changing snowmelt. *Nat. Clim. Chang.* 10, 459–465,
1817 doi:10.1038/s41558-020-0746-8, 2020.
- 1818 Querol, A. Tobías, N. Pérez, A. Karanasiou, F. Amato, M. Stafoggia, C.P. García-Pando, P. Ginoux, F. Forastiere, S. Gumy,
1819 P. Mudu: Monitoring the impact of desert dust outbreaks for air quality for health studies. *Environ. Int.*, 130, p. 104867,
1820 2019.
- 1821 Raiswell, R., Hawkings, J. R., Benning, L. G., Baker, A. R., Death, R., Albani, S., Mahowald, N., Krom, M. D., Poulton, S.
1822 W., and Wadham, J.: Potentially bioavailable iron delivery by iceberg-hosted sediments and atmospheric dust to the polar
1823 oceans, *Biogeosciences*, 13, 3887-3900, 2016.
- 1824 Ranjbar, K., O’Neill, N.T., Ivanescu, L., King, J., Hayes, P.L.: Remote sensing of a high- Arctic, local dust event over Lake
1825 Hazen (Ellesmere Island, Nunavut, Canada), *Atmospheric Environment*, 118102, ISSN 1352-2310,
1826 doi:10.1016/j.atmosenv.2020.118102, 2021.
- 1827 Richards-Thomas, T., McKenna-Neuman, C., and Power, I.M. Power: Particle-scale characterization of volcanoclastic dust
1828 sources within Iceland. *Sedimentology*, 68,3, 1137-1158, doi: 10.1111/sed.12821, 2021.
- 1829 Romanias M.N., Y. Ren, B. Grosselin, V. Daele, A. Mellouki, P. Dagsson-Waldhauserová, F. Thevenet: Reactive uptake of
1830 NO₂ on volcanic particles: A possible source of HONO in the atmosphere, *Journal of Environmental Sciences*, Vol 95, pp
1831 155-164, September 2020. doi: 10.1016/j.jes.2020.03.042, 2020.
- 1832 Ryan-Keogh, T. J., Macey, A. I., Nielsdottir, M. C., Lucas, M. I., Steigenberger, S. S., Stinchcombe, M. C., Achterberg, E. P.,
1833 Bibby, T. S., and Moore, C. M.: Spatial and temporal development of phytoplankton iron stress in relation to bloom dynamics
1834 in the high-latitude North Atlantic Ocean, *Limnology and Oceanography*, 58, 533-545, doi: 10.4319/lo.2013.58.2.0533, 2013.

- 1835 Rymer, K.: Aeolian activity in central Spitsbergen (Ebba Valley) in the years 2012–2017. In Proceedings of the XXXVII Polar
1836 Symposium “Polar Change—Global Change”, Poznan, Poland, 7–10 June 2018; p. 61, 2018.
- 1837 Rymer, K.G., Rachlewicz, G., Buchwal, A., Temme, A.J.A.M., Reimann, T., van der Meij, W.M.: Contemporary and past
1838 aeolian deposition rates in periglacial conditions (Ebba Valley, central Spitsbergen). *Catena* 211, 105974, 2022.
- 1839 Samonova O.A. and Aseyeva E.N.: Particle size partitioning of metals in humus horizons of two small erosional landforms in
1840 the middle Protva basin – a comparative study. *GEOGRAPHY, ENVIRONMENT, SUSTAINABILITY*, 13, 1, 260-271,
1841 doi:10.24057/2071-9388-2019-116, 2020.
- 1842 Sanchez-Marroquin, A. O. Arnalds, K. J. Baustian-Dorsi, J. Browse, P. Dagsson-Waldhauserová, A. D. Harrison, E. C. Maters,
1843 K. J. Pringle, J. Vergara-Temprado, I. T. Burke, J. B. McQuaid, K. S. Carslaw, B. J. Murray: Iceland is an episodic source of
1844 atmospheric ice-nucleating particles relevant for mixed-phase clouds. *Science Advances* 6, 26, eaba8137,
1845 doi:10.1126/sciadv.aba8137, 2020.
- 1846 Šantl-Temkiv, T., R. Lange, D. Beddows, U. Rauter, S. Pilgaard, M. Dall’Osto, N. Gunde-Cimerman, A. Massling, and H.
1847 Wex: Biogenic Sources of Ice Nucleating Particles at the High Arctic Site Villum Research Station, *Environ. Sci. Technol.*,
1848 53, 18, 10580-10590, doi:10.1021/acs.est.9b00991, 2019.
- 1849 Schroth, A. W., Crusius, J., Sholkovitz, E. R. and Bostick, B. C.: Iron solubility driven by speciation in dust sources to the
1850 ocean, *Nat. Geosci.*, 2, 5, 337–340, doi:10.1038/ngeo501, 2009.
- 1851 Schroth, A. W., Crusius, J., Gassó, S., Moy, C. M., Buck, N. J., Resing, J. A., and Campbell, R. W.: Atmospheric deposition
1852 of glacial iron in the Gulf of Alaska impacted by the position of the Aleutian Low, *Geophysical Research Letters*, 44, 5053-
1853 5061, doi: 10.1002/2017gl073565, 2017.
- 1854 Schuler, T. V., Kohler, J., Elagina, N., Hagen, J. O. M., Hodson, A. J., Jania, J. A., Kääb, A. M., Luks, B., Małecki, J., Moholdt,
1855 G., Pohjola, V. A., Sobota, I., and Van Pelt, W. J. J.: Reconciling Svalbard Glacier Mass Balance, *Front Earth Sci.*, 8, 156,
1856 doi:10.3389/feart.2020.00156, 2020.
- 1857 Semenkov, I. N. and Koroleva, T. V.: The spatial distribution of fractions and the total content of 24 chemical elements in soil
1858 catenas within a small gully’s catchment area in the Trans Urals, Russia, *Appl. Geochemistry*, 106, 1–6, doi:
1859 10.1016/j.apgeochem.2019.04.010, 2019.
- 1860 Semenkov, I. and Yakushev, A.: Dataset on heavy metal content in background soils of the three gully catchments at Western
1861 Siberia, *Data Br.*, doi:10.1016/j.dib.2019.104496, 2019.

- 1862 Semenov, I. N., Usacheva, A. A. and Miroshnikov, A. Y.: Distribution of global fallouts cesium-137 in taiga and tundra
1863 catenae at the Ob River basin, *Geol. Ore Depos.*, 57, 2, 138–155, doi:10.1134/S1075701515010055, 2015a.
- 1864 Semenov, I. N., Miroshnikov, A. Y., Asadulin, E. E., Usacheva, A. A., Velichkin, V. I. and Laverov, N. P.: The Ob river
1865 basin as a source of Kara Sea contamination with global fallout of Cesium-137, *Dokl. Earth Sci.*, 463, 1, 704–706,
1866 doi:10.1134/S1028334X1507003X, 2015b.
- 1867 Semenov, I. N., Krupskaya, V. and Klink, G.: Data on the concentration of fractions and the total content of chemical elements
1868 in catenae within a small catchment area in the Trans Urals, Russia, *Data in Brief*, 29, doi: 10.1016/j.dib.2019.104224, 2019.
- 1869 Semenov, I. N., Sharapova, A. V., Koroleva, T. V., Klink, G. V., Krechetov, P. P. and Lednev, S. A.: Nitrogen-containing
1870 substances in the snow of the fall areas of the Proton launch vehicle stages in 2009 – 2019, *Led i sneg*, 61, 301-310, doi:
1871 10.31857/S2076673421020090, 2021.
- 1872 Sharapova, A. V., Semenov, I. N., Koroleva, T. V., Krechetov, P. P., Lednev, S. A. and Smolenkov, A. D.: Snow pollution
1873 by nitrogen-containing substances as a consequence of rocket launches from the Baikonur Cosmodrome, *Sci. Total Environ.*,
1874 709, 136072, doi: 10.1016/j.scitotenv.2019.136072, 2020.
- 1875 Shepherd, G., Terradellas E., Baklanov A., Kang A., Sprigg W., Nickovic S., Darvishi Bolorani A., Al-Dousari A., Basart
1876 S., Benedetti A. et al.: Global assessment of sand and dust storms, UNEP, WMO, UNCCD; United Nations Environment
1877 Programme, 123 p., [URL:http://apps.unep.org/publications/pmtdocuments/Global_assessment_of_sand_and_dust_storms-](http://apps.unep.org/publications/pmtdocuments/Global_assessment_of_sand_and_dust_storms-2016.pdf)
1878 [2016.pdf](http://apps.unep.org/publications/pmtdocuments/Global_assessment_of_sand_and_dust_storms-2016.pdf), 2016.
- 1879 Shi, Z., Krom, M. D., Jickells, T. D., Bonneville, S., Carslaw, K. S., Mihalopoulos, N., Baker, A. R., and Benning, L. G.:
1880 Impacts on iron solubility in the mineral dust by processes in the source region and the atmosphere: A review, *Aeolian*
1881 *Research*, 5, 21-42, doi: 10.1016/j.aeolia.2012.03.001, 2012.
- 1882 Shugar, D. H., Clague, J. J., Best, J. L., Schoof, C., Willis, M. J., Copland, L., Roe, G. H.: River piracy and drainage basin
1883 reorganization led by climate-driven glacier retreat. *Nature Geoscience* 10, 370, 2017.
- 1884 Sofiev, M., Vira, J., Kouznetsov, R., Prank, M., Soares, J., Genikhovich, E.: Construction of the SILAM Eulerian atmospheric
1885 dispersion model based on the advection algorithm of Michael Galperin, *Geosci. Model Developm.* 8, 3497-3522, 2015.
- 1886 Speirs, J.C., McGowan, H.A. and Neil, D.T. Meteorological controls on sand transport and dune morphology in a polar-desert:
1887 Victoria Valley, Antarctica. *Earth Surf. Proc. Land.*, 33, 1875–1891, 2008.

- 1888 Spolaor A, Moroni B, Luks B, Nawrot A, Roman M, Larose C, Stachnik Ł, Bruschi F, Koziol K, Pawlak F, Turetta C, Barbaro
1889 E, Gallet J-C and Cappelletti D. Investigation on the Sources and Impact of Trace Elements in the Annual Snowpack and the
1890 Firn in the Hansbreen (Southwest Spitsbergen). *Front. Earth Sci.* 8:536036, doi: 10.3389/feart.2020.536036, 2021.
- 1891 Stockdale, A., Krom, M. D., Mortimer, R. J., Benning, L. G., Carslaw, K. S., Herbert, R. J., Shi, Z., Myriokefalitakis, S.,
1892 Kanakidou, M., and Nenes, A.: Understanding the nature of atmospheric acid processing of mineral dusts in supplying
1893 bioavailable phosphorus to the oceans, *Proc Natl Acad Sci U S A*, 113, 14639-14644, doi: 10.1073/pnas.1608136113, 2016.
- 1894 Stojiljkovic, A., Kauhaniemi, M., Kukkonen, J., Kupiainen, K., Karppinen, A., Denby, B. R., Kousa, A., Niemi, J. V., and
1895 Ketzel, M.: The impact of measures to reduce ambient air PM10 concentrations originating from road dust, evaluated for a
1896 street canyon in Helsinki, *Atmos. Chem. Phys.*, 19, 11199–11212, doi: 10.5194/acp-19-11199-2019, 2019.58-9, 2019.
- 1897 Storelvmo, T., I. Tan, and A. V. Korolev: Cloud Phase Changes Induced by CO2 Warming—a Powerful yet Poorly Constrained
1898 Cloud-Climate Feedback, *Current Climate Change Reports*, 1, 4, 288-296, doi:10.1007/s40641-015-0026-2, 2015.
- 1899 Sweeney M., Mason J. A., Mechanisms of dust emission from Pleistocene loess deposits, Nebraska, USA, *Journal of*
1900 *Geophysical Research* 118, 3, 1460-1471, doi:10.1002/jgrf.20101, 2013.
- 1901 Tagliabue, A., and Arrigo, K. R.: Iron in the Ross Sea: 1. Impact on CO2 fluxes via variation in phytoplankton functional
1902 group and non-Redfield stoichiometry, *Journal of Geophysical Research: Oceans*, 110, 2005.
- 1903 Tan, I., and T. Storelvmo: Evidence of Strong Contributions From Mixed-Phase Clouds to Arctic Climate Change, *Geophys.*
1904 *Res. Lett.*, 46, 5, 2894-2902, doi:10.1029/2018GL081871, 2019.
- 1905 Tang, M, Cziczo, D.J., Grassian, V. H.: Interactions of sater with mineral dust aerosol: Water adsorption, hygroscopicity, cloud
1906 condensation, and ice nucleation. *Chem. Rev.* 116, 4205-4259, 2016.
- 1907 Tarr, R. S., and L. Martin. Glacier deposits of the continental type in Alaska, *Geology*, 21, 289–300, doi:10.1086/622063,
1908 1913.
- 1909 Television Midtvest 2021, video link: [Se videoen: Kraftig blæst får biler til at forsvinde i støvsky | TV MIDTVEST](#), 2021.
- 1910 Terradellas, E., Nickovic, S., and Zhang, X. Y.: Airborne dust: a hazard to human health, environment and society. *WMO*
1911 *Bull*, 64, 2, 42-46, 2015.
- 1912 Terradellas, E., Zhang, X. Y, Farrel, D., Nickovic, S., and Baklanov, A.: Airborne dust: Overview of atmospheric dust content
1913 in 2016. *WMO Airborne Dust Bull* 1, 1-3, 2017.

- 1914 Tobo, Y. K. Adachi, P. J. DeMott, T. C. J. Hill, D. S. Hamilton, N. M. Mahowald, N. Nagatsuka, S. Ohata, J. Uetake, Y.
1915 Kondo, M. Koike: Glacially sourced dust as a potentially significant source of ice nucleating particles. *Nat Geosci*, 12, 4, 253-
1916 258, doi:10.1038/s41561-019-0314-x, 2019.
- 1917 Urupina D., Lasne, J., Romanias, M., Thiery, V., Dagsson-Waldhauserová, P., Thevenet, F.: Uptake and surface chemistry of
1918 SO₂ on natural volcanic dusts, *Atmospheric Environment*, Vol 217, pp 116942, DOI: 10.1016/j.atmosenv.2019.116942, 2019.
- 1919 UNCCD / Vukovic, A.: Sand and Dust Storms Source Base-map. Visualization Tool. <https://maps.unccd.int/sds/> and
1920 <https://www.youtube.com/watch?v=4tsbspJvuAs>, 2021.
- 1921 USGCRP: Impacts, Risks, and Adaptation in the United States: The Fourth National Climate Assessment, Volume II. In: D.
1922 R. Reidmiller, C. W. Avery, D. R. Easterling, K. E. Kunkel, K. L. M. Lewis, T. K. Maycock, and B. C. Stewart (Eds.).
1923 Washington, DC, doi:10.7930/NCA4.2018, 2018.
- 1924 Usher, C.R., Michel, A.E., and Grassian, V.H.: *Chemical Reviews*, 103, 12, 4883-4940, doi: 10.1021/cr020657y, 2003.
- 1925 Valle, H. F. Del, Elissalde, N. O., Gagliardini, D. A., and Milovich, J.: Status of desertification in the Patagonian region:
1926 Assessment and mapping from satellite imagery. *Arid Soil Research and Rehabilitation*, 12, 2, 95–121,
1927 doi:10.1080/15324989809381502, 1998.
- 1928 Varga, G., Dagsson-Waldhauserová, P., Gresina, F. and Helgadóttir A.: Saharan dust and giant quartz particle transport
1929 towards Iceland. *Scientific Reports* 11, 11891, 2021.
- 1930 Vergara-Temprado, J., A. K. Miltenberger, K. Furtado, D. P. Grosvenor, B. J. Shipway, A. A. Hill, J. M. Wilkinson, P. R.
1931 Field, B. J. Murray, and K. S. Carslaw: Strong control of Southern Ocean cloud reflectivity by ice-nucleating particles, *P. Natl.*
1932 *Acad. Sci. USA*, doi:10.1073/pnas.1721627115, 2018.
- 1933 von Friesen, L.W. and Riemann, L.: Nitrogen Fixation in a Changing Arctic Ocean: An Overlooked Source of Nitrogen?
1934 *Frontiers in Microbiology*, 11, 1664-302X, doi: 10.3389/fmicb.2020.596426, 2020.
- 1935 Vukovic, A.: Report on consultancy to develop Global Sand and Dust Source Base Map, no. CCD/18/ERPA/21, UNCCD,
1936 2019.
- 1937 Vukovic Vimic, A.: Global high-resolution dust source map, InDust webinar, 21 April 2021, [https://cost-](https://cost-indust.eu/events/indust-events)
1938 [indust.eu/events/indust-events](https://cost-indust.eu/events/indust-events), 2021.
- 1939 Wahlström E., Reinikainen, T. and Hallanaro E.-L. *Ympäristön tila Suomessa*, ISBN 951-662-523-1, 364 p., 1996.

- 1940 Wheaton, E. E.: Prairie dust storms — A neglected hazard, *Nat. Hazards*, 5, 1, 53–63, doi:10.1007/BF00127139, 1992.
1941
- 1942 Wheaton, E. E. and Chakravarti, A. K.: Dust storms in the Canadian Prairies, *Int. J. Climatol.*, 10, 8, 829–837,
1943 doi:10.1002/joc.3370100805, 1990.
- 1944 Wientjes, I. G., R. S. Van De Wal, G. J. Reichart, A. Sluijs, and J. Oerlemans: Dust from the dark region in the western ablation
1945 zone of the Greenland ice sheet, *The Cryosphere*, 5, 589–601, doi:10.5194/tc-5-589-2011, 2011.
- 1946 Winton, V. H. L., Dunbar, G. B., Bertler, N. A. N., Millet, M. A., Delmonte, B., Atkins, C. B., Chewings, J. M., and Andersson,
1947 P.: The contribution of aeolian sand and dust to iron fertilization of phytoplankton blooms in southwestern Ross Sea,
1948 Antarctica, *Global Biogeochemical Cycles*, 28, 423-436, doi: 10.1002/2013gb004574, 2014.
- 1949 Winton, V.H.L., Dunbar, G.B., Atkins, C.B., Bertler, N.A.N., Delmonte, B., Andersson, P., Bowie, A., Edwards, R.: The origin
1950 of lithogenic sediment in the south-western Ross Sea and implications for iron fertilization. *Antarctic Science*,
1951 doi:10.1017/S095410201600002X, 2016a.
- 1952 Winton, V. H. L., Edwards, R., Delmonte, B., Ellis, A., Andersson, P. S., Bowie, A., Bertler, N. A. N., Neff, P., and Tuohy,
1953 A.: Multiple sources of soluble atmospheric iron to Antarctic waters, *Global Biogeochemical Cycles*, 30, 421-437, doi:
1954 10.1002/2015gb005265, 2016b.
- 1955 Wolfe S.A., *Cold-Climate Aeolian Environments*, Reference Module in Earth Systems and Environmental Sciences,
1956 10.1016/B978-0-12-818234-5.00036-5, 2020.
- 1957 Zhu, L., Ives, A., Zhang, C., Guo, Y., and Radeloff, V.: Climate change causes functionally colder winters for snow cover-
1958 dependent organisms. *Nature Climate Change*, 9, 1-8, doi:10.1038/s41558-019-0588-4, 2019.
- 1959 Zhu, Y., Toon, O.B., Jensen, E.J. et al.: Persisting volcanic ash particles impact stratospheric SO₂ lifetime and aerosol optical
1960 properties. *Nat Commun* 11, 4526, doi:10.1038/s41467-020-18352-5, 2020.
- 1961 Zwoliński, Z., Kostrzewski, A., and Pulina, M. (Eds.): *Dawne i współczesne geoekosystemy Spitsbergenu [Ancient and*
1962 *modern geoecosystems of Spitsbergen]*, Bogucki Wydawnictwo Naukowe, Poznań, 456 p., 2013.